Département de Physique, Université de Fribourg (Suisse)

Physikdepartement, Universität Freiburg (Schweiz)

Protein and cell adsorption: topographical dependency and adlayer viscoelastic properties determined with oscillation amplitude of quartz resonator

THESE

présentée à la Faculté des Sciences de l'Université de Fribourg (Suisse) pour l'obtention du grade de *Doctor rerum naturalium* par
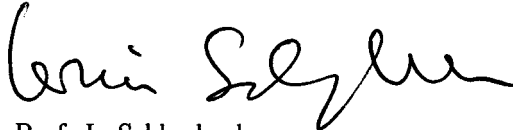
Carine Galli Marxer

de

Valcolla (TI)

Thèse Nr 1388

Acceptée par la Faculté des Sciences de l'Université de Fribourg (Suisse) sur la proposition de Prof. Louis Schlapbach, Dr. Martine Collaud Coen et Prof. Marcus Textor.

Fribourg, le 28 août 2002

Le Directeur de thèse:

Prof. L. Schlapbach

Le Doyen:

Prof. D. Baeriswyl

Table of Contents

Protein adsorption on topographically nanostructured titanium

Summary

The biocompatibility of materials in implant or biosensor fields strongly depends on first interactions occurring between a given surface and a biological environment. It is well-known that a living body brought into contact with a surface will induce protein adsorption, which creates the interface, on which proteins or cells will adsorb. The interactions can be influenced by modifying the surface properties, which are the chemistry, the surface charge and the topography of the surface. It has been shown that cells can "sense" the topography, growing along grooves of defined depth and width at the micrometer scale.

In the first part of this thesis, the fundamental addressed question is whether proteins can "sense" the topography, in analogy to what has been observed for cells on microstructures, because proteins are always present between the surface and the cells. Topographical modification have to be performed at the nanometer scale, corresponding to the size of proteins. Using an Atomic Force Microscope (AFM) and applying Local Anodic Oxidation (LAO) in ambient air, it is possible to create nanostructures of a height of $1-4nm$ and a width of $10nm$. The characterization of the surface by X-Ray Photoelectron Spectroscopy (XPS) reveals that this method assures a modification of the topography of the surface without change of its chemical composition. Surfaces structured by LAO therefore represent ideal systems to study the dependence of protein adsorption on topography. We are able to visualize the created nanostructures by AFM and successively adsorb proteins in situ, rinse and image the new surface. The densities of adsorbed proteins on the nanostructured and neat surfaces are compared and we find that the protein arrangement depends on the underlying nanostructures. A remarkable specificity of the actin filament (F-actin) adsorption on the nanostructure height is noticed. On Ti, F-actin is observed to have a low adsorption on created lines of a height of $4nm$ and the adsorbed proteins appear to be randomly oriented. In contrast, high protein adsorption is observed for structure height between 1 and $2nm$, moreover the filaments adsorb preferentially parallel to the nanostructured pattern. On Si, F-actin also adsorb preferentially along $1nm$ high lines, but the density of adsorbed proteins is higher on neat surface. We have therefore demonstrated that proteins "sense" the topography of surfaces at the nanometer scale.

Experiments performed with AFM only permit static measurements giving no information on the kinetics of protein adsorption. The second part of this thesis is devoted to the building of a Quartz Crystal Microbalance (QCM), which allows us firstly to follow the adsorption kinetics, and secondly to get information about the viscoelastic properties of the adlayer. The QCM is a rather new but ultrasensitive technique. In liquid the QCM sensitivity is $9ng/cm^2$ and under vacuum it reaches $0.135ng/cm^2$. Nevertheless quantification of the amount of adsorbed mass is still difficult to determine under liquid loading, since different phenomena influence the measured parameters. Water molecules entrapped between adsorbed mass can firstly bring an added measured mass, and secondly modification of the liquid and mass properties such as density and viscosity can bring artefacts. In contrary to commercial instruments, our home-made QCM allows us to measure the maximal oscillation amplitude of the quartz crystal. This parameter allows us to distinguish the contribution due to adsorbed mass from the one due to changes of liquid and mass properties. The interpretation of the QCM measurements is therefore enhanced. During this thesis

work experiments have been performed under liquid with different systems, such as proteins and cells, and on different surfaces. On Au more proteins adsorb on the surface, in comparison to Ti. Nevertheless the biological activity is larger on Ti at high protein concentration. Adsorption of cells involves complex phenomena, which are not yet fully determined. We demonstrate that during the first $80 min$ of adsorption, the spreading of the cell influences mostly the measured parameters. Thereafter the cytoskeleton of the cell is rearranged, inducing cell stiffening and an increase of the total cell viscosity. This phenomenon induces variations of the frequency, the amplitude and the decay time constant, although no real modification of the amount of adsorbed cell occurs. Using drugs, it has been possible to modify the polymerisation state of the cytoskeleton, inducing changes of the viscoelastic properties of the adsorbed cells. Changes of the measured frequency, amplitude and decay time constant during cell spreading could therefore be reproduced.

In summary the topography is an important parameter, which has to be taken into account in the general biomaterial field, because the structure of the surface at a nanometer scale can influence the response of biological environments. In order to better analyze the protein adsorption and the cell response against surfaces, the QCM is a very promising technique, but it is essential to measure several parameters.

Résumé

La biocompatibilité des matériaux utilisés dans les domaines des implants et des biosenseurs dépend fortement des premières interactions ayant lieu entre une surface donnée et l'environnement biologique. Il est bien connu que lorsqu'un corps vivant est mis en contact avec une surface, une adsorption de protéines est induite (rétention de protéines sur une surface), formant une interface sur laquelle d'autres protéines ou cellules vont adsorber. Les interactions peuvent être influencées en modifiant les propriétés de la surface, qui sont la chimie, la charge et la topographie. Il a été démontré que les cellules sont sensibles à la topographie, se développant le long de rainures de largeurs définies et de profondeurs à l'échelle du micromètre.

La question fondamentale abordée dans la première partie de cette thèse est de savoir si les protéines peuvent aussi "sentir" la topographie à l'échelle du nanomètre, en analogie avec le comportement des cellules. Ces investigations sont particulièrement importantes, puisque des protéines sont toujours présentes entre la surface et les cellules. Les modifications topographiques doivent être effectuées à l'échelle du nanomètre, ce qui correspond à la grandeur des protéines. Avec un Microscope à Force Atomique (AFM) et en appliquant l'Oxidation Anodique Locale (LAO) à air ambiant, il est possible de créer des nanostructures d'une hauteur de $1-4nm$ et d'une largeur de $10nm$. La caractérisation de la surface par Spectroscopie Photoélectronique à Rayons-X (XPS) révèle que la LAO assure une modification de la topographie de la surface sans aucun changement de sa composition chimique. Les surfaces structurées par LAO représentent ainsi des systèmes idéaux pour étudier l'adsorption des protéines en fonction de la topographie. Nous pouvons visualiser les nanostructures crées par l'AFM et successivement adsorber les protéines in-situ, rincer et imager la nouvelle surface. La comparaison des densités des protéines adsorbées sur les nanostructures et sur la surface vierge montre que l'arrangement des protéines dépend des nanostructures sous-jacentes. Une remarquable spécificité de l'adsorption de filaments d'actine (F-actine) est notée en fonction de la hauteur des nanostructures. Sur le titane (Ti), la F-actine adsorbe peu sur les lignes de $4nm$ de haut, et les protéines sont orientées aléatoirement. Au contraire, une grande adsorption de protéines est observée sur les structures ayant des hauteurs comprises entre 1 et $2nm$. De plus, les filaments s'adsorbent de préférence parallèlement aux nanostructures. Sur le silicium, la F-actine adsorbe également de préférence le long des lignes de $1nm$ de haut, cependant la densité des protéines adsorbées est plus grande sur la surface non-structurée. Nous avons ainsi pu démontrer que les protéines sont sensibles à la nanotopographie des surfaces.

Les expériences réalisées avec l'AFM ne permettent que des mesures statiques, et ne donnent aucune information quant à la cinétique d'adsorption des protéines. La seconde partie de cette thèse est consacrée à la construction d'une Microbalance à Crystal de Quartz (QCM) qui nous permet tout d'abord de suivre la cinétique d'adsorption, et deuxièmement d'acquérir des informations sur les propriétés viscoélastiques de la couche adsorbée. La QCM est une technique relativement nouvelle mais ultrasensible. Dans les liquides, la QCM peut détecter $9ng/cm^2$, et cette sensibilité atteint $0.135ng/cm^2$ dans le vide. Néanmoins, la quantification de la masse adsorbée est difficile à déterminer dans les milieux liquides, car différents phénomènes influencent les paramètres mesurés. Premièrement, les molécules d'eau retenues entre les partic-

ules adsorbées apportent leur contribution à la masse mesurée, et deuxièmement, une modification des propriétés du liquide ou de la masse, telles que la densité ou la viscosité, peuvent générer des artefacts. Au contraire des instruments commerciaux, la QCM que nous avons construite permet de mesurer l'amplitude maximale d'oscillation du crystal de quartz. Ce paramètre nous permet de distinguer la contribution due à la masse adsorbée de celle due aux changements de propriétés du liquide et de la masse. L'interprétation des mesures QCM est ainsi améliorée. Dans ce travail de thèse, des expériences ont été réalisées dans les liquides avec différents systèmes, comme des protéines et des cellules, ainsi que sur différentes surfaces. Une plus grande quantité de protéines s'adsorbent sur l'or que sur le Ti. Néanmoins lorsque la concentration des protéines est élevée, l'activité biologique des protéines est plus grande sur le titane. L'adsorption des cellules est régie par des phénomènes complexes qui ne sont pas encore entièrement compris. Nous démontrons que, durant les 80 premières minutes d'adsorption, l'expansion des cellules influence principalement les paramètres mesurés. Ensuite le cytosquelette est développé, induisant une rigidification de la cellule, ce qui augmente la viscosité totale de la cellule. Ce phénomène induit des variations de la fréquence, de l'amplitude et de la constante d'amortissement malgré qu'aucune modification réelle de la quantité de cellules adsorbées n'ait lieu. En utilisant des drogues, il a été possible de modifier l'état de polymérisation du cytosquelette, ce qui induit des changements des proporiétés viscoélastiques des cellules adsorbées. Les changements de fréquence, d'amplitude et de constante d'amortissement mesurés durant l'expansion cellulaire ont ainsi pu être reproduits.

En résumé, la topographie est un paramètre important qui doit être pris en considération dans le domaine général des biomatériaux, car la structure de la surface à l'échelle du nanomètre peut influencer la réponse d'un environement biologique. Afin de mieux analyser l'adsorption de protéines et la réponse cellulaire envers des surfaces, la QCM est une technique très prometteuse, permettant non seulement de mesurer la masse adsorbée, mais aussi le développement des cellules. Il est cependant essentiel de mesurer plusieurs paramètres.

Introduction

1   Presentation of the work

The understanding of protein and cell adsorption is of high importance for the production of biocompatible implants as well as for the biosensor field, where a protein layer has to be designed as a functional coating. It is well-known that a living body brought into contact with a surface will induce protein adsorption, on which further proteins or cells will adsorb. The foreign body reaction is composed of a succession of events [1]. The first protein adsorption occurs within minutes. During the first day cells (neutrophils and macrophages) will attack the foreign body. When the macrophages find they cannot digest the implant, they fuse into giant cells to engulf the object in the following next 4 days. However the implant is too large to be completely ingest, therefore inducing cytokines (messengers) secretion to alert other cells. In response fibroblasts arrive and begin synthesizing collagen during the next 10 days. After 3 weeks the implant is completely encased in an acellular and avascular collagen bag. The properties of the first protein adlayer can therefore play a crucial role in the integration of implant in the body.

Depending on the application, varying adhesion qualities are required. For example bones or tooth implants demand good protein adhesion to allow the growth of the bone and the formation of a stable and strong interphase between the implant and the bone. In contrast the protein adhesion has to be poor for catheters or contact lenses, where a low contact with the tissue is required. The interactions between proteins and a solid surface can be influenced by modifying the surface prop-

erties, which are the chemistry, the surface charge and the topography. A number of studies have shown that cells "sense" the topography of the surface at the μm scale, growing along grooves of determined width and depth (see figure 1) [2–6].
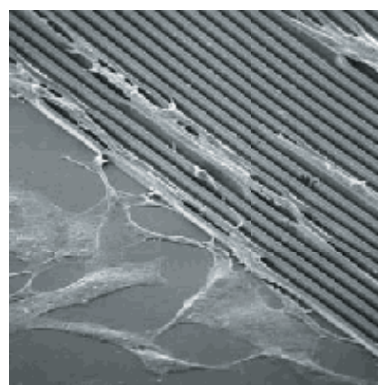
Figure 1: Spreaded cells on grooves [4]

Because proteins are always present between the cells and the substratum, the first part of my work (see Paper I and II) has been devoted to study the role of topography on protein adsorption, which had never been addressed as only parameter. Created structures had to be scaled down to reach sizes accordingly to proteins, i.e. in the nm range, which is smaller than the lithography resolution. The Scanning Probe Microscopy (SPM) permits manipulation of molecules, measuring surfaces at the atomic scale or modifying the surface at the nm scale. An Atomic Force Microscope (AFM) has been used to create nanostructures applying the Local Anodic Oxidation (LAO), which allows us to change the topography (figure 2) without modifying the surface chemistry. On the created nanostru-

Figure 2: Nanostructures created by LAO. A: The first two letters of my university FR. B: Wire netting structure

...ctures proteins have been adsorbed, and the new surface can be measured by AFM. These experiments were static giving no information on the kinetics of protein adsorption.

The second part of my work (see Paper III to V) has therefore been focussed on the building of a Quartz Crystal Microbalance (QCM), which allows us firstly to follow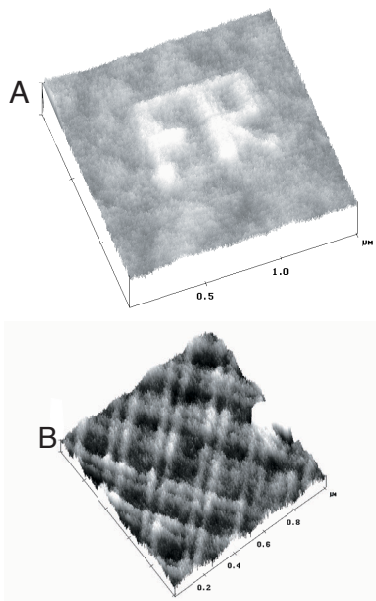 the adsorption kinetics, and secondly to get information about the viscoelastic properties of the adlayer. In comparison to commercial QCM a new parameter has been introduced, which is the maximal oscillation amplitude of the quartz crystal (see Paper III). The adsorption kinetics of different systems has bee measured. Protein A-BSA-IgG is a system well-known in immunology and fibronectin is viscoelastic in solution. For both systems the mechanical properties of the adsorbed layers have been investigated on Ti and Au surfaces (see Paper IV). Cell adsorption and spreading has also been performed with different cell types, where the cytoskeleton has been disturbed with drugs

(see Paper V). This system range has allowed us to improve the interpretation of QCM measurements, opening new applications in biotechnology research.

2   BIOCOMPATIBILITY

The notion of biocompatibility has evolved with the development of materials used in medical devices. So far a biocompatible material was defined as a material that would *do no harm*. The principle was based on inertness, as reflected by the definition of biocompatibility: "the quality of not having toxic or injurious effects on biological systems" [7]. Nevertheless recent devices began to be designed with materials that were more responsive to local biological conditions, where interactivity became the central principle. The official definition of biocompatibility is: "the ability of a material to perform with an appropriate host response in a specific application". Unfortunately *an appropriate host response* was still difficult to determine. Through tremendous advances in molecular biology and biological surface sciences, the current definition of biomaterial is "a material intended to interface with biological systems to evaluate, treat, augment, or replace any tissue, organ, or function of the body".

The biocompatibility of medical implants is influenced by different factors, such as the toxicity of the material used, the form and design of the implant, the skill of the surgeon inserting the device, the resistance of the device to chemical or structural degradation, the dynamics or movement of the device *in-situ*, and the nature of the reactions occurring at the biological interface. Naturally these factors vary with the implantation area, i.e. in soft tissue or hard tissue, or in the cardiovascular system. Therefore biocompatibility may

have to be uniquely defined for each application [8].

The prominent applications for biomaterials are:

- Orthopedics: joint replacements, bone cements, bone defect fillers, fracture fixation plates, artificial tendons and ligaments.

- Cardiovascular: vascular grafts, heart valves, pacemakers, artificial heart and ventricular assist device components and blood substitutes.

- Ophthalmics: contact lenses, corneal implants, artificial corneas and intraocular lenses.

- Other: dental implants, cochlear and ear implants, tissue screws and tacks, burn and wound dressings, artificial skin, tissue adhesives and sealants, drug-delivery systems, matrices for cell encapsulation and tissue engineering, and sutures.

A wide range of materials is used, such as metals (stainless steel, titanium, cobalt chrome, nitinol), ceramics and glasses (alumina, calcium phosphate, hydroxyapatite), synthetic and natural polymers.

Despite the large choice of existing implants, rejection phenomena still occur, encouraging further researches in order to improve the understanding of the cell mechanism and response in different environments.

3 PROTEINS AND CELLS

All living creatures are made of cells, which consist of a small lipid membrane compartment filled with a concentrated aqueous solution of chemicals. 70% of the cell weight is due to the presence of water;

proteins, nucleic acids and polysaccharides contribute to 26%. The rest are inorganic ions, sugars, amino acids, nucleotides, fatty acids and other small molecules.

3.1 Proteins

Proteins are long linear polymers of amino acids (figure 3) joined by a peptide bond between the carboxylic acid group of one amino acid and the amino group of the next. Only
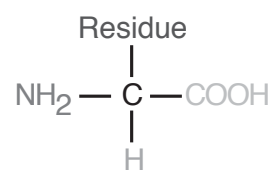
Figure 3: One amino acid

20 amino acids are common in proteins, each with a different side chain attached to the C atom. Only 5 amino acids have charged side chains, whereas the others are uncharged but reactive in specific ways. The charge of amino acids depends on pH in the solution. The isoelectric point pI of proteins corresponds to the pH, at which the total protein charge is zero.

The diverse and sophisticated functions of proteins are determined by the properties of the amino acid side chains in aggregate.

Functions The main functions of proteins can be classified as following:

- Structure: structural proteins are responsible for the mechanical stability of organs and tissues

- Transport: molecules are transported inside the body by specific proteins. For example hemoglobin transport oxygen and CO_2

- Protection: the immunological system defends our organism against

pathogen agents

- Regulation and control: proteins are involved in the biochemical signalling

- Catalyse: the enzymes participate in catalyse

- Movement: muscular contraction arise due to coordinated action of actin and myosin proteins

Protein folding [9] Proteins do not possess only one determined 3D-structure, because changes in the environment will modify the charge of the amino acid side chains, inducing modifications of the interactions between each atom. Protein can therefore fold and unfold. Three main levels of protein structure have been determined. The primary structure defines the amino acid sequence and remains therefore at the chemistry level. The secondary structure corresponds to the local arrangement of the backbone without regard to conformation of the side chain. α-helix, β-sheet or β-turn are example of the secondary structure (figure 4). Finally the global arrange-
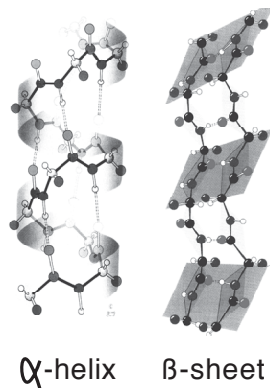

α-helix   ß-sheet

Figure 4: α-helix and β-sheet form the secondary structure of proteins.

ment of proteins represents the tertiary structure (figure 5). At the moment a lot of effort is put into solving the protein folding problem for different reasons. Firstly the function

Figure 5: Tertiary structure of Chymotrypsin Inhibitor 2 (CI2)

of proteins is defined by its chemistry and its tertiary structure. Secondly the sequencing of protein is a relative quick process, in contrast to the determination of the secondary and tertiary structure by crystallisation of proteins. The aim is to determine an algorithm, which could translate the primary structure into the tertiary one, that is the understanding of the relationship between the amino acid sequence and the native 3D-structure.

In 1920s it has been demonstrated that the process of protein folding and denaturation is reversible.It is only later, with the invention of laser, that the first experimental studies could start. In 1968 the *Levinthal paradox* is enounciated: it has been experimentally shown that proteins fold within seconds [10], what was in contradiction to the idea, that protein folding is a consequence of random rearrangement of amino acids, which would lasts 10^{62} years to fold for a protein with 83 amino acids. The approach to understand the folding pathway is based on experimental and theoretical developments. Statistical mechanics and simulation permit to compare calculations with experiments. Experimental methods are princi-

pally based on two different groups. The first one is based on crystallography, but it has to be kept in mind that protein structure *in vitro* can be different from the one *in vivo*. The second group comprise Nuclear Magnetic resonance (NMR), Circular Dichroism (CD) and fluorescence methods, which allows us to track changes of conformation in time and to determine rate constant of folding. Protein engineering can also help to understand protein folding by measuring the effect of local modification of the primary structure. Despite the complexity of proteins a general model emerges, which is the nucleation-condensation model [11, 12]. The mechanism involves the creation of a nucleus, around which further protein condensation arises. α-helix represents often a nucleus, whose consolidation arises simultaneously with complete folding of the protein. It seems that the whole molecule is involved in forming the transition state, where the nucleus is simply the best formed part of the structure. Nevertheless further experiments and calculations have to be performed in order to analyse more complex proteins, and to determine the influence of the environment on protein folding.

Adsorption When proteins come in contact with a solid surface, further modifications of the tertiary structure can occur, inducing denaturation. The protein adsorption can be divided into four main steps [13]:

1. The transport of proteins towards the interfacial region is driven by Brownian motion and gradient diffusion, which depends on the experimental conditions.

2. The first interactions occurring between the protein and the surface determine the residence time of the initial attachment.

3. During the residence time dynamic processes arise, such as movements and con-

formational changes of the proteins, which can induce stronger binding and increase residence time.

4. If the binding with the surface is too weak, desorption will occur.

It has been observed that surface properties influence the protein adsorption. Some general trends have been determined; nevertheless exceptions are always present:

- An increased exterior hydrophobicity of the protein and an increased hydrophobicity of the solid surface increases the surface affinity [14, 15], without being strongly affected by solution pH or variation in ionic strength.

- A decrease of protein stability increases the adsorption affinity on most surfaces [15, 16].

- Proteins presenting opposite charges to the surface will adsorb with a higher affinity [17, 18]. Moreover the adsorption affinity depends also on the location of the charges on the protein surface [19], so that proteins can orient at the surface to expose opposite charges toward each other.

- The size and the shape of the protein can play an important role in adsorption, since the number of binding sites per adsorbed protein will increase for larger one. The Vroman effect [20, 21] describes the competitive adsorption of protein mixtures, where smaller proteins adsorb first and are thereafter replaced by larger one.

3.2 Cells

Eucaryotic cells (animal and plant cells) have a nucleus (*caryon* in Greek), containing the majority of DNA enclosed by a double layer membrane. The genetic code is

therefore kept in a compartment, which is separated from the rest of the cell contents, the cytoplasm, where most of the cell's metabolic reactions occur. All eucaryotic cells have an internal skeleton, the cytoskeleton, which determines their shape, their capacity to move and their ability to arrange their organelles. Moreover the cytoskeleton participate in the organelle transport from one part of the cell to another.

3.2.1   The cytoskeleton

The cytoskeleton is composed of a network of protein filaments, which is a highly dynamic structure that reorganizes continuously as the cell changes its shape, divides and responds to its environment. The diverse activities of the cytoskeleton depend on 3 types of proteins, which are the actin filaments, the microtubules and the intermediate filaments. Each type of filament is formed from a different protein subunit and presents different sizes. The main subunits of the three classes of cytoskeletal polymers, as well as many of the hundreds of accessory proteins that associate with them, have been isolated and their amino acid sequences determined. It is still difficult to establish how these proteins function in the cell.

The function of the cytoskeleton depends firstly on complex assemblies of proteins, which bind in cooperative groups to the cytoskeletal filaments. It is relatively straightforward to examine the effect of a single accessory protein on a filament, but it is much more difficult to analyze the effects of a mixture of many different proteins. Secondly the cytoskeleton exerts forces and generates movements without any major chemical change. It is therefore difficult to assay the function of a cytoskeletal system that has been reconstituted *in vitro* from purified components.

The different cytoskeletal proteins show different strain versus stress [22]. Microtubule networks are easily deformed but

they rupture and begin to flow without limit when stretched beyond 50% of their original length. Actin filament networks are much more rigid, but they also rupture easily. In contrast, Vimentin networks (intermediate filaments) are easily deformed and withstand large stresses and strains without rupture.

Actin filaments [23–27] are found in all eucaryotic cells. It is the most abundant protein, often constituting 5% or more of the total cell protein. Each actin molecule is a single polypeptide of 375 amino acids long with an Adenosine Tri- Phosphate (ATP) tightly associated with it. Actin filaments are $8nm$ wide and consist of a tight helix of uniformly oriented actin molecules, also called G-actin. The polar structure of a filament shows different polymerisation rates for the two ends. The *minus end* is relatively inert and the faster-growing *plus end* polymerises up to 10 times faster. Actin is involved in a wide range of structures (see figure 6), form stiff and relatively permanent extensions at the cell surface to the dynamic 3-dimensional networks at the leading edge of a migrating cell.
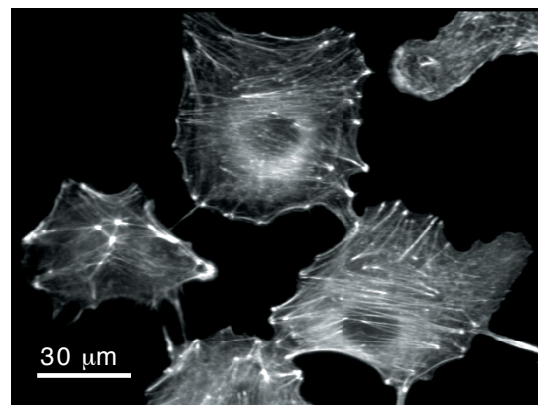

Figure 6: Actin staining of A549 cells

Three different main structures based on actin coexist in every living cell, due to two different classes of *actin filament cross-linking proteins*: *bundling proteins* and *gel-forming proteins*. The first one cross-link actin fila-

ments into a parallel array and is important for forming the tight parallel arrays found in microspikes, and the looser contractile bundles found in stress fibers. In contrast, gel-forming proteins cross-link actin filaments at intersections, creating loose gels. *Fibrin* is responsible for the tight association of actin filaments in parallel bundles at the leading edge of cells, particularly in microspikes and filopodia. α-*actinin* is concentrated in the parallel stress fibers and is responsible for the loose cross- linking of actin filaments. It also helps to form the anchorage for the ends of stress fibers at focal contacts. Finally *filamin* promotes the formation of a loose and highly viscous network in the cell-cortex by clamping together two actin filaments that cross each other.

Microtubules [28] are long and stiff polymers that extend throughout the cytoplasm. They govern the location of membrane-bound organelles and other cell components. Hollow tubes with diameters of $25nm$ are formed from tubulin, which is a heterodimer consisting of two closely related and tightly linked globular polypeptides α-tubulin and β-tubulin. Tubulin is present in all eucaryotic cells and at least six forms of α-tubulin and β-tubulin exist in mammalian cells, each of them being encoded by a different gene. Similarly to actin filaments, the two ends of microtubules polymerise at different rates. The fast-growing end is defined as the *plus end* and the other one as the *minus end*, which polymerises 3 times slower. The centrosomes defines the primary site of microtubule nucleation in animal cells. As it can be seen in figure 7, the greatest density of microtubules is located around the nucleus. Stabilization of microtubules is performed by the binding of other proteins, the microtubule-associated proteins or MAP's. There are many kinds of MAP's, some are widely distributed in most cells.
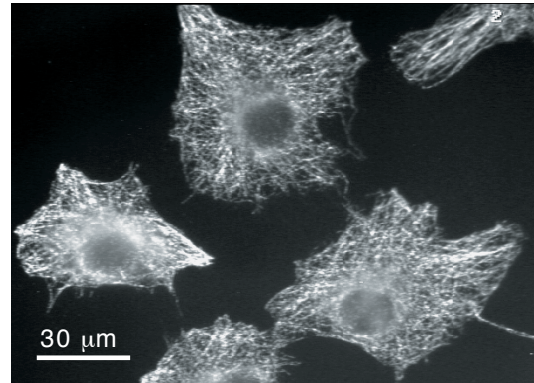

Figure 7: Microtubule staining of A549 cells

Intermediate filaments [29–32] are tough and durable protein fibers, which are found in most of animal cells, that are subjected to mechanical stress. They have a diameter of $8 - 10nm$. The filaments surround the nucleus and extend out to the cell periphery, where they interact with the plasma membrane. Unlike actin and tubulin, which are globular proteins, many types of intermediate filament protein monomers are highly elongated fibrous molecules, that have an amino-terminated *head*, a carboxyl- terminal *tail* and a central *rod domain*. Two of the coiled-coil dimers associate in an antiparallel manner to form a tetrameric subunit, which constitutes a nonpolarized structure, in contrast to actin filaments and microtubules. Finally it seems that tetramers add to an elongating intermediate filament in a simple binding reaction, in which they align along the filament axis and pack together in a helical pattern. Three classes of cytoplasmic intermediate filaments exist in vertebrate cells: (a) *keratin filaments*, (b) *vimentin* and *vimentin-related filaments* and (c) *neurofilaments*, each formed by polymerisation of their corresponding subunit proteins.

3.2.2 *Cell adsorption and spreading*

[33–35] Actin forms the basis of animal cell migration. Nevertheless it undergoes many different transformations as the cell moves for-

ward. Three distinct processes can be broadly identified in the crawling movements of animal cells: (1) *protrusion*, in which lamellipodia and microspikes (or filopodia) are extended from the front of the cell, (2) *attachment*, where the actin cytoskeleton makes a connection with the substratum, and (3) *traction*, where the body of the cell moves forward.

Protrusion is a function of the leading edge of the cell, which is driven by actin polymerisation, although this is still debated.

Attachment is performed through focal contacts, where the plasma membrane is attached to components of the extracellular matrix that has adsorbed to the solid surface. When fibroblasts grow on a culture dish, most of their cell surface is separated from the substratum by a gap of more than $50nm$. At the focal contacts, this distance is reduced to 10 to $15nm$. Staining has shown that the stress fibers attach indirectly to the membrane with the *attachment proteins*, such as vinculin, paxillin and talin [33]. Focal contacts can also relay signals from the extracellular matrix to the cytoskeleton. Several protein kinases are localized to focal contacts, and there are indications that their activity changes with the type of substratum. Regulation for the survival, growth, morphology, movement, and differentiation of cells can therefore occur in response to the extracellular matrix in their environment.

Traction is the most mysterious part of cell locomotion. It is thought that the necessary force is generated near the front of the cell and that the nucleus and bulk cytoplasm are dragged forward passively. In many experiences cells are spread on a deformable polymer [36, 37] in order to track contractile activity of cells.

3.2.3 Influence of the topography on cell adsorption

During the 1980s, the approaches to design implant surfaces were optimization of mechanical retention and imitation of nature. Nevertheless the interactions with the body were not understood, and these solutions illustrate the principle that "existing biomaterials, although demonstrating generally acceptable clinical success, look like dinosaurs poised for extinction in light of the winds of change blowing through the biomedical, biotechnological and physical science" enunciated by Ratner in 1993 [38]. Surface nano- and micropatterning was the envisioned tool, which became reality with improvements of micro- and nanofabrication methods that enable a precise control of topographic features. It has been effectively demonstrated that topographic guidance of cells is a very robust phenomena that can be exhibited by diverse cell types on diverse surfaces such as glass and silica [39], polyvinyl chloride [40], epoxy [41], araldite [42], polystyrene [43], polycarbonate [2, 3], titanium and titanium alloys [41, 44–46], extra-cellular matrices of oriented collagen fibers [47], extracellular-matrix fibrils from amphibian gastrulae [48], fractured enamel [49] and fish scales [50].

Cells reacts on different profiles, such as truncated V-shaped grooves [51], rectangular profiles [2, 3, 42, 52], cylindrical fibers [53] and hemispherical grooves and ridges [40]. Groove depth and spacing interact so that the more closely spaced topographic cues, the more the cells will react to features of a given depth [2, 3]. With increasing step height the proportion of aligned cells increases [54]. Nevertheless the formation of epithelial cell-cell contacts appears to decrease their topographic sensitivity [2, 3]. However the fibroblasts' responses to guiding topography is amplified at high density [55].

The intracellular distribution of cytoskeletal proteins is modified for cells

guided on grooves. It has been found that various filaments segregate preferentially with time into subcellular locations defined by the substratum. Microtubules are the first proteins to reform and align. Moreover they are first observed in the deepest portion of the grooves. In contrast actin filaments form later and are typically first located close to the groove-wall/ridge edge [56], as well as vinculin [57]. This cytoskeletal control probably accounts for the marked effect on cell shape.

Nevertheless it has to be mentioned that all these experiments are performed *in vitro*, which does not mean that similar behaviors will occur *in vivo*, where cells have the opportunity to make contact with all surfaces in all three dimensions. Moreover modification of cell shape can also alter the cell functions. The effect is not yet known *in vivo*, but preliminary experiments have been performed *in vitro*. Cell metabolism can effectively be affected at the very basic level of mRNA and mRNA metabolism [58]. Therefore the good news is that it seems possible to select specific topographies that produce a cell shape that enhances the production of a specific protein. The bad news is that other proteins might be secreted, which have deleterious effects on implant integration.

3.2.4 *Influence of the hydrophobicity on cell adsorption*

The topography can influence the cell adsorption, but also the hydrophobicity of the substratum. Differential adhesiveness is known to be capable of guiding cells and growth cones [59–62]. On hydrophobic surfaces almost no cells adsorb and spread [63]. In case of pattern, the periodicity seems to be an important parameter, similarly to topography [59]. The cell orientation increases with increasing pattern period.

In vivo proteins are always present between the adsorbed cells and the implant surface, so that experiments with living cells have to be performed with pre-adsorbed proteins. It has been shown that after pre-adsorption of laminin on a hydrophobically patterned surface, neurons adhere and exhibit neuritic outgrowth on the previously hydrophobic regions [60]. In fact laminin preferentially adsorbed on the hydrophobic regions of the pattern. Similar phenomena have been shown with other cells and other substrata [64].

This example shows how important the study and the characterization of protein adsorption on different surfaces is, in order to better understand the cell responsivity during cell adsorption and spreading.

4 THE QCM

The Quartz Crystal Microbalance (QCM) is a powerful technique to follow the adsorption kinetics of quite different systems, such as atoms, molecules, proteins or even living cells. The physical phenomenon of the sensor is based on the piezoelectric effect, whose discovery is attributed to Pierre and Jacques Curie. In 1880 they showed that crystals of Rochelle salt could produce electricity when pressure is applied in certain crystallographic directions. One year later they showed the reverse effect, which consists of the production of strain by the application of electricity [65]. Nevertheless it is only at the end of the 1950s that this phenomenon has been investigated. AT-cut quartz crystal is the most used cut for frequency control applications, because it has nearly zero frequency drift with temperature (see figure 8).

Two electrodes are evaporated on each side of the thin quartz plate for the application of an alternative voltage, which induces oscillation of the crystal. In 1959 Sauerbrey published an article showing that the frequency shift of quartz crystals is
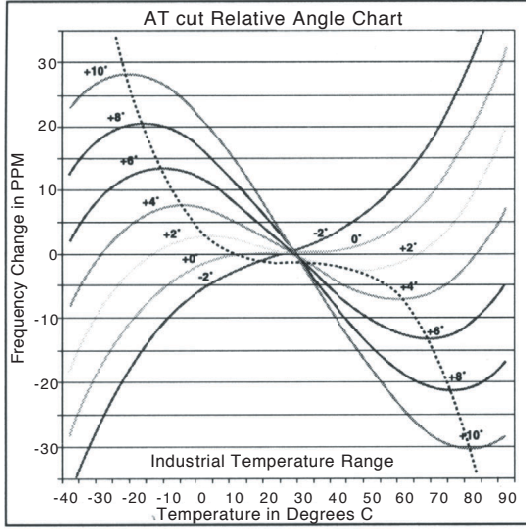
Figure 8: Temperature vs frequency of AT cut crystal resonators.

proportional to the adsorbed mass under vacuum [66]. The QCM was born.

In 1981 the application field of QCM is enlarged to liquid environments [67], opening new research insights in biotechnologies and electrochemistry.

The general setup of our QCM is presented in figure 9. It is composed of three different main components, which are the sensor environment, the QCM-computer interface and the computer with the program allowing to acquire, treat and present the data.

4.1 The sensor environment

10MHz quartz crystals have been used, whose electrodes show two different diameters. Only the larger one enters in contact with liquids, in order to avoid perturbating effects due to the electrical properties of the liquid [68]. The quartz crystal is entrapped between two plexiglas pieces, which are sealed with VITON O-rings.
The liquid exchanges are performed manually with micropipettes and a tubing system.

The sensor and the solutions are placed in a temperature control box in order to main-

tain a constant temperature of $T \pm 0.1^{o}C$ by water circulating inside its walls. No artefacts due to thermal modification of liquid properties can therefore occur.

It is possible to combine the QCM with microscopy, by mounting the crystal under an optical or fluorescence microscope.

4.2 The QCM-computer interface

The electronic interface controls the relay and digitizes, stores and sends the measured data to the computer.

A frequency generator excites the crystal near its series resonance frequency f and a second frequency generator determines the sampling frequency $f_{sampling}$. The relation between the measured alias frequency and the quartz resonance frequency is given by the following relation:

$$f_{alias} = f_{sampling} \cdot frac(\frac{f}{f_{sampling}})$$

When $f_{sampling} \approx f$, $\Delta f_{sampling} = \Delta f$, so that measured shifts of the alias frequency are proportional to resonance frequency shifts.

The relay is closed about $3ms$ to excite the crystal, and is thereafter opened. Due to energy losses occurring in the system the crystal amplitude A begins to decrease according to

$$A(t) = A_0 e^{-t/\tau} sin(2\pi f t + \phi)$$

where τ is the decay time constant, f the measured frequency and ϕ the phase angle. One measurement under liquid lasts about $1.5ms$. During the measurement the amplitude signal is digitized and stored in the RAM. It is thereafter transmitted to the computer with the GPIB bus, and a new measurement can be performed by closing the relay.

4.3 The program

A program has been developed in Lab-View in order to acquire, treat and show the
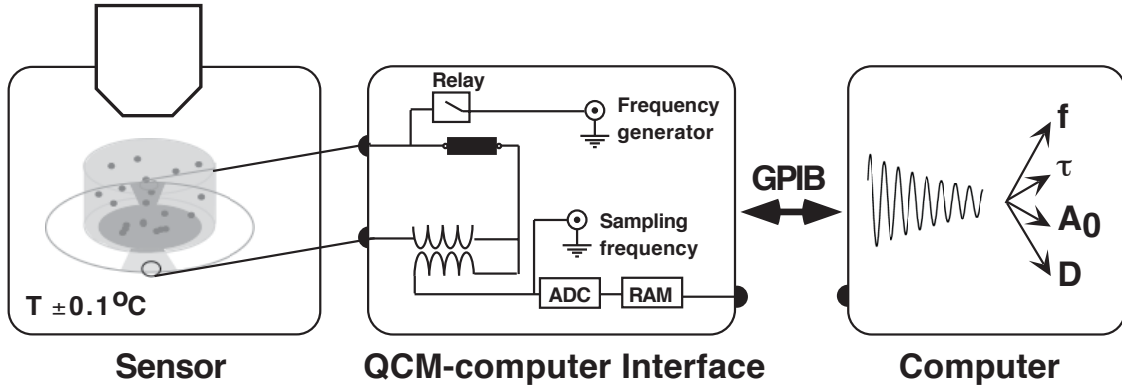
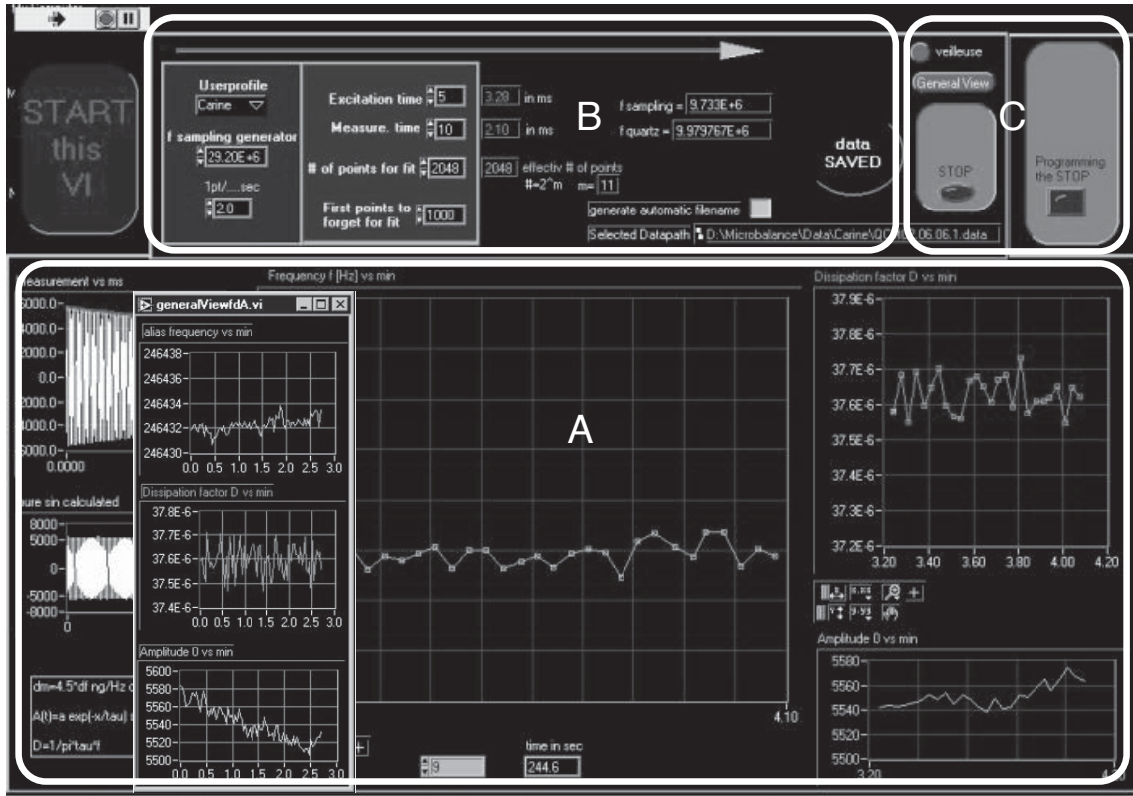Figure 9: Setup of our home-made Quartz Crystal Microbalance

Figure 10: GUI of the developed program in order to control the general QCM.

data over hours. The measured amplitude is transmitted to the computer via the GPIB bus, and the program fits the data in order to determine f, τ and A_0 each $300ms$. The Dissipation factor $D = 2/(\omega\tau)$ is also calculated.

Figure 10 shows the developed Graphical User Interface (GUI). It is composed of three different parts.

In part A the acquired data are monitored. First of all the amplitude decrease of each mea-

surement is shown in the left part. It allows us to adjust precisely the frequency generator at the resonance frequency of the crystal and to control continuously the crystal behavior. The decay time constant is determined and the exponential decrease is also shown in this first graph. The amplitude decrease is transformed in a pure sinusoidal curve in order to determine the resonance frequency. This signal is presented under the amplitude decrease. For each measurement f, D and A_0 are plotted in two different ways. The general overview of the adsorption kinetics is visualized in the three small graphs (middle of part A). The parameters of the last 60 measurements are shown in the three larger graphs in the right part.

The input parameters such as the user profile, the measurement time, the acquisition rate and the created file name have to be given in part B.

Finally the part C allows us to control the Start/Stop of the measurements. The user can choose to start/stop the data acquisition directly or at a scheduled date and time (see figure 11). Similarly the measurement can be immediately stopped, or its end can be determined.

4.4   The resolution

Under vacuum we obtain an excellent resolution of $f \pm 0.03Hz$, $\tau \pm 1.5E - 8sec$, $A \pm 3a.u.$ and $D \pm 0.5E - 7$. The measured mass sensitivity corresponds therefore to $m \pm 0.135ng/Hzcm^2$ using the Sauerbrey relation.

Under liquid loading the resolution decreases due to damping of the liquid. When nanodeionized water is in contact with the quartz at 25^oC, we reach a resolution of $f \pm 2Hz$, $\tau \pm 0.5E^{-6}sec$, $A \pm 50a.u.$ and $D \pm 1E^{-6}$. The mass sensitivity is $m \pm 9ng/Hzcm^2$, corresponding to the better resolution which is possible to obtain with 10MHz quartz crystals.

BIBLIOGRAPHY

[1] D. G. Castner, B. D. Ratner, Biomedical surface science: foundations to frontiers, Surf. Sci. 500 (2002) 28–60.

[2] P. Clark, P. Connolly, A. S. G. Curtis, J. A. T. Dow, C. D. W. Wilkinson, Topographical control of cell behaviour II. Multiple grooved substrata, Development 108 (1990) 635–644.

[3] P. Clark, P. Connolly, A. S. G. Curtis, J. A. T. Dow, C. D. W. Wilkinson, Cell guidance by ultrafine topography in vitro, J. Cell Sci. 99 (1991) 73–77.

[4] A. Curtis, C. Wilkinson, Topographical control of cells, Biomaterials 18 (1997) 1573–1583.

[5] B. Wojciak, J. Crossan, A. S. G. Curtis, C. Wilkinson, J. Mat. Sci. Mat. Medicine 6 (1995) 266–271.

[6] B. Wojciak-Stothard, A. Curtis, W. Monaghan, K. MacDonald, C. Wilkinson, Guidance and activation of murine macrophages by nanometric scale topography, Exp. Cell. Res. 223 (1996) 426–435.

[7] D. F. Williams, The Williams Dictionary of Biomaterials, Liverpool University Press, 1999.

[8] B. D. Ratner, A. S. Hoffman, F. J. Schoen, J. E. Lemons, Biomaterials Science, An introduction to materials in medicine, Academic Press, 1996.

[9] A. Fersht, Structure and mechanism in protein science, W.H. Freeman and Company, New York, 2000.

[10] C. Levinthal, Are there pathways for protein folding?, J. Chim. Phys. 65 (1968) 44–45.

[11] L. S. Itzhaki, D. E. Otzen, A. R. Fersht, The structure of the transition state for folding of chymotrypsin inhibitor 2 analysed by protein engineering methods: evidence for a nucleation-condensation mechanism for protein folding, J. Molec. Biol. 254 (1995) 260–288.

[12] A. R. Fersht, Nucleation mechanisms in protein folding, Curr. Opin. Struct. Biol. 7 (1997) 3–9.

[13] J. L. Brash, P. W. Wojciechowski, Interfacial Phenomena and Bioproducts, JL Brash, PW Wojciechowski, eds, Marcel Dekker, 1996.

[14] J. D. Andrade, V. Hlady, A. P. Wei, C. H. Ho, A. S. Lea, S. I. Jeon, Y. Lin, E. Stroup, Proteins at interfaces: principles, multivariate aspects, protein resistant surfaces, and direct imaging and manipulation of adsorbed proteins, Clinical Materials 11 (1992) 67–84.

[15] D. W. Urry, C. H. Luan, Proteins at interfaces II, TA Horbett and JL Brash Edition, no. 602 in ACS Symposium series, Washington DC, 1995.

[16] J. McGuire, M. C. Wahlgren, T. Arnebrandt, Structural stability effects on the adsorption and Dodecyltrimethylammonium Bromide-Mediated, elutability of bacteriophage T4 lysozyme at silica surfaces, Journal of Colloid and Interface Science 179 (1995) 182–192.

Figure 11: GUI of the developed program in order to control the timer of the QCM. In this case the stop of the measurement is defined.

[17] W. Norde, Driving forces for protein adsorption at solid surfaces, Macromolecular Symposium 103 (1996) 5–81.

[18] E. Blomberg, P. M. Claesson, Proteins at interfaces II, TA Horbett and JL Brash Edition, no. 602 in ACS Symposium series, Washington DC, 1995.

[19] J. D. Andrade, V. Hlady, In Advances in polymer science 79 (1986) 1–63.

[20] S. M. Slack, A. M. Horbett, Proteins at interfaces II, ta horbett and jl brash Edition, no. 602 in ACS Symposium series, Washington DC, 1995.

[21] L. Vroman, A. L. Adams, Findings with the recording ellipsometer suggesting rapid exchange of specific plasma proteins at liquid/solid interfaces, Surf. Sci. 16 (1969) 438–446.

[22] P. Janmey, Mechanical properties of cytoskeletal polymers, Curr. Opin. Cell Biol. 3 (1991) 4–11.

[23] W. Kabsch, J. Vandekerckhove, Structure and function of actin, Annu. Rev. Biophys. Biomol. Struct. 21 (1992) 49–76.

[24] E. M. Bonder, D. J. Fishkind, M. S. Mooseker, Direct measurement of critical concentrations and assembly rate constants at the two ends of an actin filament, Cell 34 (1983) 491–501.

[25] M.-F. Carlier, Actin: protein structure and filament dynamics, J. Biol. Chem. 266 (1991) 1–4.

[26] T. J. Mitchison, Compare and contrast actin filaments and microtubules, Mol. Biol. Cell 3 (1992) 1309–1315.

[27] A. Bretscher, Microfilament structure and function in the cortical cytoskeleton, Annu. Rev. Cell Biol. 7 (1991) 337–374.

[28] J. F. Hyams, C. W. Lloyd, Microtubules, Wiley-Liss, 1993.

[29] K. Albers, E. Fuchs, The molecular biology of intermediate filament proteins, Int. Rev. Cytol. 134 (1992) 243–279.

[30] R. B. Cary, M. W. Klymkowsky, Finding filament function, Curr. Biol. 2 (1992) 43–45.

[31] P. M. Steinert, D. R. Roop, Molecular and cellular biology of intermediate filaments, Annu. Rev. Biochem. 57 (1988) 593–625.

[32] M. Stewart, Intermediate filament structure and assembly, Curr. Opin. Cell Biol. 5 (1993) 3–11.

[33] K. Burridge, K. Fath, T. Kelly, G. Nuckolls, C. Turner, Focal adhesions: transmembrane junctions between the extracellular matrix and the cytoskeleton, Annu. Rev. Cell. Biol. 4 (1988) 487–525.

[34] J. P. Heath, B. F. Holifield, Cell locomotion: new research tests old ideas on membrane and cytoskeletal flow, Cell Motil. Cytoskeleton 18 (1991) 245–257.

[35] T. P. Stossel, On the crawling of animal cells, Science 260 (1993) 1086–1094.

[36] B. Hiny, G. Celetta, J. J. Tomasek, G. Gabbiani, C. Chaponnier, Alpha-smooth muscle actin expression upregulates fibroblast contractile activity, Molecular Biology of the cell 12 (2001) 2730–2741.

[37] K. Burton, J. H. Park, D. L. Taylor, Keratocytes generate traction forces in two phases, Mol. Biol. Cell 10 (1999) 3745–3769.

[38] B. D. Ratner, New ideas in biomaterials science- a path to engineered biomaterials, J. Biomed. Mat. Res. 27 (1993) 837–850.

[39] G. A. Dunn, Contact guidance of cultured tissue cells: a survey of potentially relevant properties of the substratum, In Cell behavior, ed. R. Bellairs, A.S.G. Curtis, and G. Dunn, London: Cambridge U niversity Press (1982) 247–280.

[40] Y. A. Rovensky, I. L. Slavnaya, Spreading of fibroblast-like cells on grooved surfaces, Exp. Cell Res. 84 (1974) 199–206.

[41] B. Chehroudi, T. R. L. Gould, D. M. Brunette, Effects of grooved epoxy substratum on epithelial cell behavior *in vitro* and *in vivo*, Biomed. Mater. Res. 2 (1988) 459–473.

[42] J. Meyle, K. Gultig, H. Wolburg, A. F. Von Recum, Fibroblast anchorage to microtextured surfaces, J. Biomed. Mater. Res. 27 (1993) 1553–1557.

[43] P. T. Ohara, R. C. Buck, Contact guidance in vitro, Exp. Cell Res. 121 (1979) 235–249.

[44] D. M. Brunette, The effects of implant surface topography on the behavior of cells, Int. J. Oral Maxillofac. Imp. 3 (1988) 231–246.

[45] B. Chehroudi, T. R. L. Gould, D. M. Brunette, Titanium-coated micromachined grooves of different dimensions affect epithelial and connective-tissue cells differently in vivo, J. Biomed. Mater. Res. 24 (9) (1990) 1203–1219.

[46] T. Inoue, J. E. Cox, R. M. Pilliar, A. H. Melcher, Effects of the surface geometry of smooth and porous-coated titanium alloy on the orientation of fibroblasts in vitro, J. Biomed. Mater. Res. 21 (1987) 107–126.

[47] G. A. Dunn, T. Ebendal, Contact guidance on oriented collagen gels, Exp. Cell Res. 111 (1978) 475–479.

[48] N. Nakatsuji, K. E. Johnson, Experimental manipulation of contact guidance system in amphibian gastrulation by mechanical tension, Nature 307 (1984) 453–455.

[49] S. J. Jones, Boyde, Colonization of various natural substrates by osteoblasts *in vitro*, Scann. Electron Microscopy 11 (1979) 529–538.

[50] P. Weiss, A. Taylor, Fish scale as substratum for uniform orientation of cells in vitro, Anat. Rec. 124 (1956) 381.

[51] D. M. Brunette, Fibroblasts on micromachined substrata orient hierarchically to grooves of different dimensions, Exp. Cell Res. 164 (1986) 11–26.

[52] D. M. Brunette, Spreading and orientation of epithelial cells on grooved substrata, Exp. Cell Res. 167 (1986) 203–217.

[53] A. S. G. Curtis, M. Varde, Control of cell behavior: topological factors, J. Natl. Cancer Inst. 33 (1964) 15–26.

[54] B. Wojciak-Stothard, A. Curtis, W. Monaghan, K. MacDonald, C. Wilkinson, Guidance and activation of murine macrophages by nanometric scale topography, Exp. Cell. Res. 223 (1996) 426–435.

[55] A. S. G. Curtis, P. Clark, The effects of topographic and mechanical properties of materials on cell behavior, Crit. Rev. Biocompat. 5 (1990) 343–362.

[56] C. Oakley, D. M. Brunette, The sequence of alignment of microtubules, focal contacts, and actin filaments in fibroblasts spreading on smooth and grooved titanium substrata, J. Cell Sci. 106 (1993) 343–354.

[57] E. T. den Braber, J. E. de Ruijter, L. A. Ginsel, A. F. von Recum, J. A. Jansen, Orientation of ecm protein deposition, fibroblast cytoskeleton, and attachment complex components on silicone microgrooved surfaces, J. Biomed. Mater. Res. 40 (2) (1998) 291–300.

[58] H. L. Hong, D. M. Brunette, Effect of cell shape on proteinase secretion, J. Cell Sci. 87 (1987) 259–267.

[59] P. Clark, P. Connolly, G. R. Moores, Cell guidance by micropatterned adhesiveness *in vitro*, J. Cell Sci. 103 (1992) 287–292.

[60] P. Clark, S. Britland, P. Connolly, Growth cone guidance and neuron morphology on micropatterned laminin surfaces, J. Cell Sci. 105 (1993) 203–212.

[61] A. Ohl, K. Schröder, D. Keller, A. Meyer-Plath, Chemical micropatterning of polymeric cell culture substrates using low-pressure hydrogen gas discharge plasmas, J. Mat. Sci. Mat. Medicine 10 (1999) 747–754.

[62] C. A. Scotchford, E. Cooper, G. J. Leggett, S. Downes, Growth of human osteoblast-like cells on alkanethiol on gold self-assembled monolayers: the effect of surface chemistry, J. Biomed. Mater. Res. 41 (1998) 431–442.

[63] S. T. Britland, P. Clark, P. Connolly, G. R. Moores, Micropatterned substratum adhesiveness: a model for morphogenetic cues controlling cell behavior, Exp. Cell Res. 198 (1992) 124–129.

[64] M. Lampin, R. Warocquier-Clérout, C. Legris, M. Degrange, M. F. Sigot-Luizard, Correlation between substratum roughness and wettability, cell adhesion, and cell migration, J. Biomed. Mater. Res. 36 (1997) 99–108.

[65] D. Salt, Handbook of quartz crystal devices, Van Nostrand Reinhold (UK) Co.Ltd, 1987.

[66] G. Sauerbrey, Verwendung von Schwingquartzen zur Wägung dünner Schichten und zur Mikrowägung, Z. Phys. 155 (1959) 206–222.

[67] T. Nomura, M. Iijima, Electrolytic determination of nanomolar concentrations of silver in solution with a piezoelectric quartz crystal, Anal. Chim. Acta 131 (1981) 97–102.

[68] M. Rodahl, F. Höök, B. Kasemo, QCM operation in liquids: an explanation of measured variations in frequency and Q factor with liquid conductivity, Anal. Chem. 68 (1996) 2219–2227.

Paper I

SURFACE SCIENCE

ELSEVIER
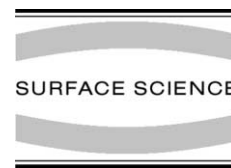
Surface Science Letters

Protein adsorption on topographically nanostructured titanium

C. Galli [a,*], M. Collaud Coen [a], R. Hauert [b], V.L. Katanaev [c], M.P. Wymann [d], P. Gröning [a], L. Schlapbach [a]

[a] *Solid State Physics Department, University of Fribourg, Pérolles, CH-1700 Fribourg, Switzerland*
[b] *Swiss Federal Laboratories for Materials Testing and Research (EMPA), Überlandstrasse 129, CH-8600 Dübendorf, Switzerland*
[c] *College of Physicians and Surgeons, Columbia University, 701 West 168th Street, NY 10032, USA*
[d] *Institute of Biochemistry, University of Fribourg, Pérolles, CH-1700 Fribourg, Switzerland*

Abstract

We study the protein adsorption on surfaces in order to investigate their predominant role in biocompatibility. Nanostructures are created by local anodic oxidation on titanium using the atomic force microscope. A remarkable specificity of the actin filament adsorption on the nanostructure height is noticed. F-actin is observed to have a low adsorption on nanostructures of a height of 4 nm and the adsorbed proteins appear to be randomly oriented. In contrast high protein adsorption is observed for structure height between 1 and 2 nm, moreover the filaments adsorb preferentially parallel to the nanostructured pattern. © 2001 Elsevier Science B.V. All rights reserved.

1. Introduction

The understanding of protein adsorption is of crucial importance for the production of biocompatible implants as well as for the biosensor field, where a protein layer has to be designed as a functional coating. It is well-known that a living body brought into contact with a surface will induce protein adsorption, which creates the interface. Depending on the applications, varying adhesion qualities are demanded. For example bones or tooth implants require good protein adhesion to allow the growth of the bone and the formation of a stable and strong interphase between the implant and the bone. In contrast the protein adhesion has to be poor for example for catheters or contact lenses, where a low contact with the tissue is required. Adsorption is a very complex process, where proteins can change conformation and sometimes lose their biological activity. Furthermore, they can also be replaced by proteins that have a higher affinity to the surface (Vroman effect). Several surface properties can influence the protein adsorption, such as the surface topography, the surface chemistry and the surface hydrophobicity. In order to investigate

---

* Corresponding author. Tel.: +41-26-300-90-76; fax: +41-26-300-97-47.
E-mail address: carine.galli@unifr.ch (C. Galli).

the protein adsorption process and the role of the topography, we applied the local anodic oxidation (LAO) to create structures of the size of proteins, i.e. of the order of the nanometer. We are able to visualize the protein adsorption on the created nanostructures with the atomic force microscope (AFM). The fundamental question we address here concern whether the protein can "sense" the topography of nanostructures, in analogy to what has been observed for cells on microstructures.

2. Materials and methods

2.1. Protein

F-actin is built up from actin monomers of 42 kDa and is active in cell motion and in muscular contraction. The filaments have a width of 6.5–8.2 nm [1] and their isoelectrical point ranges from 5.06 to 5.27 [2]. We prepared the Rabbit muscle F-actin as described in Ref. [3], and controlled by PAGE its purity. We get only one line, which means that our actin solution contained no impurities. By rhodamine phalloidin fluorescence enhancement [4], we determined an F-actin concentration of 6.65 μM. For the F-actin adsorption, we placed a droplet of protein solution on the sample and rinsed after 4 s the surface with a micropipette by a number of sucking–rinsing processes using nanodeionized water, in order to wash out the nonadsorbed filaments.

2.2. Substrate

To measure proteins of a nanometric size with the AFM, we need substrates with a minimal roughness. We achieve this by evaporating Ti at a speed of 50 Å/s on silicon Si⟨111⟩, and obtain 10 nm thick layer of a small natural root mean square (RMS) roughness of 0.2 nm.

2.3. The atomic force microscope

A Nanoscope III (Digital Instruments Inc, USA) is used for the creation of nanostructures, for the visualization of the new surface topography and finally for the analysis of the actin adsorption on titanium (see Fig. 1). The nanostructures are created in ambient air using contact mode (CM) with a Si CM-tip. The AFM images are measured in tapping mode (TM) with a TM-tip, in order to minimize the interaction between the tip and the F-actin [5]. The relative room humidity was 30% and the room temperature was 23°C.

2.4. The local anodic oxidation

To create a defined topography on titanium, we apply the LAO which was developed in the semiconductor field [6,7]. Due to the humidity in the air, a thin water film covers all surfaces, including the sample surface (see Fig. 1). The application of a voltage between the AFM-tip and the sample dissociates the water molecules. Due to the larger size of the oxide lattice in comparison to the metal lattice, a thickening of the oxide layer induces the growth of nanometer sized structures towards the surface.

3. Results

Actin is an asymmetrical protein which forms filament. Fig. 2 shows actin filaments at high
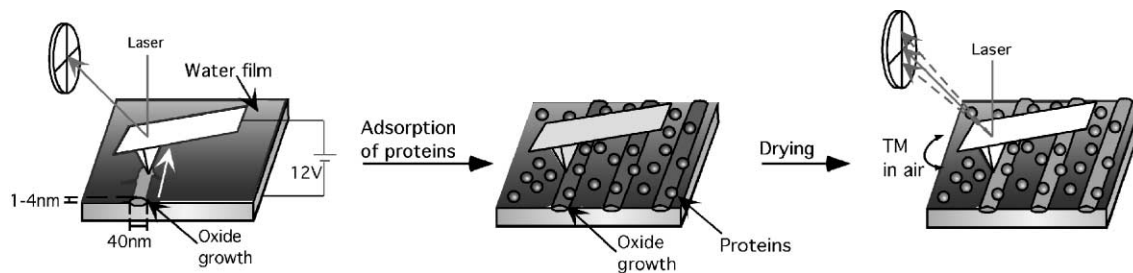

Fig. 1. The nanostructures are created by the application of a voltage between the AFM-tip and the sample during the scan.

resolution adsorbed on neat surface. Therefore the filamentous structure of actin allows us to visualise a possible orientation of adsorbed actin in contact with nanostructures. The created nanostructures on titanium are composed of lines of two distinct heights, as shown in Fig. 3. The main lines have a height of 3–4 nm and a full width at half maximum (FWHM) of 40 nm. The secondary lines are 1–2 nm high and have a similar FWHM. These differences are due to the curvature of the piezo-electrical part of the AFM, which is used to move the sample. Thus the distance between the tip and the sample is modified during the scan, which induces a change of the shape of the water film between the surface and the AFM-tip, leading to the creation of nanostructures of different heights. Generally, the height and the FWHM of the created nanostructures depend on the tip–surface distance, the humidity, the velocity of the tip over the surface and the applied voltage [8]. The large white spots seen on the sample are not produced by LAO, but are already present after the evaporation of Ti. In Fig. 4 we show the same template as shown in Fig. 3 after adsorption of F-actin. To obtain comparable images, we use the same AFM-tip, thus keeping the same tip convolution. The differences in adsorption in and out the nanostructures can be seen in Fig. 4A, while Fig. 4B represents the same magnification as shown in Fig. 3, where we can detect the differences between adsorption on regions with varying nanostructure heights. The main lines are still visible due to a low protein adsorption, in contrast to the secondary lines, which are covered by a thick layer of F-actin.
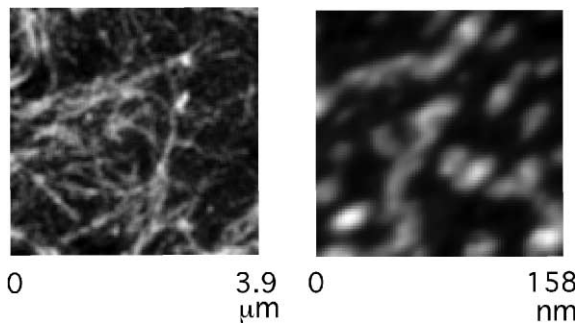

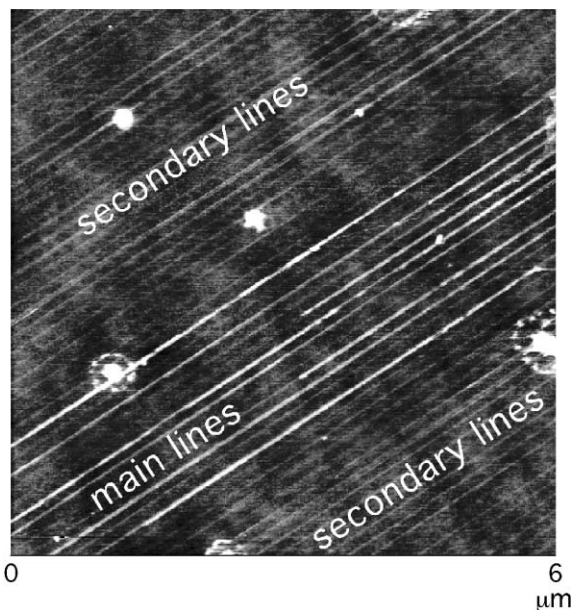
Fig. 3. Nanostructures created by LAO on titanium with a tip velocity of 2 μm/s and an applied voltage of 12 V. The main lines have a height of 3–4 nm, and the secondary lines are 1–2 nm high. The vertical scale is 8 nm.

On neat titanium, F-actin also adsorb on the surface, but in a smaller concentration. Clearly the density of adsorbed proteins depends on differences in the height of the nanostructures. Furthermore, we find that the adsorption of F-actin on the secondary lines exhibits a preferential orientation along the nanostructures. In contrast adsorbed proteins on neat titanium are oriented in all directions. Similarly there seems to be no preferential orientation for the adsorbed proteins on the main lines. Thus we find that in addition to the increased adsorption on the smaller sized nanostructures, the proteins have a tendency to adsorb preferentially along these nanostructures.

4. Discussion

X-ray spectroscopy (XPS) measurements show that the composition of the created nanostructures on titanium is pure TiO_2. Therefore, we are confident that LAO leads to change in the surface topography without changing the surface chemis-

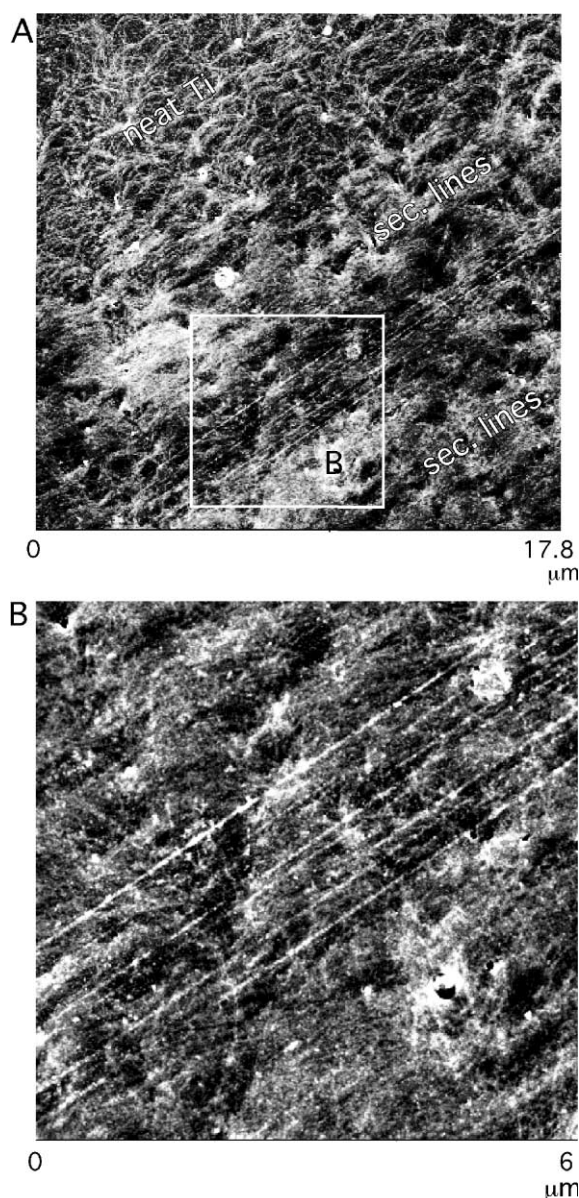Fig. 2. Actin filaments adsorbed on neat surface. The vertical scale is 8 nm.

Fig. 4. Adsorption of the actin filaments on and outer the nanostructures. The vertical scale is 8 nm. A: general view of the protein adsorption. B: adsorption of the F-actin on the main lines.

try. We presume that the proteins are not sensitive at layers being some nm from the sample surface, and that they only "sense" the titanium surface and not the metallic Ti and silicon support. From the fact that we find no Ti in XPS measurements we can deduce that the native Ti oxide layer is thicker than 2–3 nm. Therefore there is no differences in static surface charges between the lower and the upper parts of the topographical structures, which could induce a preferential adsorption.

It appears that the real key parameter for the observed protein adsorption is indeed of geometrical nature with differences in height. Similar dependencies are observed for cells [9], where the relevant length scale, however, is of the order of the μm. Clark et al. [10,11] showed that the degree of cell orientation increases with increasing groove depth. Similarly to the results shown here they find a cut off at which the preferential order along the topography is lost. A lower limit for the preferential cell adsorption is also found and can be as small as 44 nm [12,13]. For F-actin we find very similar behavior, where a preferential adsorption with a well-defined orientation is found for the structures with heights around 1 nm, while a lower and random adsorption is found for the flat surface and structures with heights around 4 nm.

Therefore the range of structure sizes, where specific adsorption occurs seems to be very narrow for proteins. We could imagine that a lock and key mechanism is responsible for this specificity. Depending on the size and shape of the protein an optimal topography for adsorption could be found.

In conclusion, we have demonstrated that proteins can also "sense" the topography, confirming the important role of the nanotopography in the biocompatibility.

For future work, we are planning to investigate the influence of the specific adsorption on the biological activity and we want to explore the possibility to improve the functional coating in biosensor by such a mean.

Acknowledgements

References

[1] T.D. Pollard, J.A. Rooper, Annu. Rev. Biochem. 55 (1986) 987–1035.

[2] J.M. Corbett, C.H. Wheeler, M.J. Dunn, Electrophoresis 16 (1995) 1524–1529.

[3] J.K. Pardee, J.A. Spudich, Meth. Enzymol. 85 (1982) 164–181.

[4] Vl. Katanaev, M.P. Wymann, Anal. Biochem. 264 (1998b) 185–190.

[5] A. Ikai, Surf. Sci. Reports 26 (1996) 261–332.

[6] R.S. Becker, J.A. Golovchenko, B.S. Swartzentruber, Nature 325 (1987) 419.

[7] Ja. Dagata, J. Schneir, H.H. Harary, C.J. Evans, Appl. Phys. Lett. 56 (1990) 2001.

[8] R.J.M. Vullers, M. Ahlskog, C. Van Haesendonck, Appl. Surf. Sci 144 (1999) 584–588.

[9] A. Curtis, C. Wilkinson, Biomaterials 18 (1997) 1573–1583.

[10] P. Clark, P. Connolly, A.S.G. Curtis, J.A.T. Dow, C.D.W. Wilkinson, Development 108 (1990) 635–644.

[11] P. Clark, P. Connolly, A.S.G. Curtis, J.A.T. Dow, C.D.W. Wilkinson, J. Cell. Sci. 99 (1991) 73–77.

[12] B. Wojciak-Stotard, A. Curtis, W. Monaghan, K. Macdonald, C. Wilkinson, Cell. Res. 226 (1996) 426–435.

[13] B. Wojciak, J. Crossan, A.S.G. Curtis, C.D.W. Wilkinson, J. Mat. Sci. Mat. Medicine 6 (1995) 266–271.

Paper II

Creation of nanostructures to study the topographical dependency of protein adsorption

C. Galli [a],*, M. Collaud Coen [a], R. Hauert [b], V.L. Katanaev [c], P. Gröning [a], L. Schlapbach [a]

[a] *Solid State Physics Research Group, University of Fribourg, Pérolles, CH-1700 Fribourg, Switzerland*
[b] *Swiss Federal Laboratories for Material Testing and Research (EMPA), Überlandstrasse 129, CH-8600 Dübendorf, Switzerland*
[c] *Institute of Biochemistry, University of Fribourg, Pérolles, CH-1700 Fribourg, Switzerland*

Abstract

Nanostructures of sizes comparable to protein dimensions are created on Si and Ti surfaces by local anodic oxidation (LAO) using the atomic force microscope (AFM). The characterization of the surface by X-ray photoelectron spectroscopy (XPS) reveals that this method assures a modification of the topography of the surface without a change of its chemical composition. Surfaces structured by LAO therefore represent ideal systems to study the dependence of protein adsorption on topography. We are able to visualize the created nanostructures with an AFM and successively adsorb the proteins in situ, rinse and image the new surface. The densities of adsorbed proteins on the nanostructured and neat surfaces are compared and we find that the protein arrangement depends on the underlying nanostructures, showing that proteins can ''sense'' the topography of surfaces at the nanometer scale. This result can be considered as the nanoscale analogous of the adsorption found for cell systems on micrometer structures. © 2002 Elsevier Science B.V. All rights reserved.

Keywords: Nanostructures; Topography; Protein; Adsorption; Surface

1. Introduction

The biocompatibility of materials in implant or biosensor fields strongly depends on first interactions occurring between a given surface and a biological environment. It is possible to influence these interactions by modifying the surface properties, which are the chemistry, the surface charge and the topography of the surface. In this paper, we are especially interested in the only role of the topography. A number of studies have shown that cells 'sense' the topography at the μm scale, growing along grooves of determined width and depth [1–5]. Nevertheless proteins are always present on surfaces, forming an interface layer, on which further proteins or cells will adsorb, because protein adsorption is the first phenomenon which takes place when a foreign material is brought

---

* Corresponding author. Tel.: +41-26-300-9076; fax: +41-26-300-9747.

E-mail address: carine.galli@unifr.ch (C. Galli).

into contact with biological environment. Therefore we focus our study in the role of topography on protein adsorption, which has never been addressed as only parameter. Created structures have to be scaled down to reach sizes accordingly to proteins, i.e. in the nm range, which is smaller than the lithography resolution. The scanning probe microscopy (SPM) permits manipulation of molecules, measuring surfaces at the atomic scale or modifying the surface at the nm scale. Therefore an AFM is used to create nanostructures applying the LAO, which allows us to change the topography without modifying the surface chemistry.

The topographical dependency of actin adsorption on Ti has already been published elsewhere [6]. As a complement, we describe here the method used for the nanostructure creation, and present the dependence of different parameters as well as the chemical composition analysis of the nanostructured surfaces. As application of the method, we describe the adsorption of different protein systems, which allows us to study the biological activity of adsorbed proteins as well as the orientation of adsorbed proteins on nanostructures. Comparison of the actin adsorption on Ti and Si shows that the amount of adsorbed filaments is higher on Si.

2. Materials and methods

2.1. Proteins

For this study, three different proteins have been used: two standard proteins for immunology tests (protein A and IgG) and F-actin, which forms filaments and is active in the cell motion and muscular contraction. Proteins A (soluble extracellular from *Staphylococcus aureus*, Fluka, Buchs, Switzerland) are globular proteins of 44.2 kDa. They have an average diameter of 3 nm [7] and their isoelectrical point is pI = 5.1 [8]. We diluted them in nanodeionized water, which has been stocked under air conditions, so that due to the CO_2 absorption, the water pH was comprised between 5 and 6, near

the pI of protein A. The concentration was 2.4 µM. The IgG antibodies (Fluka, Buchs, Switzerland) have a Y shape measuring 13.7 nm in width at their extreme and 10.4 nm in height [9]. Their weight is 150 kDa and they can bind specifically on protein A by their Fc domain. We also diluted them in nanodeionized water, at a concentration of 1 µM.

F-actin is built up from actin monomers of 42 kDa and forms filaments having a width of 6.5–8.2 nm [10]. Their isoelectrical point ranges from 5.06 to 5.27 [11], and is thus similar to protein A. Rabbit muscle F-actin was prepared as described in [12] and its purity has been controlled by PAGE. We get only one line, which means that our actin solution contained no impurities. A F-actin concentration of 6.65 µM was determined by rhodamine phalloidin fluorescence enhancement [13].

For all the protein adsorptions, we placed a droplet of protein solution on the sample during different times, and rinsed the surface with a micropipette by a number of sucking–rinsing processes using nanodeionized water, so that non-adsorbed proteins or non-specifically bounded IgG were washed out.

2.2. Substrates

In order to measure proteins of some nanometers with the AFM, we need extremely flat substrates. Native silicon Si⟨111⟩ meets this condition having a natural root mean square (RMS)-roughness of 0.2 nm over 10 µm². To study the protein adsorption on Ti surface that is known to be biocompatible [14,15], we also evaporated a 10 nm thick titanium layer on Si at a speed of 50 Å/s. The RMS-roughness of this Ti layer is 0.35 nm for 10 µm² surfaces.

2.3. The atomic force microscope (AFM)

The creation of the nanostructures, the imaging of the new surface topography and the adsorbed proteins were performed by an AFM (NanoScope III from Digital Instruments Inc, Santa Barbara, USA). The nanostructures were

created in ambient air in Contact Mode (CM) with Si CM-tip (448 μm-long cantilever and 0.1–0.31 Nm^{-1} force constant) or TappingMode™-tip (127 μm-long cantilever and 53–88 Nm^{-1} force constant). All the AFM images are measured in air in TM if not otherwise specified. Because proteins are soft materials, the applied force is minimized so as not to deform them [16]. All AFM images shown are original unprocessed and unfiltered data. The room temperature is 23 °C and the relative humidity is about 30%.

2.4. The X-ray photoelectron spectroscopy (XPS)

We measure the Si$\langle 111 \rangle$ native surface and a 100 μm square of nanostructured Si with a Quantum 2000 XPS from PHI with 10 μm lateral resolution. The radiation was monochromatized Al Kα (1486.6 eV) and the X-ray source was operated at 4.9 W. In order to focus the measurement on or outer the nanostructures, a scanning X-ray image (SXI) has been performed, which showed a well contrasted square of nanostructures on the secondary electron image. The surface composition was calculated from the integral corrected with the atomic sensitivity factor of the O1s, C1s and Si2p (Si and SiO$_2$ compounds) peaks after a Shirley background subtraction. We measured with a 20 μm large X-ray spot at the angles of 0, 30, 45 and 55° reported from the normal of the surface in order to determine the oxide layer thickness d. The intensities of the Si and Si^{4+} signals are

$$I_{\mathrm{Si}} = \mathrm{e}^{-\frac{d}{\varLambda_{\mathrm{Si}_{\mathrm{oxide}}} \cos \theta}} \int_d^{\infty} \sigma_{\mathrm{Si}} T n_{\mathrm{Si}} \, \mathrm{e}^{-\frac{z-d}{\varLambda_{\mathrm{Si}} \cos \theta}} \, \mathrm{d}z \qquad (1)$$

$$dz I_{\mathrm{Si}_{\mathrm{oxide}}} = \int_0^d \sigma_{\mathrm{Si}_{\mathrm{oxide}}} T n_{\mathrm{Si}_{\mathrm{oxide}}} \, \mathrm{e}^{-\frac{z}{\varLambda_{\mathrm{Si}_{\mathrm{oxide}}} \cos \theta}} \, dz \qquad (2)$$

where $\varLambda$ is the mean free path of the Si2p photoelectrons, which is 23 Å in Si [17] and 34.9 Å in Si^{4+} [17]. σ is the photoionization cross section for the Si2p level electron, which is assumed to be equal [18,19] for the bulk and for the oxide layer. T is the analyzer transmission function that we assume equal for all signals and θ is the angle between the normal of the surface and the photoelectron direction. n is the atomic density, which can be easily obtained from $n = \rho / M$, where ρ is the density (2.33 g/cm^3 for SiO$_2$ and 2.66 g/cm^3 for Si) and M is the molecular weight (28.1 g for Si and 60.1 g for SiO$_2$).

For the different measured angles, the oxide thickness is given by the ratio of the intensities of the Si signal over the Si^{4+} signal, which is finally

$$d = \varLambda_{\mathrm{Si}_{\mathrm{oxide}}} \cos \theta \, \ln \left(1 + \frac{I_{\mathrm{Si}_{\mathrm{oxide}}} n_{\mathrm{Si}} \varLambda_{\mathrm{Si}}}{I_{\mathrm{Si}} n_{\mathrm{Si}_{\mathrm{oxide}}} \varLambda_{\mathrm{Si}_{\mathrm{oxide}}}} \right) \qquad (3)$$

3. Results and discussion

3.1. Creation and characterization of nanostructures

3.1.1. The local anodic oxidation (LAO)

We use the LAO method, which has been developed in the semiconductor research domain [20,21] to create defined nanopattern on Si or Ti surfaces. In LAO, advantage is taken of the fact that the sample is covered by a thin water film, due to the humidity of the air (see Fig. 1). By applying a voltage between the AFM-tip and the
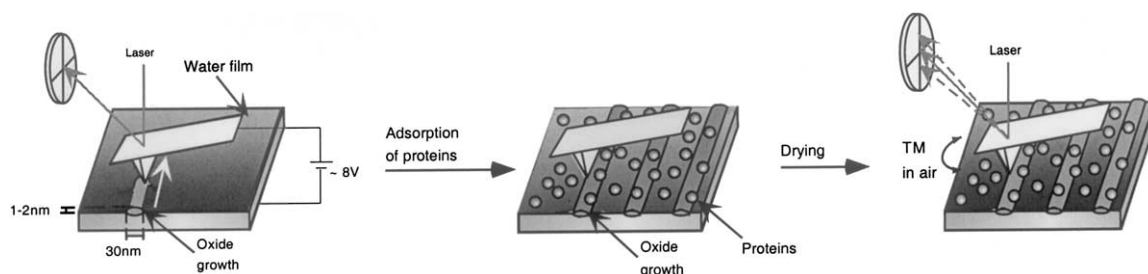

Fig. 1. The LAO allows us to create nanostructures by applying a voltage between the AFM-tip and the sample. We adsorb proteins on the new topography, dry the sample and image by AFM the adsorbed proteins in TM.
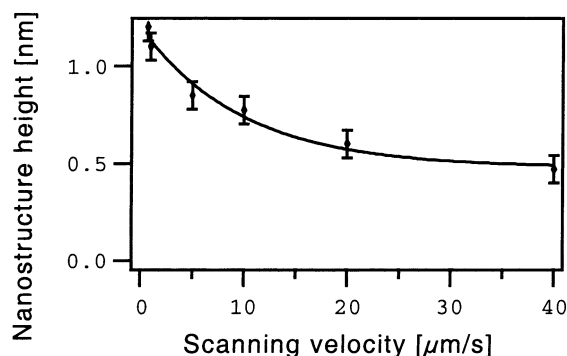
Fig. 2. Nanostructure height as a function of the scanning tip velocity. The applied voltage between the tip and the sample is 8 V.

sample surface, the water molecules dissociate locally [21,22], and OH^- ions adsorb subsequently onto the surface. Due to the larger lattice constant of oxide compared to the metal lattice constant, a thickening of the native oxide layer by LAO induces the creation of nanostructures above the surface. The formation of the nanostructures depends typically on the substrate, the degree of relative humidity [23,24], the tip shape [25], the distance between the tip and the sample [26], the tip velocity (see Fig. 2) and the applied voltage (see Fig. 3).

We explore the effect of scanning velocity on the creation of nanostructures and find that the height of the nanostructures systematically decreases as the scanning velocity is increased. In
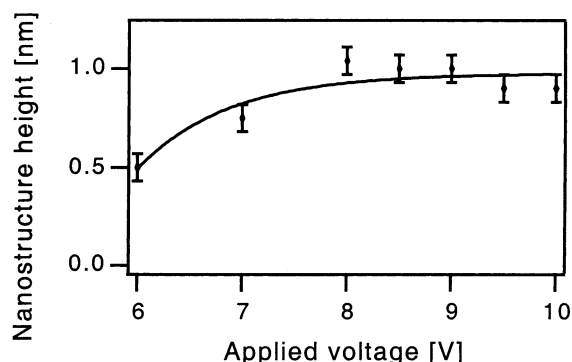

Fig. 3. Nanostructure height as a function of the voltage applied between the AFM-tip and the sample for a tip velocity of 1 μm/s.

Fig. 2 the result of a set of structuring scans are shown, where the same CM-tip has been used. The applied voltage between the tip and the sample was 8 V and the distance between the tip and the sample was kept constant. All images in this section were measured in CM. The nanostructure height decreases continuously with increasing scanning velocities, to reach 0.5 nm for a tip velocity of 40 μm/s. The highest homogeneous nanostructures are obtained with a scanning velocity of 0.7 μm/s and have a size of 1.2 nm. At lower tip velocities the water film between the AFM-tip and surface tends to disrupt, such that the nanostructures present interruptions. We determine the limit in velocity, below which the formation of nanostructures cannot be well controlled for our setup to be 1 μm/s for an applied voltage of 8 V.

The height of the nanostructures depends not only on the scanning velocity but also on the applied voltage. In Fig. 3 we show the results of a set of experiments, where again the same CM-tip was used and the tip-sample distance was kept constant. The tip velocity was chosen to be 1 μm/s to ensure the creation of homogeneous structures. The height of the nanostructures drastically increases for voltages between 6 and 8 V, and then remains constant at a maximal value of 1 nm for higher voltages.

The full width at half maximum (FWHM) is found to be independent of the scan velocity and the applied voltage. For the two sets of experiments shown in Figs. 2 and 3 we determine a FWHM of 100 nm. However, we are able to vary the FWHM by varying the tip shape and the tip-sample distance. We have been able to create structures with FWHM of 20 nm, which is to our knowledge the best lateral resolution which can be achieved [23,25,27].

LAO not only enables us to control the height and width of nanostructures, figures of any shape can also be created by programming the path of the tip over the sample surface. Two examples are shown in Fig. 4a and b. The two first letters of our university city FR and the wire netting structure are created in CM with a CM-tip at the optimal applied voltage of 8 V and a tip velocity of 1 μm s^{-1}. The wire netting structure is made in

In ambient air native oxidation takes place and the native oxidation process will differ from one material to another. This difference affects the oxidation by LAO, such that the creation of nanostructures will differ depending on the material used. For silicon the oxide layer grows slowly and reaches a defined maximal thickness after a couple of days [28]. As a result of that the Si nanostructures obtained by LAO present a maximal thickness, which is the limit through which the OH^- ions can diffuse. The creation of Si nanostructures presents no particular difficulties.

In contrast Ti oxide is formed spontaneously in a fraction of a second [29] after exposure to air and grows continuously [30]. Creation of nanostructures on Ti presents different difficulties in ambient air. The tip-sample distance is a very sensitive parameter. Simply due to the non-linear curvature of the piezoelectrical part of the AFM, which is used to move the sample, nanostructures of different heights are obtained. Also the creation of nanostructures with our voltage setup limit of 12 V becomes impossible to achieve if the native oxide layer is too thick.

3.1.2. Characterization of the nanostructured surfaces by X-ray photoelectron spectroscopy (XPS)

XPS is a standard method used to analyze the chemical composition of a surface. By illuminating the surface with X-rays, electrons of the different surface elements will be excited and leave the surface. They are collected and counted in regard to their kinetic energy, which is specific for each photoelectron coming from a defined shell of an element. XPS measurements of both native and nanostructured $Si\langle 111 \rangle$ reveals the presence of silicon, oxygen and contaminations of carbon. Fig. 5 shows Si2p peaks measured on the native Si surface (Fig. 5a) and on the nanostructured Si surface (Fig. 5b), where the $Si2p_{3/2}$ peaks are normalized. The Si2p core level (Si) from the bulk is found at a binding energy of 99.5 eV and the Si2p from the SiO_2 layer (Si^{4+}) at a binding energy of 103.3 eV. All the spectra measured on nanostructured and neat Si present exactly the same shape with peaks at the same binding energies. Therefore we can affirm that the nanostruc-
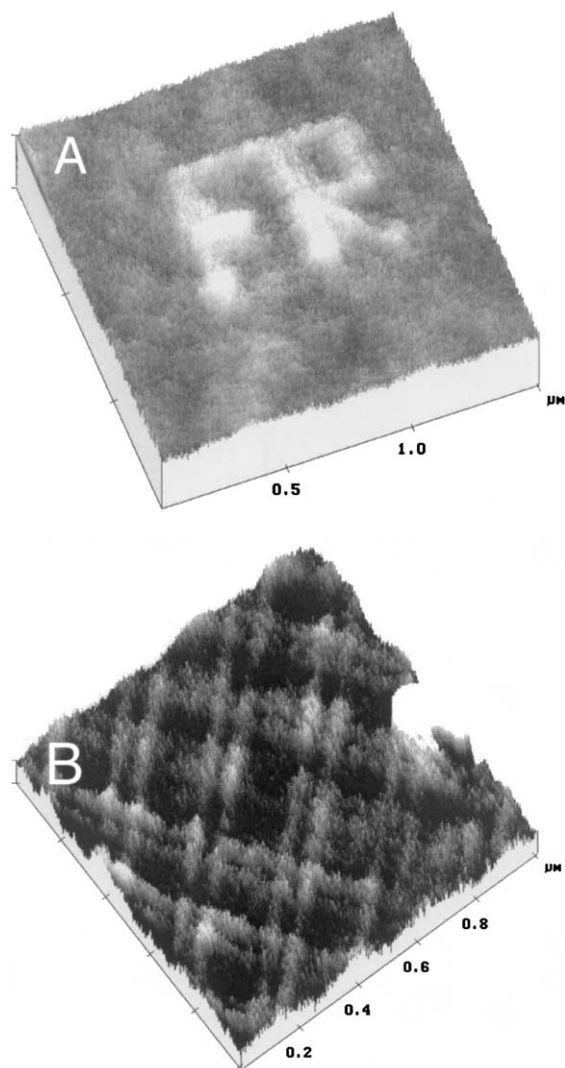

Fig. 4. LAO allows us to create nanostructures of different shapes. (a) The first two letters of our university city FR. (b) Wire netting structures created in two steps.

two steps: in a first scan parallel lines are created, and in a second scan the lines perpendicularly to the first one are produced. The simple lines have a height of 0.8 nm but the height at the intersections is nearly 50% higher. Scanning once more over the intersection areas does not lead to further growth. It seems that for an applied voltage of 8 V, the LAO permits an increase of the oxide thickness up to a maximal limit of 2 nm on Si.

tures present exactly the same chemistry as neat Si, and that the LAO treatment does not change the surface chemistry. The topography is therefore the only modified surface parameter for protein adsorption.

XPS measurements also allow us to determine the oxide thickness present before and after LAO treatments due to the fact that the mean free path of an electron depends on its kinetic energy and is therefore constant for a defined photoelectron. By varying the analysis angle reported from the normal of the surface it is possible to analyze the chemical composition at a different depth from the surface. If the metallic Si signal is always
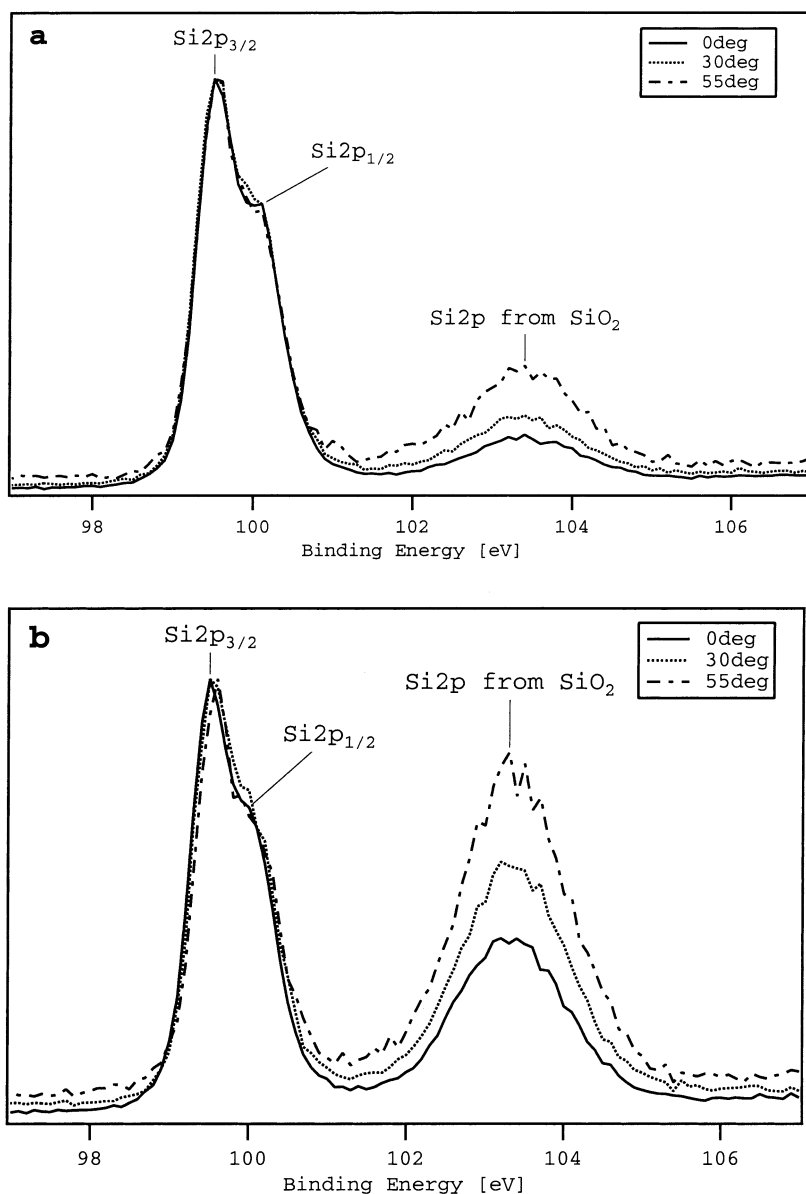

Fig. 5. XPS measurement of (a) the native Si surface and (b) the nanostructured Si surface. The $Si2p_{3/2}$ peaks are normalized in both figures.

dominant, a greater amount of Si^{4+} is present on nanostructures (Fig. 5b). No Si^{x+} ($x \leq 3$) peak of binding energy comprised between 100.5 and 102 eV [31] is measured on native Si and on the nanostructured Si. This result demonstrates that the interface between the SiO_2 and the bulk is abrupt and remains essentially unchanged after LAO treatments. The mean value of the oxide layer thickness calculated for the different angles gives 6.9 ± 1 Å for the native oxide and 20.3 ± 1 Å for the nanostructures. The difference of 13.4 Å represents the created oxide thickness due to the LAO treatment, which is in agreement to the height difference measured with the AFM. The created oxide thickness corresponds to the growth of six added monolayers, considering that the thickness of one monolayer of silicon oxide is 2.2 Å [32]. This suggests that the oxide growth due to the LAO follows the same layer-by-layer growth as Si in air at room temperature [32,33].

XPS measurements on Ti show that the composition of the created nanostructures is pure TiO_2. Because no metallic Ti signal is measured we can deduce that the native oxide layer is thicker than 2–3 nm.

On Si and on Ti, the native oxide thicknesses are thick enough to assume no differences in static surface charges between the lower and the upper parts of the topographical structures, which could induce a preferential protein adsorption due to changes in electrostatic interactions.

3.2. Protein adsorption on nanostructures

In order to be able to study protein adsorption on the nanostructures, we developed techniques which enable us to treat the surfaces in situ, by means without removing the sample from its location in the AFM. This is necessary, as it is nearly impossible to find the very small nanostructured area once the sample has been removed from its original location. After creation and characterization of a nanostructured surface, proteins are adsorbed during a defined amount of time and the surface is subsequently rinsed and dried. This procedure ensures a defined adsorption step and possible problems of desorption–readsorption processes during the imaging are avoided [34], as

well as the difficulty to image in different buffer solutions. AFM measurements are therefore performed in air. In order to be able to compare images it is important to keep the tip convolution artefact constant. We thus always use the same AFM-tip and measure in the same mode (TM in our case) for a given set of experiments.

We explore the adsorption of two proteins on nanostructured surfaces, where the nanostructures consist of parallel lines, and the two proteins differ in shape and size: protein A is a globular protein with a diameter of 3 nm; F-actin forms filaments with a cross-sectional diameter of 6.5–8.2 nm. For the globular protein A, we additionally test for its biological activity after adsorption, by adsorbing in a second step IgG antibodies.

A Si nanostructured surface is shown in Fig. 6a. The lines have a FWHM of 30 nm and the spacing between them is not always regular. The corresponding height histogram (Fig. 6b) can be fitted by two Gaussian curves. The first one corresponds to the neat Si surface and the second one to created lines. We determine from the peak-to-peak distance the mean height of the nanostructures, which corresponds with 1.1 nm to roughly a third of the diameter of protein A in solution.

Shown in Fig. 7a is the surface obtained after 45 s adsorption of protein A on the nanostructured surface shown in Fig. 6a. The lines are covered by protein A but their shape remains visible despite the large amount of adsorbed protein A on the sample surface. The histogram comprises two peaks. The first peak corresponds to the protein A adsorbed on the neat surface. It is wide owing to the presence of holes in the protein layer. The second peak corresponds to the protein adsorbed on top of the created lines. This peak is much smaller, because due to the globular shape of the proteins only a few points on top of the proteins are depicted as maximum height. The peak-to-peak distance remains essentially unchanged compared to the one obtained for the surface before protein adsorption (see Fig. 6b). Profiles (not shown) on nanostructured and neat Si reveal that the height of the protein layer is in both cases of the order of 1 nm, which corresponds to the first monolayer of adsorbed protein A on Si [35]. Furthermore we find that the RMS
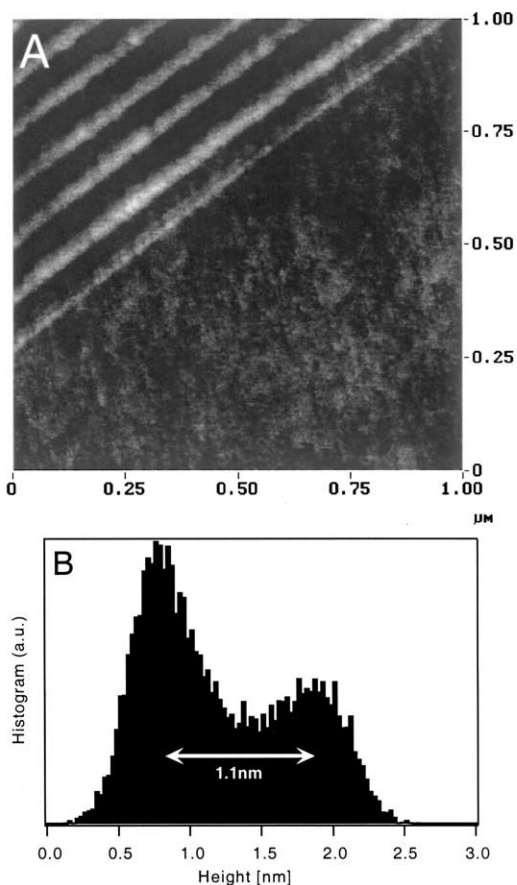
Fig. 6. AFM image (a) and height histogram (b) of nanostructured Si. The vertical scale is 5 nm.

by the protein layer. The decreasing part of this curve is shifted by 1.1 nm compared to the histogram obtained for the neat Si, which corresponds to the nanostructure height. The nanostructure histogram is peaked around 4.7 nm, which is much lower than the height expected for a specific binding of IgG to protein A (13.4 nm). Clearly, the IgG is not in a standing position, independent of the underlying structure. The adsorbed protein A layer (Fig. 7) contains holes and no site blocking proteins have been adsorbed after the protein A deposition. It has been shown that the protein A of the first monolayer adsorbed on Si is 1 nm high and biologically non-active [35]. Therefore IgG can adsorb non-specifically

roughness is identical on nanostructured and neat Si. Clearly, there are no differences in adsorption behavior of protein A on nanostructured or neat Si.

We test for potential differences in the biological activity of the adsorbed protein A on nanostructures, by proceeding to a second adsorption step, where IgG are adsorbed during 45 s (Fig. 8) on the previous adsorbed protein A. The nanostructure shape remains visible, but one line with IgG corresponds to two lines with protein A due to the larger size of IgG (13.7 nm). Different histograms on and around the nanostructured areas have been calculated. The histogram on the nanostructures is wider due to the larger roughness of the surface and the incomplete coverage
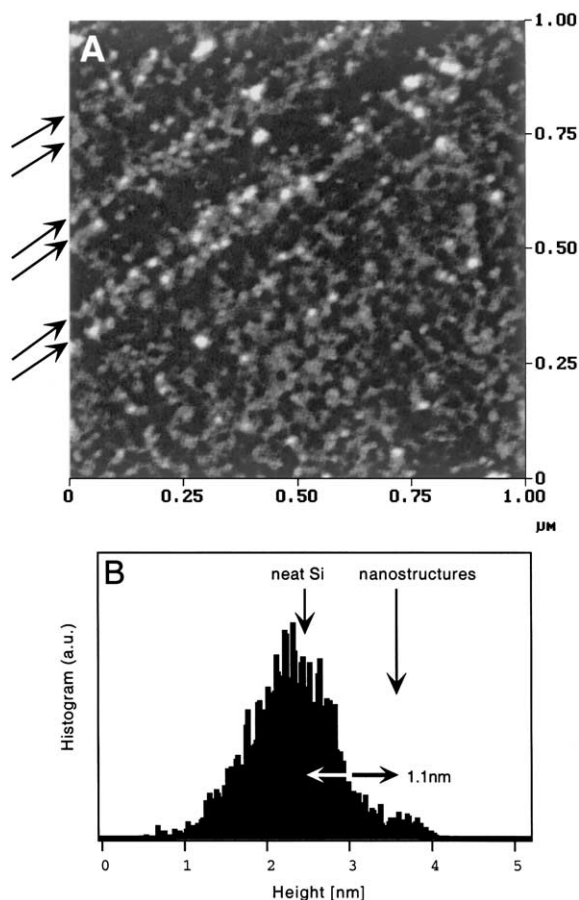

Fig. 7. AFM image (a) and height histogram (b) of protein A adsorption on the previous Si nanostructures. The vertical scale is 5 nm.
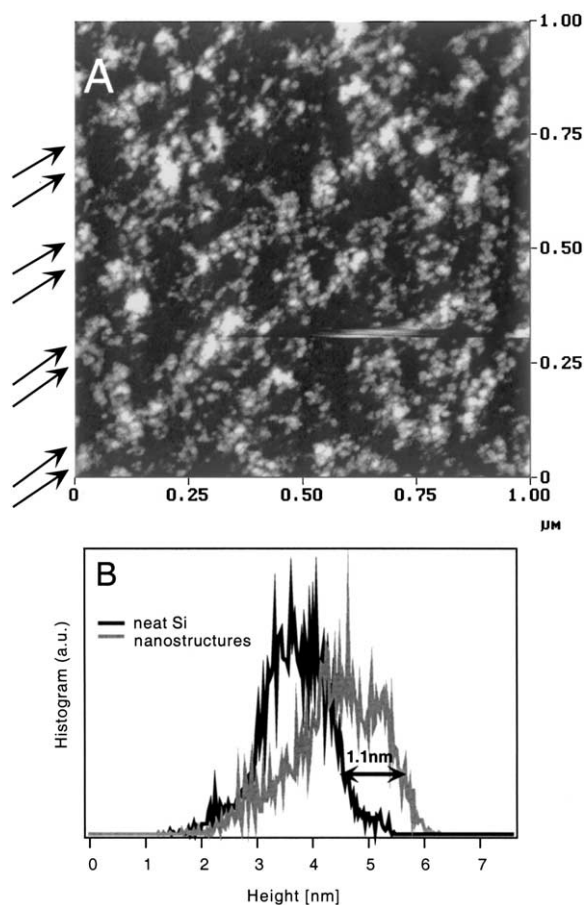
Fig. 8. (a) AFM image of IgG adsorbed on the preadsorbed protein A. The vertical scale is 5 nm. (b) Height histograms on neat Si and on nanostructures.

between the protein A on neat Si as on nanostructures, and no preferential adsorption is noted on nanostructures.

Similar Si nanostructures have been used to adsorb filamentous proteins, in order to measure a possible orientation specificity of adsorbed proteins in contact with nanostructures. The 5 s F-actin adsorption is shown in Fig. 9a. F-actin covers the neat Si and the nanostructures are still visible due to a low protein density. Fig. 9b is a magnification of the F-actin adsorbed on the nanostructures. The adsorbed filaments are forming a kind of neuronal network composed of large intersection areas, which are interconnected by different filament bundles. Even if F-actin adsorbs
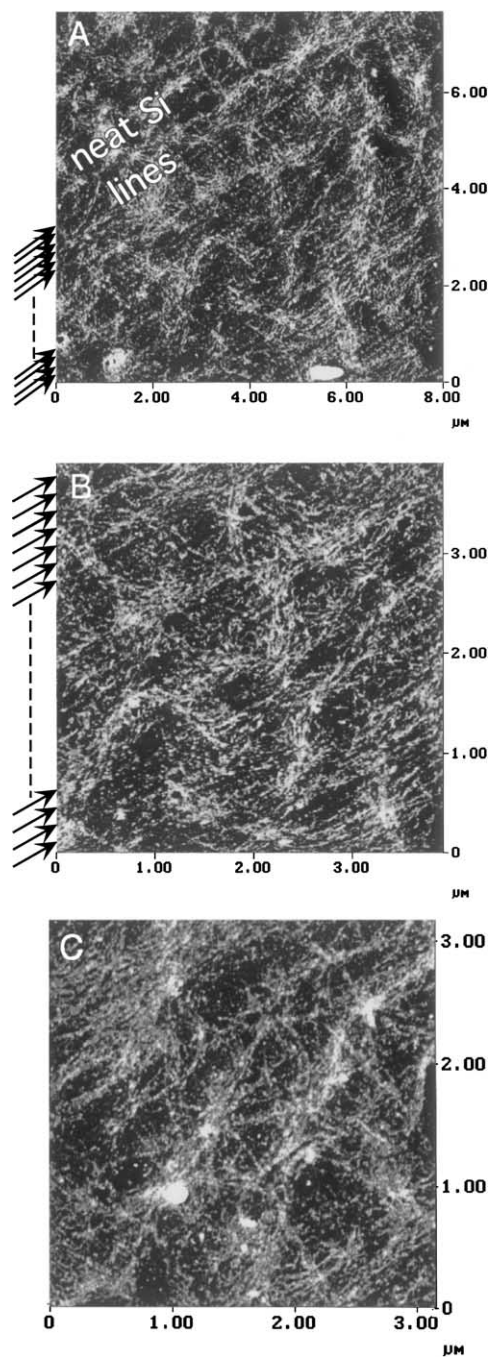

Fig. 9. Adsorption of F-actin on and outer Si nanostructures. The vertical scales are 10 nm. (a) General view of the adsorbed F-actin. (b) Enlargement of the nanostructure area. (c) Enlargement of the neat Si area.

in different directions, a preferential orientation along the nanostructures is visible. F-actin filaments are actually present in a cone of 18° towards the lines. For angles between 18 and 55°, no filaments are present. Therefore it seems that if a filament in solution approaches the nanostructures under an angle of less than 55°, the attraction between the filament and the nanostructures is high enough to twist it and it will consequently adsorb along the nanostructures. In contrast, filaments approaching the nanostructures with angles larger than 55° will simply feel the nanostructures as a general roughness of the sample. On neat Si the filaments are again forming a similar neuronal network, as can been seen in Fig. 9c. The intersection points are however smaller and single filaments spread over the neat Si in all directions without preferential orientation. The density of adsorbed filaments is higher on neat Si than on the nanostructures. Therefore in contrast to protein A, we find that in addition to a lower adsorption on the nanostructures, F-actin has a tendency to adsorb preferentially along the created nanostructures.

As shown previously [6], we observe similar F-actin adsorption on Ti, which depends furthermore on nanostructure height. Fig. 10a shows the created lines which present two distinct heights. The main lines have a height varying between 3 and 4 nm and have a FWHM of 40 nm. The secondary lines are 1–2 nm high with a similar FWHM. This height difference is due to a modification of the tip-sample distance during the scan. The large white spots visible on the figure were produced during the Ti evaporation, and were already present before the LAO treatment. Fig. 10b shows the same nanostructures covered by a 4 s F-actin adsorption. The main lines are still visible in contrast to the secondary lines, which are covered by a thick layer of F-actin. On neat Ti, the concentration of filaments is lower than on the secondary lines, but higher than on the main lines. Therefore the density of adsorbed proteins depends on the topography height. Furthermore F-actin adsorbs preferentially along the nanostructures being 1–2 nm high, in contrast to the 3–4 nm high nanostructures and to the neat Ti where no preferential orientation of adsorbed filaments is noted.
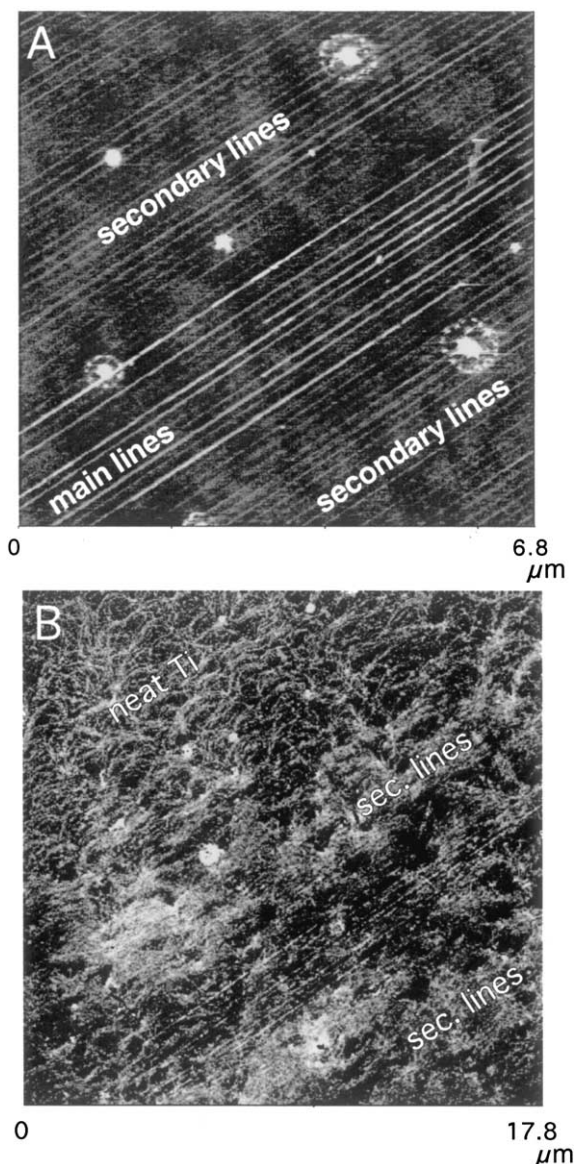
Fig. 10. (a) Nanostructures created on Ti. (b) F-actin adsorbed on nanostructured Ti. The vertical scales are 8 nm.

It appears that the nanotopography is an important parameter for the protein adsorption. On Ti as on Si an oriented adsorption of F-actin occurs on 1 nm high parallel lines. Such a topography increases the RMS-roughness up to 0.5 nm, therefore increasing the contact area between the surface and the proteins, favoring the protein adhesion along the lines. On Ti the 3–4 nm high

nanostructures nevertheless represent an upper cut off, where the adsorbed F-actin density is very low and no preferential orientation of adsorbed proteins is noted. This height, which corresponds to half of the F-actin diameter, seems too rough to favor protein adsorption. Similar height dependencies are observed for cells [1,2,5], where the relevant length scale, however, is of the order of the μm.

On Ti the highest density of adsorbed F-actin occurs on 1 nm high nanostructures, in contrast to Si where the F-actin adsorption is higher on neat Si surface. This difference could be explained by the different chemistries and therefore different biocompatibilities of Si and Ti towards proteins. For biocompatible surfaces as Ti, the contact area between the adsorbed proteins and the sample surface is maximized, in contrast to non-biocompatible surfaces, as for example Si, where the contact area between the adsorbed proteins and the sample surface is minimized. Furthermore the RMS-roughness of Ti is already greater for neat surfaces in comparison to Si, so that between the Ti nanostructures the surface is rougher than on Si.

In contrast to F-actin, the protein A shows no preferential adsorption on 1 nm high nanostructures. Due to their globular shape the contact area on nanostructured or neat Si remains constant, so that no adsorption difference can be noted. A pattern composed of circular lines of diameter similar to protein A could perhaps locally increase the density of adsorbed protein A.

be created. Therefore no difference in static surface charge can be considered between the lower and upper parts of the nanostructures. Furthermore the chemistry of the created nanostructures is similar to the native oxide. To date, LAO is the only technique which permits modification of the surface topography in a nanometer range without changing the surface chemistry. We demonstrated that this technique allows us to study the biological activity of adsorbed proteins on nanostructures. Protein A shows no adsorption difference on parallel 1 nm high nanostructures on Si. The non-specifically bounded IgG also shows no preferential adsorption on or outer the nanostructures covered with protein A. In contrast, the F-actin adsorbs preferentially along 1 nm high lines on Si. Furthermore the density of protein adsorbed on neat Si is higher than on nanostructures. On neat Ti nanostructures of different heights have been created. The F-actin adsorption is the highest on the 1–2 nm high lines with a defined orientation along the lines, in contrast to a low and non-oriented protein adsorption on the 3–4 nm high nanostructures. In order to approach the in vivo conditions, further experiments have to be performed under aqueous conditions and in solutions where different proteins are present.

In short we have demonstrated that protein can ''sense'' the nanotopography similarly to the cells at micrometer scales. The topography is therefore an important parameter, which has to be taken into account in the general biomaterial field because the structure of the surface at a nanometer scale can influence the response of biological materials.

4. Conclusion

The LAO combined with AFM measurements is a very promising technique, which can be applied to study the reaction of biological systems in contact with a defined topography at the nm scale. XPS measurements have shown that the native oxide thickness is 0.69 nm for neat Si and 2.03 nm on the highest Si nanostructures. Ti presents a native oxide layer thicker than 2–3 nm, and nanostructures of 1–4 nm height can

References

[1] P. Clark, P. Connolly, A.S.G. Curtis, J.A.T. Dow, C.D.W. Wilkinson, Topographica control of cell behaviour II. Multiple grooved substrata, Development 108 (1990) 635–644.

[2] P. Clark, P. Connolly, A.S.G. Curtis, J.A.T. Dow, C.D.W. Wilkinson, Cell guidance by ultrafine topography in vitro, J. Cell Sci. 99 (1991) 73–77.

[3] B. Wojciak, J. Crossan, A.S.G. Curtis, C. Wilkinson, J. Mater. Sci.: Mater. Med. 6 (1995) 266–271.

[4] B. Wojciak-Stothard, A. Curtis, W. Monaghan, K. MacDonald, C. Wilkinson, Guidance and activation of murine macrophages by nanometric scale topography, Exp. Cell Res. 223 (1996) 426–435.

[5] A. Curtis, C. Wilkinson, Topographical control of cells, Biomaterials 18 (1997) 1573–1583.

[6] C. Galli, M. Collaud Coen, R. Hauert, V.L. Katanaev, M.P. Wymann, P. Gröning, L. Schlapbach, Protein adsorption on topographically nanostructured titanium, Surf. Sci. 474 (2001) L180–L184.

[7] Brookhaven Database of Proteins.

[8] J.J. Langone, Protein A of *Staphylococcus aureus* and related immunoglobulin receptors produced by streptococci and pneumonococci, Adv. Immunol. 32 (1982) 157–252.

[9] A. Müller, E. Diemann, A. Banding, M. Richter, J. Frey, W. Engelhardt, Comment on the imaging of immunoglobulin G by scanning tunneling microscopy, J. Vac. Sci. Technol. B 11 (2) (1993) 337–338.

[10] T.D. Pollard, J.A. Rooper, Actin and actin-binding proteins, a critical evaluation of mechanisms and functions, Annu. Rev. Biochem. 55 (1986) 987–1035.

[11] J.M. Corbett, C.H. Wheeler, M.J. Dunn, Moelectrophoreses of cardiac tissue from human, dog, rat and mouse: towards the establishment of an integrated two-dimensional protein database, Electrophoresis 16 (1995) 1524–1529.

[12] J.K. Pardee, J.A. Spudich, Purification of muscle actin, Methods Enzymol. 85 (1982) 164–181.

[13] V.L. Katanaev, M.P. Wymann, Microquantification of cellular and in vitro F-actin by rhodamine phalloidin fluorescence enhancement, Anal. Biochem. 264 (1998) 185–190.

[14] D.F. Williams, Titanium as a metal for implantation: Part1: physical properties, J. Med. Eg. Technol. 1 (4) (1977) 195–198.

[15] H. Zitter, H.J. Plenk, The electrochemical behavior of metallic implant materials as an indicator of their biocompatibility, J. Biomed. Mater. Res. 21 (7) (1987) 881–896.

[16] A. Ikai, STM and AFM of bio/organic molecules and structures, Surf. Sci. Rep. 26 (1996) 261–332.

[17] A. Ishizaka, S. Iwata, Y. Kamigaki, Si–SiO_2 interface characterization by ESCA, Surf. Sci. 84 (1979) 355–374.

[18] V.I. Nefedov, N.P. Sergushin, I.M. Band, M.B. Trzhaskovskaya, Relative intensities in X-ray photoelectron spectra, J. Electron Spectrosc. Related Phenomena 2 (1973) 383–403.

[19] J.H. Scofield, Hatree/slater subshell photoionization cross-section at 1254 and 1487 eV, J.Electron Spectrosc. Related Phenomena 8 (1976) 129–137.

[20] B.S. Becker, J.A. Golovchenko, B.S. Swartzentruber, Atomic-scale surface modifications using a tunneling microscope, Nature 352 (1987) 419.

[21] J.A. Dagata, J. Schneir, H.H. Harary, C.J. Evans, Modification of hydrogen-passivated silicon by a scanning tunneling microscope operating in air, Appl. Phys. Lett. 56 (1990) 2001.

[22] R.S. Becker, J.A. Golovchenko, B.S. Swartzentruber, Atomic-scale surface modifications using a tunneling microscope, Nature 325 (1987) 419.

[23] R. Held, T. Heinzel, P. Studerus, K. Ensslin, Nanolithography by local anodic oxidation of metal films using an atomic force microscope, Physica E 2 (1998) 748–752.

[24] H. Sugimura, T. Uchida, N. Kitamura, H. Masuhara, Tip-induced anodization of titanium surfaces by scanning tunneling microscopy: A humidity effect on nanolithography, Appl. Phys. Lett. 63 (9) (1993) 1288–1290.

[25] C.R.K. Marrian, E.S. Snow, Proximal probe lithography and surface modification, Microelectronic Eng. 32 (1996) 173–189.

[26] F. Pérez-Murano, G. Abdal, N. Barniol, X. Aymerich, J. Servat, P. Gorostiza, F. Sanz, Nanometer-scale oxidation of Si (100) surfaces by tapping mode atomic force microscopy, J. Appl. Phys. 78 (11) (1995) 6797–6801.

[27] M. Wendel, B. Irmer, J. Cortes, R. Kaiser, H. Lorenz, J.P. Kotthaus, A. Lorke, Nanolithography with an atomic force microscope, Superlattices Microstructures 20 (3) (1996) 349–356.

[28] F. Bozso, P. Avouris, Thermal and photochemical oxidation of Si(111): doping effect and the reaction mechanism, Phys. Rev. B 44 (1991) 9129–9131.

[29] B. Kasemo, J. Lausmaa, Surface science aspects on inorganic biomaterials, CRC Crit. Rev. Biocompatibility 2 ∼ (4) (1986) 335–380.

[30] B. Gasser, Reintitan und Varianten seiner Oberflaeche in der Implantologie, Master's thesis, University of Fribourg, Switzerland, dissertation Nr. 1204, 1998.

[31] M.T. Sieger, D.A. Luh, T. Miller, T.-C. Chiang, Photoemission extended fine structure study of the SiO_2/Si(111) interface, Phys. Rev. Lett. 77 (13) (1996) 2758–2761.

[32] M. Morita, T. Ohmi, E. Hasegawa, M. Kawakami, M. Ohwada, Growth of native oxide on a silicon surface, J. Appl. Phys. 68 (3) (1990) 1272–1281.

[33] H. Watanabe, K. Fujita, M. Ichikawa, Atomic-step observation at buried SiO_2/Si(111) interfaces by scanning reflection electron microscopy, Surf. Sci. 385 (1997) L952–L957.

[34] M. Collaud Coen, C. Galli, M. Bielmann, R. Lehmann, P. Gröning, L. Schlapbach, Imaging adsorption of proteins on chemically and topographically modified sur-

faces by SPM, Langmuir (2001) submitted for publication.

[35] M. Collaud Coen, R. Lehmann, P. Gröning, M. Biel-mann, C. Galli, L. Schlapbach, Adsorption and bioactivity of protein A on silicon surfaces studied by AFM and XPS, J. Colloid Interface Sci. 233 (2001) 180–189.

Paper III

Interpretation of Quartz Crystal Microbalance measurements improved using the maximal oscillation amplitude and the transient decay time constant

C. Galli Marxer[a,1], M. Collaud Coen[a], H. Bissig[b], U.F. Greber[c] and
L. Schlapbach[a]

[a] *Solid State Physics Research Group, University of Fribourg, Pérolles, CH-1700 Fribourg (Switzerland)*
[b] *Soft Condensed Matter Physics Group, University of Fribourg, Pérolles, CH-1700 Fribourg (Switzerland)*
[c] *Institute of Zoology, University of Zürich, Winterthurerstrasse 190, CH-8057 Zürich (Switzerland)*

Abstract

The behavior of the oscillation amplitude A_0 and the decay time constant τ of quartz during adsorption of proteins and cells is studied with a home-made Quartz Crystal Microbalance (QCM). We are able to measure simultaneously the frequency shift f, the dissipation factor D, the maximal amplitude A_0 and the transient decay time constant τ each $300\,ms$ under liquid, gaseous or vacuum environments. This enables distinguished analyses between adsorption and modifications of liquid/mass properties. Furthermore the surface coverage and the stiffness of the adlayer can be estimated.

1 INTRODUCTION

The Quartz Crystal Microbalance (QCM) is an ultrasensitive technique, which allows us to follow in real time the adsorption kinetics of molecules, proteins and cells onto a surface [1]. Its sensor consists of a thin quartz crystal (generally AT-cut) sandwiched between two evaporated metal electrodes [2]. The application of an alternative voltage with a frequency similar to the quartz resonance frequency induces oscillation of the quartz. The first measurements have been performed by Jones et al. and Meiure et al. under vacuum for deposition of metals [3, 4]. In this case the Sauerbrey relation [5] predicts a linear relation between the adsorbed mass and the measured resonance frequency shift:

$$\Delta f = -\frac{2f_0^2}{\sqrt{\mu_q \rho_q}}\frac{\Delta m}{A} = -\frac{2f_0^2}{\nu_q \rho_q}\frac{\Delta m}{A} = \frac{1}{C}\cdot\Delta m$$

[1]Corresp. author: Carine.Galli@unifr.ch, Tel: ++41 26 300 90 76, Fax:++41 26 300 97 47

where Δf is the measured frequency shift, f_0 the resonance frequency, Δm the adsorbed mass and C the quartz sensitivity constant, which depends on intrinsic properties of the quartz crystal only ($\nu_q = 3340\,m/s$ the velocity of the acoustic shear waves perpendicular to the quartz surface, $\mu_q = 2.947E^{11}\,gcm^{-1}s^{-2}$ the shear modulus of quartz, $\rho_q = 2.648\,gcm^{-3}$ the quartz density and A the area of the electrodes). This equation assumes the following properties: a) the adsorbed mass is perfectly bounded to the electrode and does not slip on the surface; b) it is elastic, i.e. it does not undergo viscoelastic deformations; c) the mass is forming an uniform layer and d) the material acoustic impedance is identical with that of the quartz. Since Nomura [6] showed that the QCM can not only operate in vacuum and air but also under liquid, the interest for QCM greatly increased due to potential applications in electrochemistry, immunology, biotechnology and cell biology. Nevertheless, measure-

ments in liquid environment are much more complex than under vacuum and the Sauerbrey equation is no more valid. It has been shown that for large molecules, as for example proteins, the adsorbed mass calculated with the Sauerbrey equation is systematically overestimated [7], because water molecules trapped between the adsorbed proteins vibrate simultaneously
with the protein adlayer, bringing an added measured mass. Moreover changes in the mass and liquid properties (density, viscosity) also influence the measured resonance frequency.

Therefore it is essential to measure simultaneously all possible parameter(s) and not only the frequency. Various groups have developed methods to measure the dissipation factor $D = D(f, \tau)$ [8] or Q-factor $Q = 1/D$ [9] in addition to f. Nevertheless, this technique does not allow to determine if the frequency shift is due to an adsorbed mass or as a result of modifications of the liquid/mass properties since f is contained in D. It has been shown that the interpretation of QCM data is enhanced using steady state techniques by measuring the resistance in addition to the resonance frequency [10–13].

The aim of this paper is to present the additional information given by the maximal oscillation amplitude and the decay time constant in the case of a transient technique. It allows us to get information about pur energy losses, to separate the contributions of liquid and adsorbed mass in the measured frequency and to detect modifications in stiffness of the adlayer. The interpretation of data is therefore improved, especially concerning the adsorption of viscoelastic mass. Different systems in liquid have been chosen, such as water-ethanol mixtures, proteins and cells.

2 MATERIALS AND METHODS

2.1 Proteins

Two proteins different in size and shape have been used for this study. Protein A

(Staphylococcus Aureus, Fluka, Buchs, Switzerland) is a globular protein of $44.2 kDa$. Its average diameter is $3nm$ [14] and the isoelectric point is $pI = 5.1$ [15]. The concentration was $1.6\mu M$ and it was diluted in nanodeionized water kept in air, inducing a water pH ranged between $5 - 6$.

Fibronectin (Sigma, Buchs, Switzerland) is a large multidomain glycoprotein, which is almost $130nm$ long [16]. Studies of the hydrodynamic properties of fibronectin in solution suggested a flexible conformation [17]. The stock solution was $1.1mg/ml$ in $0.05M$ Tris buffered saline solution at a $pH = 7.5$ and we diluted it to a final concentration of $0.55mg/ml$.

2.2 Cells

TC7 african green monkey kidney epithelial cells were grown on plastic dishes in a humidified $5\%CO_2$ air atmosphere at 37^oC in DMEM (Gibco) with $20mM$ Hepes containing 10% FBS (Hyclone) and $2mM$ glutamine as described earlier [18]. Near confluent cells were detached from the substratum by short trypsinisation $(0.5mg/ml)$ at 37^oC and immediately resuspended in RPMI medium (Gibco) supplemented with 10% FBS, $2mM$ Glutamine, 1% nonessential amino acids, $100U/ml$ penicillin and $0.1mg/ml$ streptomycin. Cells were immediately transferred to the QCM.

THP1 acute monocytic leukemia cells were maintained in suspension as described in [19]. $31 \cdot 10^4$ cells/ml were collected by centrifugation and resuspended in Iscove's medium (Life Technologies) supplemented with 10% FBS, $2mM$ Glutamine, $100U/ml$ penicillin and $0.1mg/ml$ streptomycin and transferred to the QCM.

2.3 The Quartz Crystal Microbalance (QCM)

The Quartz Crystal Microbalance used for this study is a home-made microbalance, which

can measure simultaneously the series resonance frequency f, the dissipation factor D, the maximal oscillation amplitude A_0 of the quartz and the transient decay time constant τ. The experimental set-up shown in figure 1 is used for experiments in liquid environments, but it can also be employed in air or under vacuum.
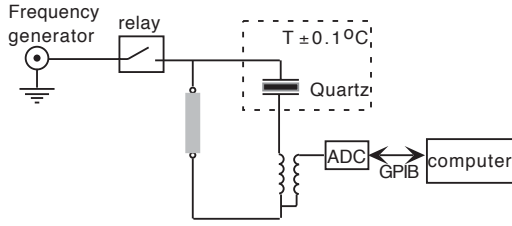

Figure 1: Experimental setup of our home-made QCM.

When the relay is closed, a frequency generator (Agilent 33120A) excites the quartz crystal at its resonance frequency, which is constantly adjusted during the experiment. The drive voltage supplied by the signal generator is kept constant. After almost 3 ms the relay is open and the quartz amplitude decays as an exponentially damped sinusoidal [8, 20]:

$$A(t) = A_0 e^{\frac{-t}{\tau}} sin(\omega t + \phi), \qquad t \geq 0$$

where τ is the transient decay time constant, and ϕ the phase. The decay curve is recorded with a sampling frequency f_s of a second frequency generator (Stanford DS345), so that due to aliasing the measured frequency f_m is

$$f_m = f_s \cdot frac\left(\frac{f}{f_s}\right)$$

f_m is lower than the oscillation frequency f of the quartz crystal. Nevertheless, the frequency shifts Δf and Δf_m are similar, allowing us to detect the true frequency shifts during adsorption. The amplitude is digitized and stored in the Analogic-Digital Converter (ADC), and the values are then transmitted to

the computer via the GPIB interface. While this measurement is fitted to obtain the different parameters, the relay is already closed for the next measurement. A programm developped in LabView (National Instruments) acquires, treats and shows the data over hours. The resolutions obtained for $3Hz$ measurement rate are $f \pm 2Hz$, $D \pm 0.5E-6$, $A_0 \pm 50$ (a.u.) and $\tau \pm 1.4E - 6sec$ for $10MHz$ quartz crystals operating into deionized water at $25 \pm 0.1^o C$. Under vacuum the resolution is much better with $f \pm 0.03Hz$, $D \pm 0.5E - 7$, $A_0 \pm 3$ (a.u.) and $\tau \pm 1.5E - 8sec$. Using the Sauerbrey relation it corresponds to changes in mass of $m \pm 9ng/cm^2$ in liquid and $m \pm 0.135ng/cm^2$ under vacuum.

The quartz crystal and the solutions are placed in a temperature control box at $T \pm 0.1^o C$. Therefore the temperature remains constant during the whole experiment and during the solution exchanges, preventing additional frequency shift due to changes in the density and the viscosity of the liquid and due to modification of the quartz sensitivity. The quartz is sandwiched between two plexiglas pieces sealed with VITON O-rings, where liquid exchanges are possible due to the presence of a tubing system. Only one side of the crystal is in contact with $90\mu l$ of liquid. This experimental setup ensures that no evaporation of liquid can occur during the measurements.

All experiments have been performed with quartz having smooth Au electrodes (Internal Crystal Manufacturing Co,Inc, OK, USA). The side of the crystal in contact with the liquid has a larger electrode area, so that no influence of the conductivity and dielectric constant of the liquid can disturb the measurements [21].

Before each protein experiment, the system has been equilibrated with deionized water at a temperature of $25 \pm 0.1^o C$. The cell experiment has been performed at $37 \pm 0.1^o C$ and the system has been preequilibrated with media lacking cells.

3   THEORY AND RESULTS

3.1   Equivalent circuit and physical properties

An AT-cut quartz crystal can be described by an electrical equivalent circuit, as shown in figure 2. It is composed of the series branch
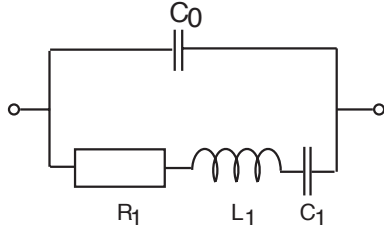

Figure 2: Equivalent circuit of a quartz. R_1, L_1 and C_1 represent the total resistance, inductance and capacitance. Under mass and liquid loading, these values are modified in comparison to vacuum.

or motional branch in parallel with a capacitance C_0, which is the static capacitance of the quartz resonator with the electrodes. The motional branch defines the electromechanical characteristics of the quartz resonator with the inertial component L_1, the compliance of the quartz C_1 and the energy dissipation during oscillation R_1. This model can also be converted to a mechanical one, where the mass is related to L_1, the energy stored during oscillation to C_1 and the energy losses to R_1 [22]. All these components are also related to the measured QCM parameters. Upon liquid loading the series resonance frequency is given by [23]

$$f = \frac{1}{2\pi\sqrt{L_1 C_1}}(1 + \frac{C_0 D^2}{2C_1})$$

where $D = R_1/\omega L_1$. Kanazawa [24] found the following relation for the frequency shift under liquid without adsorbed mass compared to vacuum:

$$\Delta f = -f_0^{3/2}\sqrt{\frac{\rho_l \eta_l}{\pi \mu_q \rho_q}}$$

where f_0 is the resonance frequency, ρ_l and η_l are the density and viscosity of the liquid, and ρ_q and μ_q are the density and the shear modulus of the quartz crystal, respectively. In the equivalent circuit, this correction to the Sauerbrey equation would be represented by the addition of a resistance R_l and an inductance L_l in the motional branch. This equation shows that the measured frequency is not only sensitive to mass changes (Sauerbrey), but also to changes in liquid properties. Similarly, changes in viscosity and density of adsorbed mass will also induce additional frequency shifts. Moreover it has been shown that the frequency sensitivity in terms of frequency change per mass density increases with increasing deposition for soft films [25].

The dissipation factor measures the dissipated energy over the stored energy and is given by

$$D = \frac{R_1}{2\pi f L_1} = \frac{2}{\omega \tau}$$

Changes of R_1, L_1 or C_1 will therefore induce changes of D, and it is therefore difficult to determine which real physical properties (adsorbed mass, energy stored, energy losses, density, viscosity) have induced the D variation.

The use of additional parameter(s) is therefore required in order to improve the interpretation of QCM data, especially for viscoelastic systems. In this view the maximal oscillation amplitude A_0 of the voltage across the quartz crystal, which is proportional to the mechanical vibration amplitude of the quartz crystal, can be easily used in the case of a transient technique. Indeed it has been shown that when the parallel capacitance is eliminated, what is our case, a change in the voltage is proportional to the change in the motional resistance [26–28]. It has been also directly derived that a modification of the vibration amplitude of the quartz crystal is proportional to the change of the motional resistance [29].

Experiments performed under vacuum have shown that the maximal oscillation amplitude of a vibrating quartz crystal is linear proportional to the quartz quality factor $Q = 1/D$ for a given applied voltage [30], confirming the theory developed for a bare quartz crystal [25]. The same behavior is observed for quartz in contact with different liquids, where no mass adsorption occurs. Figure 3 presents the maximal oscillation amplitude as a function of the dissipation factor for mixtures of water and ethanol at different relative concentrations. The maximal amplitude decreases

Figure 4: The maximal amplitude and the transient decay time constant are proportional to liquid properties, such as the density and the viscosity.
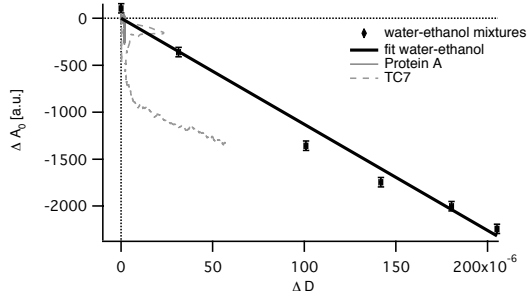

Figure 3: Maximal oscillation amplitude A_0 as a function of dissipation factor D for water-ethanol mixtures, protein A and TC7 cell adsorption.

linearly (water-ethanol curve) with an increase of the dissipation factor D. An increase of the liquid density ρ_l and viscosity η_l product results in an increase of dissipated energy and therefore a decrease of amplitude, which is proportional to $\sqrt{\rho_l \eta_l}$ (see figure 4). The measurement is in accordance to different models [31, 32] and similar results have been obtained using steady state techniques [33]. Nevertheless, the proportionality between A_0 and D is no more valid as soon as biological material is adsorbed. A_0 decreases continuously during protein A adsorption, in contrast to D, which presents a saturation value (figure 3). During the adsorption of cells, which are forming a viscoelastic system, A_0 as well as D decrease, increase and then continue to decrease. Therefore additional information about

viscoelastic properties of adlayer may be comprised in the measured maximal amplitude A_0. The theoretical value of A_0 is difficult to estimate and has not yet been exactly determined, since it contains all mechanisms of energy dissipation. For thin films in contact with the quartz, energy dissipation can arise from changes of the storage modulus (G') or shear modulus (μ), loss modulus (G'') or viscosity (η) and/or thickness of the adlayer [34]. For a constant loss tangent $\alpha = G''/G'$, the dissipated energy increases with increasing thickness of adlayer [35–37], except for some given thicknesses, where film resonance appears. For most adlayer thickness, the dissipated energy increases as α increases [37]. Moreover if the adsorbed mass slips on the surface or with increasing surface roughness, changes in the motional resistance can also occur.

Figure 5 shows the amplitude as a function of the frequency shift for different systems. The curve A represents the line obtained with the only modification of the liquid density and/or viscosity (water-ethanol mixtures), where the amplitude decrease is linearly proportional to the frequency decrease. With pure mass (rigid) adsorption and no energy losses, curve B would arise, where the frequency decreases but the ampli-
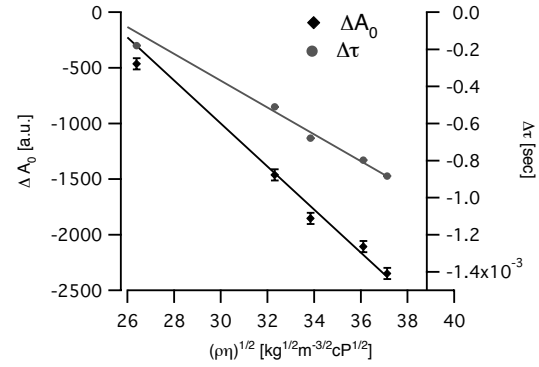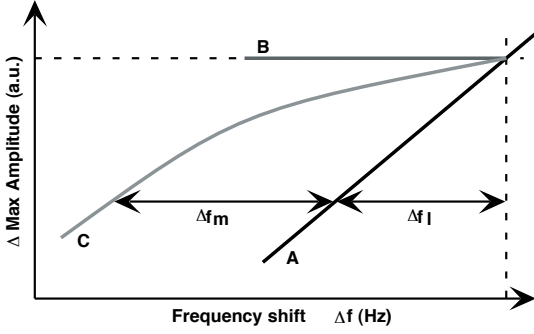
Figure 5: Measuring the amplitude allows us to distinguish the contribution in frequency shift of liquid loading Δf_l to adsorbed mass Δf_m. a: water-ethanol mixtures b: rigid adsorbed mass c: rigid adsorbed mass with changes in liquid properties.

tude   remains constant.

Finally the curve C corresponds to the adsorption of a rigid mass, where the solution viscosity and/or density are higher in comparison to the liquid present before the adsorption. The frequency decreases according to the Sauerbrey relation due to the adsorbed mass, but it also decreases due to changes in the liquid properties according to Kanazawa's relation [24]. By modification of the mechanical properties of the adsorbed mass during adsorption, an additional frequency shift would occur. If the curve A is known, it is possible to distinguish between the contribution of the mass adsorption Δf_m and the contribution of the modification of the liquid properties Δf_l.

The last parameter that we can measure is τ, which allows to calculate the dissipation factor. Figure 4 shows that under liquid loading, τ is linear proportional to the product of liquid density and viscosity, similarly to f, D and A_0. τ decreases with increasing liquid density-viscosity product. Moreover with adsorption of soft mass or if the adsorbed mass becomes softer, τ decreases according to

$$\tau = \frac{2L_1}{R_1}$$

τ represents therefore the mass over the energy losses.

In summary the different measured parameters and their dependencies to the physical properties of liquid and adlayer are listed on table 1. The storage modulus G' and the loss modulus G'' can be related to the shear elastic modulus μ and the viscosity η.

Under liquid and mass loading, Δf can be due to an increase of adsorbed mass and/or changes in the mechanical properties of the liquid and of the mass; ΔA_0 is proportional to energy losses due to changes of liquid and/or mass properties; $\Delta \tau$ represents the changes of decay time due to different stiffness of the adlayer and/or of the liquid; and finally ΔD occurs due to adsorbed mass and/or viscoelastic changes of the adlayer and/or liquid.

3.1.1 Protein and cell adsorption

The adsorption of proteins induces a decrease of frequency, as it can be seen in figure 6. The behavior is similar for cells af-
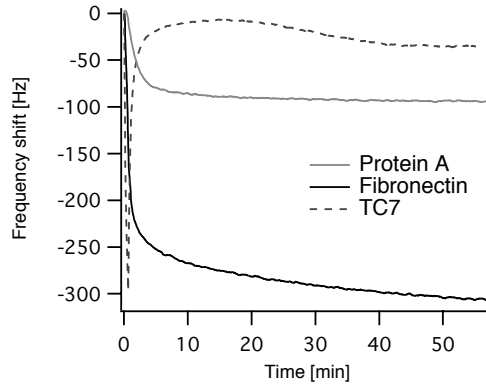

Figure 6: The frequency decreases during adsorption of proteins or cells.

ter $16min$ (see explanation further). It corresponds therefore to adsorption of mass. Nevertheless, modification of the adlayer viscoelastic properties can influence the measured frequency shift, so that we have to consider the other measured parameters.

Measured parameter	Equivalent circuit	Physical properties of liquid and adlayer
Δf	$= -\Delta(\frac{1}{\sqrt{L_1 C_1}})$	$m, \rho_{l,m}, \eta_{m,l}$
ΔA_0	$= -\Delta R_1$	$thickness_m, \rho_{m,l}, \eta_{m,l}, \mu_{m,l}$
$\Delta \tau$	$= \Delta(\frac{L_1}{R_1})$	$mass/E_{loss}$
ΔD	$= \Delta(\frac{R_1}{fL_1})$	$thickness_m, \rho_{m,l}, \eta_{m,l}, \mu_{m,l}$

Table 1: Relationship between the measured parameters and the components of the equivalent circuit, as well as their dependencies to the physical properties, where the indices m and l correspond to the adsorbed mass and to the liquid, respectively. m is the adsorbed mass, ρ the density, η the viscosity and μ the shear elastic modulus.

Figure 7 shows the amplitude A_0 as a function of the frequency shift Δf for water-ethanol mixtures, protein and cell systems. First of all
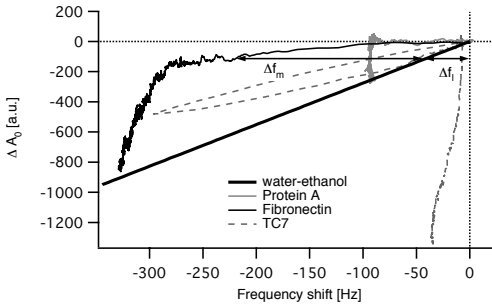

Figure 7: Amplitude vs frequency shift for water-ethanol mixtures, protein and cell adsorption.

it can be seen that the progressive exchange of water with ethanol induces a decrease of A_0 linearly proportional to the decrease in frequency, because both parameters are linearly proportional to the product of liquid density and viscosity (figure 4).

In contrast to water-ethanol exchanges, the adsorption of protein A shows different kinetics. The protein A has been diluted in water and rheological measurements have shown that no viscosity changes occur in comparison to pure water ($\eta = 1 \pm 0.01 mPa \cdot s$ at 25^oC), so that no amplitude or frequency decrease

can be attributed to changes in liquid properties. The curve remains above the water-ethanol one, and the adsorption can be globally fitted with 2 slopes. During the first $4min$ the amplitude remains constant and the frequency decreases. These first minutes of protein A adsorption correspond to a pure mass adsorption, where no energy losses occur (similarly to the curve B in figure 5). This phase corresponds to the formation of the first protein A layer [38]. Afterwards the amplitude begins to decrease and the frequency remains almost constant. The formation of the second monolayer occurs slower and energy losses arise. Similar behaviors have been observed during adsorption of different proteins [39–41] and cells [42–47]. This phenomenon can be principally due to the height increase of the protein adlayer and/or due to the increase of the constant loss tangent α. It has been shown that the first protein A monolayer is denaturated and presents a height of $1nm$, in contrast to the second monolayer, which is $3nm$ high [48]. Therefore the decrease in amplitude during the formation of the second monolayer can be due to the increase in height of the adlayer. Nevertheless, changes of α have also to occur, because the conformation of proteins is different in the first and second layer by presenting a less compact geometry in the

second layer. Moreover the presence of water molecules entrapped inside the protein layer influences the mechanical properties of the adlayer. By rinsing the surface with deionized water, the second layer is washed out [38] and the frequency increases and reaches the end point of the first slope. During this process the amplitude shows a further small decrease of $128 a.u.$, which corresponds to additional energy losses due to the rinsing of some proteins.

The adsorption of a viscoelastic protein has been measured with fibronectin (figure 7). Rheological measurements have demonstrated that fibronectin solutions are very viscoelastic by presenting dependencies of G' and G" with application of different shear stress (data not shown). We found that the large decrease in frequency happens simultaneously with a large decrease in amplitude. In contrast to protein A, the amplitude begins to decrease almost immediately after the introduction of the solution, showing that the changes of solution properties towards water contributes to the decrease of f and A_0. If the adsorbed fibronectin would induce no energy losses, the real frequency shift due to adsorbed mass would be Δf_m and Δf_l would correspond to the contribution of changes in liquid properties. However, the liquid density and viscosity are constantly modified due to protein adsorption, so that it is difficult to determine the precise influence of liquid properties, adlayer properties and mass adsorption on the frequency shift. But similarly to protein A, the amplitude vs frequency shift curve can be fitted by at least 2 different lines. After $22 min$, A_0 decreases drastically in comparison to Δf. We can estimate that at that stage the contribution of the liquid remains rather constant, because most of the protein adsorption has already occurred. The amplitude decrease corresponds to an increase of α and/or of the thickness of the protein adlayer.

Finally, we studied the adsorption of the TC7 cells (figure 7). Before the introduction

of the cell solution, the QCM has been stabilized with cell culture mediums, so that the electrode surface contains already adsorbed proteins and ions. With the TC7 introduction, the frequency drastically decreases during $40 sec$ ($\Delta f = -380 Hz$) and thereafter increases during $16 min$ to reach the initial frequency. A_0 shows similar behavior. The slopes of the decrease and increase of Δf and A_0 during the first $16 min$ are similar, meaning that a same process of adsorption-desorption occurs. Afterwards the frequency decreases less than $50 Hz$ in $40 min$, in contrast to A_0, which shows a strong decrease in time. We have measured that a solution of non-adsorbing THP1 cells induces no frequency shift and an insignificant decrease of amplitude. Therefore the frequency and amplitude changes are most likely due to adsorbing cells. At present, little is known about the precise temporal and molecular changes occurring at the interface between cells and the electrode surface during cell adsorption. We can assume that the shape of the cell gradually changes during adsorption, expanding laterally and reducing the total cell height. During this process, focal points of contact with the substratum are developed [49, 50]. This suggests that the non-slip condition is not valid, because the development of focal points may not be instantaneous. Formation of focal contact points also reshapes the cytoskeleton and this process changes the mechanical properties of the cytoplasm. It is likely that the mechanical properties of the cytoplasm affect the A_0 decrease.

All these processes participate to the measured energy losses and it can be helpful to consider A_0 and f vs the decay time constant τ (figure 8A and B), which represents the ratio of adsorbed mass over the energy losses. It can be seen that the behavior of proteins and cells differs considerably. For protein A and fibronectin, $\Delta \tau$, Δf and A_0 decrease constantly during the first $2 - 3 min$. Afterwards τ remains constant and the amplitude and frequency continue to decrease. In contrast, τ
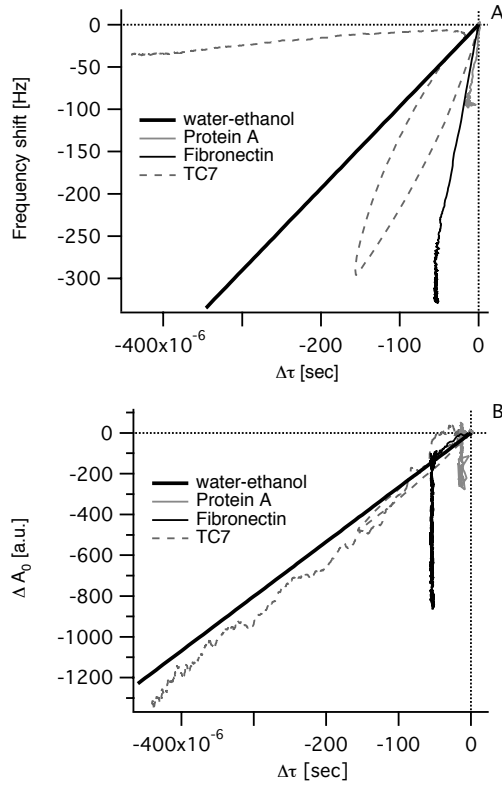
Figure 8: A: The frequency shift vs the decay time constant shift for liquid mixtures, proteins and cells. B: The amplitude vs the decay time constant shift for the same adsorptions. Cell behavior differs from protein adsorption.

is constantly modified during the cell adsorption. Similarly to f and A_0, it decreases during the first $40 sec$, increases thereafter during $16 min$ to reach the initial value and decreases afterwards. Interestingly all A_0 vs τ values move along a specific slope, which lies just under the water-ethanol line (figure 8B).

It seems to indicate that τ decreases as long as changes in density and/or viscosity of liquid/mass occur directly on the electrode surface. After its full coverage with the new adlayer mass (for proteins) or the new liquid (for mixtures), a second slope appears in the A vs τ curve. For protein A, τ decreases during the formation of the first monolayer and remains constant during the formation of the

second monolayer. In the second phase the amplitude decreases continuously, so that the kinetic energy due to the oscillation of the adsorbed mass (L_1) increases. During the formation of the second layer, the mechanical properties of the adlayer are therefore conserved. Fibronectin shows a different behavior during the first minutes of adsorption. A_0 vs τ follows the water-ethanol curve due to changes of the density and viscosity of the protein solution in comparison to water. Simultaneously, fibronectin adsorbs and covers the whole electrode surface. Similarly to protein A, the second adsorption phase occurs with a constant τ, so that the adsorbed mass increases and dissipates energy losses proportionally to Δm. The stiffness of the new adlayer is therefore conserved during adsorption. For cell adsorption τ, f and A_0 decrease during the first minutes, probably due to the solution exchange, where many cells enter in contact with the surface. Afterwards suspension equilibrates and all parameters increase to reach initial values. This phenomenon occurs more slowly than with proteins, because cells are larger and diffusion takes therefore longer. After $16 min$, cell adsorption leads to an increase of the surface coverage, so that τ and A_0 decrease again. Optical measurements have shown that the surface coverage with cells is not completed after $40 min$, where $\Delta f = -35 Hz$, $A_0 = -1330 a.u.$ and $\tau = -440 E-6 sec$. The slope of the A_0 vs τ curve follows the water-ethanol curve, so that the viscosity-density product of the cells in expansion has to increase and is the main effect. It has to be mentioned that the QCM is only sensitive to $180 nm$ over the surface when water is in contact with the electrode, because the generated waves decrease exponentially into the liquid and the penetration depth depends on the density and viscosity of the liquid [24]. Therefore an increase of adsorbed mass can be detected during the cell expansion, although the number of adsorbing cells remains constant. Similarly the total density

just over the electrode surface can be increased during cell adsorption. Nevertheless, the cell density is similar to water and the frequency shifts measured are smaller than for protein A adsorption, so that the density is not much larger than the water density. A_0 and τ are nevertheless much larger than for protein A and it follows the water-ethanol curve, so that an increase of the cell viscosity has to occur. This result is not so surprising, because it is known that the cytoskeleton is reshaped during cell adsorption, and the cell becomes stiffer. Moreover the increase in cell viscosity can influence the quartz sensitivity, which would explain the small decrease of frequency after $16 min$ of adsorption. Therefore adsorption of cells induces changes of density and viscosity at the electrode surface, which are not negligible, so that the frequency shift can be underestimated.

4   CONCLUSION

The QCM is a powerful method to follow the adsorption kinetics of different systems, from molecules to living cells. Nevertheless, different physical properties such as the liquid and mass viscosity can influence the measured frequency shift. Measuring additional parameters beside the frequency f is essential to distinguish between the contribution of the liquid and mass, as well as between mass adsorption and modification of viscoelastic properties. Here we present the information that is contained in the maximal oscillation and in the decay time constant in transient technique. The maximal oscillation A_0, which is proportional to the vibration amplitude of the quartz crystal, represents only changes of the motional resistance. Therefore, it is possible to detect other contributions as the adsorbed mass in frequency shift. The decay time constant τ represents the ratio of the kinetic energy of the adsorbed mass over its energy losses. It allows us to determine firstly, if the surface coverage is completed, and sec-

ondly, how the stiffness of the adlayer is changing with time. The interpretation of the QCM measurements is therefore enhanced by measuring f, A_0 and τ, but additional experiments and modeling will be necessary to quantify modification of each physical property.

BIBLIOGRAPHY

[1] A. Janshoff, H.-J. Galla, C. Steinem, Piezoelectric mass-sensing devices as biosensors - An alternative to optical biosensors?, Angew. Chem. Int. Ed. 39 (2000) 4004–4032.

[2] D. Salt, Handbook of quartz crystal devices, Van Nostrand Reinhold (UK) Co.Ltd, 1987.

[3] J. L. Jones, J. P. Meiure, A piezoelectric transducer for determination of metals at the micromolar level, Anal. Chem. 41 (1969) 484.

[4] J. P. Meiure, J. L. Jones, Electrogravimetric trace analysis on a piezoelectric detector, Talanta 16 (1969) 149–150.

[5] G. Sauerbrey, Verwendung von Schwingquartzen zur Wägung dünner Schichten und zur Mikrowägung, Z. Phys. 155 (1959) 206–222.

[6] T. Nomura, M. Iijima, Electrolytic determination of nanomolar concentrations of silver in solution with a piezoelectric quartz crystal, Anal. Chim. Acta 131 (1981) 97–102.

[7] W. Saenger, In Annual review of biophysics and biophysical chemistry, annual reviews Palo Alto, CA Edition, Engelman DM Cantor RC Pollard TD, 1987.

[8] M. Rodahl, B. Kasemo, A simple setup to simultaneously measure the resonance frequency and the absolute dissipation factor of a quartz crystal microbalance, Rev. Sci. Instrum. 67 (9) (1996) 3238–3241.

[9] T. Nakamoto, T. Kobayashi, Development of circuit for measuring both Q variation and resonant frequency shift of quartz crystal microbalance, IEEE Trans. Ultrason., Ferroelect., Freq. Contr. 41 (6) (1994) 806–811.

[10] S.-W. Lee, W. D. Hinsberg, Determination of the viscoelastic properties of polymer films using a compensated phase-locked oscillator circuit, Anal. Chem. 74 (2002) 125–131.

[11] K. A. Marx, T. Zhou, R. Sarma, Quartz crystal microbalance measurement of self-assembled micellar tubules of the amphiphilic Decyl Ester of D-Tyrosine and their enzymatic polymerization, Biotechnol. Prog. 15 (1999) 522–528.

[12] H. Muramatsu, A. Egawa, T. Ataka, Reliability of correlation between mass change an resonanat frequency change for a viscoelastic-film-coated quartz crystal, Journal of Electroanalytical Chemistry 388 (1995) 89–92.

[13] H. Muramatsu, K. Kimura, Quartz crystal detector for microrheological study and its application to phase transition phenomena of Langmuir-Blodgett films, Anal. Chem. 64 (1992) 2502–2507.

[14] Brookhaven Database of Proteins .

[15] J. J. Langone, Protein A of staphylococcus aureus and related immunoglobulin receptors produced by streptococci and pneumonococci, Adv. Immunology 32 (1982) 157–252.

[16] J. Engel, E. Odermatt, A. Engel, J. Madri, H. Furthmayr, H. Rohde, R. Timpl, Shapes, domain organizations and flexibility of laminin and fibronectin, two multifunctional proteins of the extracellular matrix, J. Mol. Biol 150 (1981) 97–120.

[17] S. Alexander, G. Colonna, H. Edelhoch, The structure and stability of human plasma cold-insoluble globulin, J. Biol. Chem 254 (5) (1979) 1501–1505.

[18] M. Suomalainen, M. Y. Nakano, S. Keller, K. Boucke, R. P. Stidwill, U. F. Greber, Microtubule-dependent plus- and minus end-directed motilities are competing processes for nuclear targeting of adenovirus, J. Cell Biol. 144 (1999) 657–672.

[19] C. Ebbinghaus, A. Al-Jaibaji, E. Operschall, A. Schöffel, I. Peter, U. F. Greber, S. Hemmi, Functional and selective targeting of adenovirus to high-affinity Fcγ receptor If-positive cells by using a bispecific hybrid adapter, Journal of Virology 75 (1) (2001) 480–489.

[20] R. J. Matthys, Crystal oscillator circuits, Wiley, New York (1983) 69–77.

[21] M. Rodahl, F. Höök, B. Kasemo, QCM operation in liquids: an explanation of measured variations in frequency and Q factor with liquid conductivity, Anal. Chem. 68 (1996) 2219–2227.

[22] D. A. Buttry, M. D. Ward, Measurement of interfacial processes at electrode surfaces with the electrochemical quartz crystal microbalance, Chem. Rev. 92 (1992) 1355–1379.

[23] M. Yang, M. Thompson, Multiple chemical information from the thickness shear mode acoustic wave sensor in the liquid phase, Anal. Chem. 65 (1993) 1158–1168.

[24] K. K. Kanazawa, J. G. Gordon, Frequency of a quartz microbalance in contact with liquid, Anal. Chem. 57 (1985) 1770–1771.

[25] K. K. Kanazawa, Mechanical behaviour of films on the quartz microbalance, Faraday Discuss 107 (1997) 77–90.

[26] A. Arnau, T. Sogorb, Y. Jiménez, Circuit for continuous motional series resonant frequency and motional resistance monitoring of quartz crystal resonators by parallel capacitance compensation, Rev. Sci. Instrum. 73 (7) (2002) 2724–2737.

[27] C. Chagnard, P. Gilbert, A. N. Watkins, T. Beeler, D. W. Paul, An electronic oscillator with automatic gain control: EQCM applications, Sens. Actuators B 32 (1996) 129–136.

[28] J. Auge, P. Hauptmann, J. Hartmann, S. Rösler, R. Lucklum, New design for QCM sensors in liquids, Sens. Actuators B 24.

[29] C. Zhang, G. Feng, Contributions of amplitude measurement in QCM sensors, IEEE Trans. Ultrason., Ferroelect., Freq. Contr. 43 (5) (1996) 942–947.

[30] B. Borovsky, B. L. Mason, J. Krim, Scanning tunneling microscope measurements of the amplitude of vibration of a quartz crystal oscillator, J. Appl. Phys. 88 (7) (2000) 4017–4021.

[31] S. J. Martin, V. E. Granstaff, G. L. Frye, Characterization of a Quartz Crystal Microbalance with simultaneous mass and liquid loading, Anal. Chem. 63 (1991) 2272–2281.

[32] H. Muramatsu, J. M. Dicks, E. Tamiya, I. Karube, Piezoelectric crystal biosensor modified with protein A for determination of immunoglobulin, Anal. Chem. 59 (1987) 2760–2763.

[33] S. J. Geelhood, C. W. Frank, K. Kanazawa, Transient quartz crystal microbalance behaviors compared, J. Electrochem. Society 149 (1) (2002) H33–H38.

[34] M. A. M. Noël, P. A. Topart, High-frequency impedance analysis of quartz crystal microbalances. 1. General considerations, Anal. Chem. 66 (1994) 484–491.

[35] H. L. Bandey, S. J. Martin, R. W. Cernosek, Modeling the responses of thickness-shear mode resonators under various loading conditions, Anal. Chem. 71 (1999) 2205–2214.

[36] M. V. Voinova, M. Rodahl, M. Jonson, B. Kasemo, Viscoelastic acoustic response of layered polymer films at fluid-solid interfaces: continuum mechanics approach, Physica Scripta 59 (1999) 391–396.

[37] T. W. Schneider, S. J. Martin, Influence of compressional wave generation on thickness-shear mode resonator response in a fluid, Anal. Chem. 67 (1995) 3324–3335.

[38] C. Galli Marxer, M. Collaud Coen, L. Schlapbach, Study of adsorption and viscoelastic properties of proteins with a quartz crystal microbalance by measuring the oscillation amplitude, J. Colloid Interface Sci., accepted 2002 .

[39] D. Shen, M. Huang, L.-M. Chow, M. Yang, Kinetic profile of the adsorption and conformational change of lysozyme on self-assembled monolayers as revealed by quartz crystal resonator, Sensors and Actuators B 77 (2001) 664–670.

[40] F. Höök, M. Rodahl, B. Kasemo, P. Brzenzinski, Structural changes in hemoglobin during adsorption to solid surfaces: Effects of pH, ionic strength and ligand binding, Proc. Natl. Acad. Sci. 95 (21) (1998) 12271–12276.

[41] F. Höök, M. Rodahl, P. Brzezinski, B. Kasemo, Energy dissipation kinetics for protein and antibody-antigen adsorption under shear oscillation on a quartz crystal microbalance, Langmuir 14 (1998) 729–734.

[42] K. A. Marx, T. Zhou, A. Montrone, H. Schulze, S. J. Braunhut, A quartz crystal microbalance cell biosensor: detection of microtubule alterations in living cells at nM nocodazole concentrations, Biosensors and Bioelectronics 16 (2001) 773–782.

[43] T. Zhou, K. A. Marx, M. Warren, H. Schulze, S. J. Braunhut, The quartz crystal microbalance as a continuous monitoring tool for the study of endothelial cell surface attachment and growth, Biotechnol. Prog. 16 (2000) 268–277.

[44] J. Wegener, J. Seebach, A. Janshoff, H.-J. Galla, Analysis of the composite response of shear wave resonators to the attachment of mammalian cells, Biophys. J. 78 (2000) 2821–2833.

[45] K. Otto, H. Elwing, M. Hermansson, Effect of ionic strength on initial interactions of escherichia coli with surfaces, studied on-line by a novel quartz crystal microbalance technique, Journal of Bacteriology 181 (17) (1999) 5210–5218.

[46] C. Fredriksson, S. Khilman, B. Kasemo, In vitro real-time characterization of cell attachment and spreading, J. Mater. Sci. Mater. Med. 9 (1998) 785–788.

[47] A. Janshoff, J. Wegener, M. Sieber, H.-J. Galla, Double-mode impedance analysis of epithelial cell monolayers cultured on shear wave resonators, Eur. Biophys. J. 25 (1996) 93–103.

[48] M. Collaud Coen, R. Lehmann, P. Gröning, M. Bielmann, C. Galli, L. Schlapbach, Adsorption and bioactivity of protein A on silicon surfaces studied by AFM and XPS, J. Colloid Interface Sci. 233 (2001) 180–189.

[49] R. K. Vadlamudi, L. Adam, D. Nguyen, M. Santos, R. Kumar, Differential regulation of components of the focal adhesion complex by heregulin: role of phosphatase SHP-2., J. Cell Physiol. 190 (2) (2002) 189–199.

[50] C. A. Gaudry, E. Verderio, R. A. Jones, C. Smith, M. Griffin, Tissue transglutaminase is an important player at the surface of human endothelial cells: evidence for its externalization and its colocalization with the beta(1) integrin, Exp. Cell Res. 252 (1) (1999) 104–113.

Paper IV

Study of adsorption and viscoelastic properties of proteins with a Quartz Crystal Microbalance by measuring the oscillation amplitude

C. Galli Marxer [1], M. Collaud Coen and L. Schlapbach

Solid State Physics Research Group, University of Fribourg, Pérolles, CH-1700 Fribourg (Switzerland)

Abstract

The adsorption kinetics of protein A, BSA, IgG and Fibronectin have been investigated using a home-made Quartz Crystal Microbalance. Information about the energy losses appearing in the system are measured with the maximal oscillation amplitude and the dissipation factor. Nevertheless, only the maximal oscillation amplitude allows us to distinguish the different contributions of liquid and mass in the total frequency shift. The adsorption of proteins has been performed on Ti and Au surfaces at different concentrations. The amount of irreversible adsorbed protein A and IgG increases with increasing bulk concentrations. On Au more proteins adsorb, but their biological activity is reduced in comparison to Ti. Protein A forms the first monolayer in a few seconds, which shows practically no energy losses, and following this a second monolayer is formed. The adsorption rate for the second monolayer is much smaller and energy losses are present. Fibronectin is forming a very viscoelastic system, whose mechanical properties are affected by immersion in different buffer solutions.

Keywords: protein A, BSA, IgG, Fibronectin, adsorption, QCM, amplitude, dissipation factor, viscoelasticity

1 INTRODUCTION

The interactions occurring between proteins from aqueous solutions and solid surfaces are basic phenomena, which are important in many different research areas such as implants, biosensors, cell cultures or pharmaceutical technologies [1]. Nevertheless, different properties of the adsorbed proteins are required for each application. Specific arrangement and conformation of adsorbed proteins on biochips are, for example, essential in order to ensure a good biofunctionality of the sensor surface and subsequently, the best precision of the medical diagnostic. Different implants will also require different adhesion qualities of adsorbed proteins. A poor protein adhesion is demanded for catheters and contact lenses, which is in contrast to bone implants, where strong adhesion is necessary in order to built a compact implant-bone interface.

The main phenomena leading to protein adsorption are electrostatic interactions, steric interactions, changes in the state of protein hydration and rearrangement in the protein structure [1]. It has been shown that the surface charge [2], the topography [3, 4] and the surface chemistry [2, 5] can influence protein adsorption. For most proteins reversible and irreversible adsorption can occur. Moreover, irreversible adsorption is sometimes linked with a protein denaturation. When a mixture of proteins is present in solution, the smaller one will adsorb faster and can then be replaced by proteins showing higher surface affinities

[1] Corresp. author: Carine.Galli@unifr.ch, Tel: ++41 26 300 90 76, Fax:++41 26 300 97 47

(Vroman effect).

Several experimental methods have been used to study protein adsorption. X-Ray Photoelectron Spectroscopy (XPS) [6–8] and Atomic Force Microscopy (AFM) [8, 9] allows us to get static information. In contrast Ellipsometry [10–14], Surface Plasmon Resonance (SPR) [15–17], Total Internal Reflection Fluorescence (TIRF) [18], Optical Wave Light Spectroscopy (OWLS) [19, 20] and Quartz Crystal Microscopy (QCM) [21–23] can follow the kinetics of the protein adsorption. A feature of the QCM is that it can obtain information not only on the amount of adsorption but also information on the viscoelastic properties of the adlayer by measuring the maximal amplitude (A_0) of quartz oscillation [24] and the dissipation factor (D). However, the measurement of D does not allow us to separate the contribution of the liquid properties from that of the adsorbed mass, because D contains the frequency shift f, which depends on the adsorbed mass and on the viscoelasticity of the liquid.

In this paper we analyse the adsorption of two different protein systems with a home-made QCM, which measures simultaneously the frequency shift f, the maximal oscillation amplitude A_0 and the dissipation factor D. First, a standard protein system in immunology (Protein A, BSA, IgG) is studied, and particularly the protein adsorption kinetics and the biological activity of adsorbed Protein A on Au and Ti. The second protein studied, Fibronectin, constitutes a very viscoelastic solution. Its adsorption as well as the effect of immersion in different buffers are studied.

2   MATERIALS AND METHODS

2.1   *Proteins and buffers*

Four different proteins have been used for this study: three standard proteins for immunology tests (protein A, BSA and IgG) and Fibronectin, which forms filaments and is found in connective tissue, on cell surfaces, in plasma

and other body fluids.

Proteins A (soluble extracellular from Staphylococcus Aureus, Fluka, Buchs, Switzerland) are globular proteins of $44.2kDa$. They have an average diameter of $3nm$ [25] and their isoelectrical point is $pI = 5.1$ [26]. The concentration ranged between $16 - 1600nM$. Bovine Serum Albumin (BSA)(Fluka, Buchs, Switzerland) was used as a side-blocking protein because it does not bind to protein A and IgG. The molecular weight is $66.43kDa$ and the isoelectrical point is $pI = 4.9$. The concentration of BSA was $300\mu M$ for all experiments. We diluted the BSA in nanodeionized water (nanofiltration), which was stocked under air conditions, so that due to CO_2 absorption, the water pH was between 5 and 6, near the pI of protein A and BSA. The IgG antibodies (Fluka, Buchs, Switzerland) have an Y shape measuring $13.7nm$ in width at their extreme and $10.4nm$ in height [27]. Their weight is $150kDa$ and they can bind specifically on protein A by their Fc domain. They were also diluted in nanodeionized water, at a concentration of $5\mu M$.

Fibronectin (Sigma, Buchs, Switzerland) is a large multidomain glycoprotein, which is almost $130nm$ long [28]. Studies of the hydrodynamic properties of fibronectin in solution suggest a flexible conformation [29]. The stock solution was $1.1mg/ml$ in $0.05M$ Tris buffered saline solution at $pH = 7.5$, and it was diluted in nanodeionized water.

Hepes-NaOH buffer was prepared at a concentration of $10mM$ with a $pH = 7.4$. The Citrate-phosphate solution had a $pH = 7.4$ and a concentration of $50mM$.

2.2   *The Quartz Crystal Microbalance (QCM)*

The Quartz Crystal Microbalance used for this study is a home-made microbalance, which can measure not only the series resonant frequency f and the dissipation factor D, but also the maximal oscillation amplitude A_0 of

the quartz each $300ms$ [24]. The maximal amplitude A_0 allows us to determine pure energy losses of the system, which are represented by the motional resistance in the equivalent circuit. It is then possible to distinguish frequency shifts due to an adsorbed mass and due to changes in the liquid properties. In contrast, the dissipation factor also contains this information, but is combined with the frequency.

$10MHz$ AT-cut quartz (Internal Crystal Manufacturing Co,Inc, OK, USA) were used, and all experiments were driven in the fundamental frequency. The quartz crystal and the solutions were placed in a temperature control box at $25^o \pm 0.1^oC$, so that the temperature (T) remained constant during the whole experiment and during the solution exchanges. Keeping the T of the whole system constant is extremely important, because changes of temperature can modify the liquid properties, and therefore influence the frequency, A_0 and D. The quartz is entrapped between two plexiglas pieces sealed with VITON O-rings. Only one side of the crystal is in contact with liquid. This experimental setup ensures that no evaporation of liquid is possible during the experiments. Moreover, the electrode in contact with the liquid completely covers the quartz in order to prevent any influence of the conductivity and dielectric constant of the liquid [30].

The resolution of our QCM is $f \pm 2Hz$, $D \pm 0.5E - 6$ and $A_0 \pm 50$ (a.u.) when operating in nanodeionized water at 25^oC. This corresponds to mass changes of $m \pm 9ng/cm^2$ according to the Sauerbrey equation:

$$\Delta m = -C \cdot \Delta f$$

where Δm is the adsorbed mass, Δf the measured frequency shift and C the quartz sensitivity, which is $C = 4.5ng/cm^2 Hz$ for our quartz. A decrease of the frequency shift therefore corresponds to an increase of adsorbed mass. Nevertheless, changes in liquid properties can also influence the frequency [31].

Before each measurement, stabilization of f, D and A_0 signals was achieved with nanodeionized water in contact with one side of the crystal. After protein adsorption, the quartz surface was rinsed with nanodeionized water in order to determine the total frequency shift induced by protein adsorption, without involving changes in the liquid density and viscosity.

3 RESULTS

3.1 Protein A-BSA-IgG

Protein A adsorption was performed on Au and Ti surfaces with different concentrations in order to study the protein A adsorption kinetics, as well as to measure the biological activity of adsorbed protein A. The surfaces were then blocked with BSA at a defined concentration, which was followed by the antibody adsorption. All proteins were diluted in nanodeionized water in order to minimize the presence of salt ions, which also adsorb on the surface and therefore bring confusion in the interpretation of kinetics of protein adsorption.

3.1.1 Adsorbed proteins as a function of protein A concentration

Figure 1A shows the measured frequency shift for different protein A concentrations comprised between $16 - 1600nM$. The adsorption times varied between 1 and 2 *hours* in order to obtain stabilization of the frequency, indicating that the system has reached an equilibrium; thereafter the surface was rinsed. On Au as on Ti, the amount of adsorbed protein A increases with increasing concentration, but this amount is always higher on Au. For very small concentrations such as $16nM$, no significant difference is present between both surfaces and the frequency shift Δf is equal to $-20Hz$. At higher concentrations the frequency shift on Au ranged between $-80Hz$ and $-110Hz$, which is almost twice as large
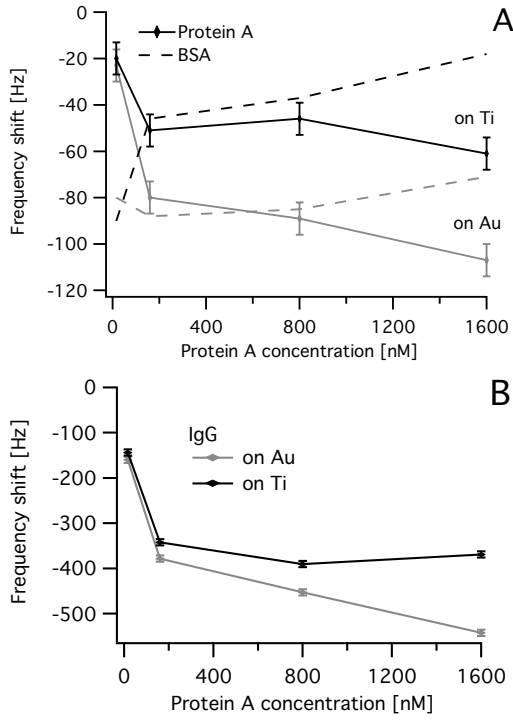
Figure 1: Frequency shift of adsorbed proteins on Au and Ti surfaces for different Protein A concentrations. a) Protein A and BSA. The error bars for the BSA are as large as for Protein A. b) IgG.

as on Ti, where Δf is about $-55Hz$. Therefore the adsorption affinity of protein A is larger on Au. This effect is especially visible for large protein concentrations.

As it is normally expected, the amount of adsorbed BSA is inversely proportional to that of the protein A (figure 1A). This phenomenon is the consequence of the side blocking effect of BSA adsorption. With increasing protein A concentration the surface coverage becomes greater preventing therefore the BSA adsorption. Nevertheless, more BSA adsorbs on Au than on Ti, similarly to protein A. At very low protein A concentrations, similar frequency shifts are measured on Au and Ti for BSA adsorption ($\Delta f = -80Hz$) and this value remains rather constant on Au. In contrast, the frequency shift on Ti diminishes with increasing protein A concentration, down

to half of the initial value ($\Delta f = -40Hz$). The adhesion of BSA is favored on Au, similarly to protein A. Therefore the density of adsorbed proteins is larger on Au than on Ti.

The adsorption of the IgG antibodies, which only specifically bind to adsorbed protein A, follows the same behavior as the protein A adsorption (figure 1B). With increasing protein A concentration the frequency shift of IgG decreases and is always larger on Au surfaces. Nevertheless, the differences of frequency shifts on Au and Ti are smaller for IgG than for protein A and BSA and shows a maximal difference of 32%. Similarly to protein A and BSA, no significant differences of frequency shifts appear at very low protein A concentrations. At concentrations higher than $160nM$, a saturation effect appears on Ti ($\Delta f = -350Hz$), which is not present for Au surfaces, where the frequency shift decreases and reaches $-550Hz$ for protein A concentrations of $1600nM$.

3.1.2   *Viscoelastic properties of adsorbed layers*

Viscoelastic properties of adlayers can be obtained by measuring the energy losses in the system during protein adsorption. The maximal oscillation amplitude A_0 can give such information more precisely than the dissipation factor D, which also contains the information of adsorbed mass due to the presence of the frequency shift [24].

The protein A solutions, as well as the IgG solutions have viscosities similar to water ($\mu = 1mPa \cdot s$ at 25^oC), so that the frequency changes cannot be attributed to changes in liquid properties. Therefore, the dissipation factor D and A_0 reflect only changes of the adlayer properties. Figure 2 shows that the dissipation factor versus the frequency shift for protein A adsorption can be globally fitted with 2 slopes. The dissipated energy generally increases with increasing adsorbed mass because

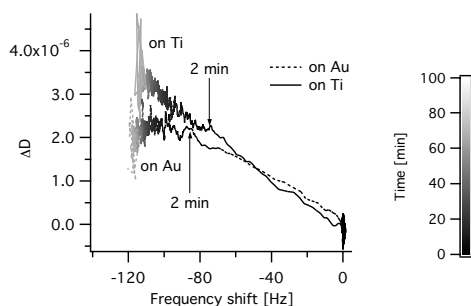firstly, proteins are soft materials and secondly,

Figure 2: ΔD vs Δf for protein A adsorbed on Au and Ti at a concentration of $1600 nM$.

Δf decreases. The timescale of adsorption is represented in figure 2 by the grey gradation scale. The frequency shift is larger on Au for a given time, so that protein A adsorbs more rapidly on Au. After $2min$ (arrow in figure 2) the adsorption rate becomes much slower. The slope is always smaller on Au than on Ti. It has been shown [8] that protein A adsorption occurs in 2 phases. The first one is very rapid and corresponds to the formation of the first monolayer of proteins, which is followed by the formation of the second layer. The first adsorption occurs within minutes, in contrary to the formation of the second layer, which takes several hours. Moreover, the thickness of the first protein layer is $1nm$ on Si, and the formation of the second protein layer increases the total thickness to $3.5nm$.

Therefore, each slope in figure 2 corresponds to the formation of each protein layer. Since more proteins are present on Au surfaces, the distance between each protein is smaller and less water molecules are trapped. On the Au surface the proteins are more squeezed than on the Ti surface and less energy is dissipated during the formation of the first and the second protein layers. A thicker adlayer dissipates more energy, and so does a layer with similar thickness but with a higher viscosity [32], or with higher viscosity-elasticity ratios [33]. Nevertheless, no additional dissipation

arises on Au during the formation of the second protein layer. In fact, a small decrease occurs, corresponding to rigidification of the adlayer. The difference in D between both surfaces corresponds therefore principally to the formation on Ti of a more viscous layer or a thicker layer with similar viscosity and elasticity.

By the rinsing of the surface, poorly bound proteins desorb and the frequency increases and reaches the value at the end of the first slope. The proteins of the second protein layer are therefore washed out, because their interactions with the electrode surface are weaker in comparison to proteins belonging to the first protein layer.

Figure 3 shows the behavior of the maximal oscillation amplitude ΔA_0 as a function of the frequency shift for the same measurement given in figure 2. During the first 2 min-
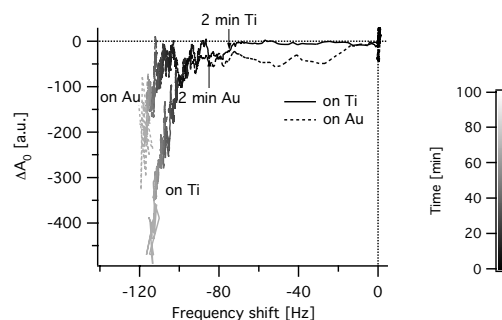

Figure 3: ΔA_0 vs Δf for protein A adsorbed on Au and Ti at a concentration of $1600 nM$.

utes of protein A adsorption, the frequency decreases with no significant changes of the maximal amplitude, corresponding to a mass adsorption with no energy losses. During the formation of the second protein layer the maximal amplitude decreases rapidly on both surfaces. Nevertheless, the pure energy losses remain smaller on Au, which reinforces the idea that the adsorbed protein A is more stressed, in accordance with the higher density measured. Figure 4 shows the maximal amplitude versus the frequency shift of kinetics of

protein A adsorption and rinsing on Au. The start of each curve is positioned at $(0; 0)$. During the rinsing of protein A, a small increase in frequency occurs with a small decrease of
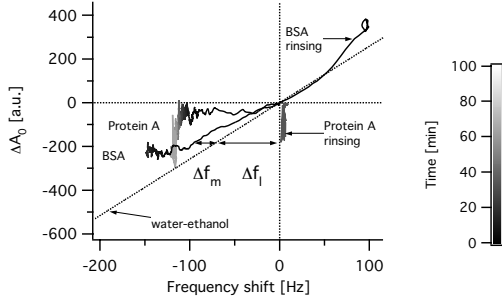

Figure 4: ΔA_0 vs Δf for adsorption and rinsing of Protein A [1600nM] and BSA [$300\mu M$] on Au. The water-ethanol curve illustrates the changes in maximal amplitude and frequency shift when liquid properties are modified with no mass adsorption. Δf_m represents the frequency shift due only to adsorbed mass, and Δf_l the contribution in frequency shift due only to changes in liquid properties.

maximal amplitude, due to desorption of the poorly adsorbed proteins, modifying the arrangement of the protein layer and inducing small changes in the viscosity-elasticity of the remaining protein layer. The adlayer is thereafter less dense.

The BSA adsorption follows the rinsing of protein A in order to block the surface for future antibody adsorption. The frequency and the maximal amplitude response of the BSA adsorption will depend on the state of the preadsorbed protein A layer and will therefore only be qualitatively described in this paper. BSA solutions show slight viscosity changes compared to water, so that a part of the frequency shift, dissipation factor and maximal amplitude is due to this change in the liquid properties. In figure 4 the water-ethanol curve corresponds to modifications of A_0 and f due only to the change of liquid density and viscosity without any mass adsorption [24]. During the first

$90sec$ of BSA adsorption, it can be seen that the maximal amplitude and the frequency decrease and that the curve follows the water-ethanol result. Therefore the real protein adsorption Δf_m occurs slowly, because the main contribution in Δf is due to changes in liquid properties Δf_l. After this the maximal amplitude remains constant, i.e., no further change in liquid properties occurs and the BSA adsorption induces a decrease of Δf_m with no modification of the dissipated energy. It is consistent with the fact that BSA does not bind to protein A, so that BSA are not forming a second protein layer, which would induce a maximal amplitude decrease as a result of a greater thickness of the adlayer. During the rinsing of BSA the maximal amplitude and the frequency increase due to the inverse changes of solution properties and also due to the decreasing viscosity-elasticity ratio of the blocked protein layer.

Antibodies of protein A have then been adsorbed on the blocked protein layer. Figure 5 shows a typical curve for IgG adsorption, where the axis scales are different than on figure 4. Similarly to protein A, IgG solu-
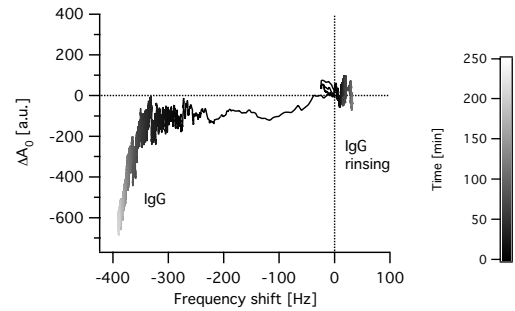

Figure 5: ΔA_0 vs Δf for IgG adsorbed on the preadsorbed Protein A and BSA on Ti. The concentration was $5\mu M$.

tion shows no viscosity changes against water, and the adsorption kinetics resemble the protein A result. Initially the frequency decreases with a slight maximal amplitude decrease, corresponding to the binding of IgG

with protein A. In the second phase the maximal amplitude shows a strong decrease with a small frequency decrease, so that great energy losses appear. IgG are 3 times larger than protein A and show an Y shape. Therefore, they can easily bring added losses to the system by trapping more water molecules than protein A, increasing the viscosity- elasticity ratio and the adlayer thickness. Moreover, only the F_c domain binds with protein A, so that the extremities of the IgG are free to move in the solution leading to additional energy dissipation. With the rinsing of IgG the maximal amplitude remains constant and only the frequency decreases. Desorption occurs and the system shows constant energy losses, i.e. constant mechanical properties.

3.1.3 Biological activity of adsorbed Protein A

In order to determine the biological activity of adsorbed protein A on Ti and on Au, we calculate the ratio of the frequency shifts of irreversibly adsorbed antibodies over irreversibly adsorbed protein A. Although more protein A and IgG adsorb on Au, the ratio shown in figure 6 is higher on Ti for all protein A concentrations. On Ti the biological activity of adsorbed protein A is therefore better conserved than on Au. A saturation effect occurs on Ti as well as on Au for protein A con-
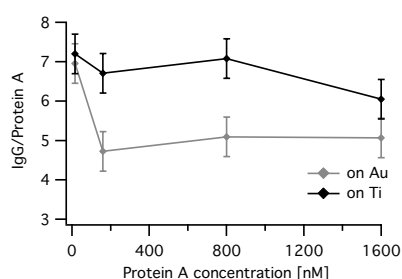

Figure 6: The biological activity is estimated for all protein concentrations with the ratio of frequency shifts of Protein A and IgG adsorption after rinsing.

centrations higher than $160nM$. The amount of adsorbed protein A and BSA is larger on Au than on Ti at these concentrations. Therefore, the density of adsorbed proteins is larger on Au, which may induce denaturation, which is readily observed. For the smallest concentration ($16nM$) the ratio is identical on Au and Ti. Therefore, the biological activity of adsorbed proteins can be influenced firstly by the density of the adsorbed proteins, and secondly by the strength of the interactions between the surface and the proteins. If the density of adsorbed proteins is too high or the interactions are too strong with the surface, the denaturation can be induced and this will decrease the biological activity of the adlayer. Moreover, the ratio of protein and antibody size can also influence the biological activity. IgG is 3 times larger than protein A; therefore, if the density of biologically active adsorbed protein A is too high it does not allow the binding of all proteins with antibodies.

3.2 Fibronectin

3.2.1 Fibronectin adsorption

Fibronectin is a filamentous protein, which forms a very viscoelastic system in solution (rheological data not shown). Therefore, it is essential to be able to distinguish if the frequency shift is due to an adsorption of mass or due to property changes of the solution and of the adlayer. When the properties of the solution change without any mass adsorption, the maximal amplitude decreases linearly with the frequency, similarly to the curve produced by exchanging water with ethanol (see figure 7) [24]. This measurement is in agreement with different models [34–37]. In the case of viscoelastic adsorption such as for fibronectin, the system becomes much more complex due to a greater number of parameters (density, elasticity and viscosity of the solution and of the fibronectin layer) changing during the protein adsorption and influencing Δf, ΔA_0 and ΔD. Figure
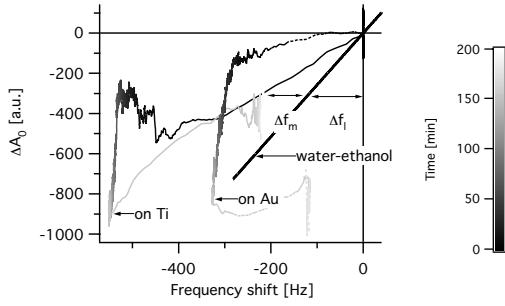
Figure 7: ΔA_0 vs Δf for adsorption of Fibronectin on Au and Ti at a concentration of $0.55 mg/ml$. The Fibronectin solutions are forming viscoelastic systems, so that Δf_m represents the frequency shift due to the adsorbed mass and Δf_l represents the contribution of the solution. The arrows indicate the point at which the surfaces were rinsed.

7 shows the maximal oscillation amplitude as a function of the frequency shift during the adsorption of fibronectin on Au and Ti at a concentration of $0.55 mg/ml$. It can be seen that the liquid contribution Δf_l is smaller on Au during the first 10 min of fibronectin adsorption. After 30 minutes the maximal amplitude decreases dramatically on Au as on Ti with a small decrease in frequency. The adsorbed fibronectin cannot be considered as being rigid [29], so that the adlayer can dissipate energy during and after the adsorption due to viscoelastic changes in the adlayer. Moreover, after 30 minutes the solution properties can be considered to be constant and can no longer dominate the frequency shift. Therefore, we can assume that the dramatic decrease of maximal amplitude corresponds to an increase of losses through the fibronectin layer with a small increase of adsorbed mass. The quantification of this added amount of mass is rather difficult to determine because it has been shown that the frequency sensitivity of the quartz increases with the deposition of softer films [38]. At the present time it is not yet known if rigidification of the adlayer occurs, and if then this

would induce the decrease of the quartz sensitivity. Nevertheless, it is certain that the height of the Fibronectin layer and/or the viscosity-elasticity ratio increase after $30 min$ of adsorption. Moreover, the fibronectin adsorption is much higher on Ti and it dissipates slightly more energy than on Au.

On Au as on Ti the adsorbed fibronectin has been rinsed with nanodeionized water at the point indicated by the arrows in figure 7. On each surface the maximal amplitude and the frequency increase with similar slopes as during the first minutes of protein adsorption. With the exchange of solution the contribution Δf_l of the liquid disappears, because the liquid properties are the same as before the protein adsorption. Simultaneously, some Fibronectin filaments are washed out because Δf_m increases during the rinsing. After the complete exchange of solution the maximal amplitude and frequency shift are smaller on Au than on Ti. Therefore, a smaller amount of Fibronectin remains on Au before and after rinsing at this protein concentration. On Au the adlayer also dissipates more energy than on Ti, so that the adlayer is thicker and/or presents a higher viscosity-elasticity ratio. At the present time it is impossible to separate the contributions of both phenomena.

3.2.2 Immersion in different buffers

After the washing of the surface with nanodeionized water, the fibronectin adlayer has been firstly immersed in a Hepes solution. Figure 8 shows that the maximal amplitude and frequency decrease on Au and on Ti. The maximal amplitude decrease is smaller on Au during the first minutes of immersion, and decreases thereafter more dramatically than on Ti. The measured negative frequency shift would correspond to an adsorption of mass, which is too large to be induced only by the adsorption of the ions present in solution. We can then conclude that the adlayer properties are modified by the introduction of Hepes buffer.
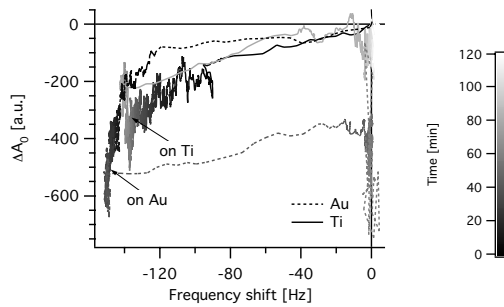
Figure 8: Immersion of the preadsorbed Fibronectin layer in Hepes solution. The arrows indicate the point at which the surfaces were rinsed.
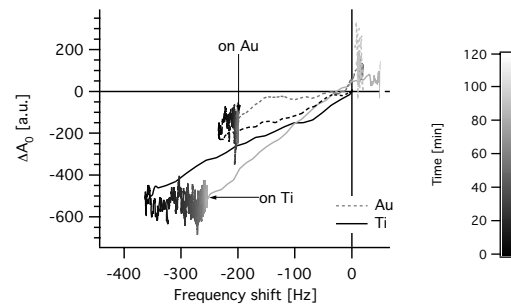

Figure 9: Immersion of the preadsorbed Fibronectin layer in Citrate-Phosphate solution. The arrows indicate the point at which the surfaces were rinsed.

During the dramatic decrease of maximal amplitude, the adlayer thickness and/or the viscosity-elasticity ratio increase due to the presence of ions in solutions, which modify the interactions inside the adlayer. By exchanging the Hepes solution with nanodeionized water (arrow on figure 8) the frequency shift and maximal amplitude increase and show similar slopes to that of the Hepes immersion. A reverse phenomenon then occurs, where ions are washed out and the adlayer recovers a new state. After the Hepes rinsing the total frequency shift is zero, so that no desorption occurred or the adlayer is stiffer and desorption occurred. The maximal amplitude is smaller than before the immersion in buffer, especially on Au, so that the thickness of the adlayer and/or the viscosity-elasticity ratio increased. In summary, two scenarios are possible: no desorption occurred with changes of the adlayer properties, or desorption occurred with a stiffening of the adlayer.

Fibronectin behaves differently in Citrate-phosphate solution, as shown in figure 9. The maximal amplitude and the frequency decrease continuously during the first minute. Similarly to immersion in Hepes, the first slope of ΔA_0 vs Δf is smaller for the Au surface. Adsorption of ions arises and the viscoelastic properties of the adlayer are mod-

ified. Nevertheless, after this the temporal dynamics differs, where the maximal amplitude remains stable and the frequency begins to increase. This phenomenon is more significant on Ti ($\Delta f = +106Hz$) than on Au ($\Delta f = +33Hz$), which corresponds to pure desorption because the maximal amplitude remains constant. By exchanging the buffer (arrow on figure 9) with nanodeionized water the total frequency shift and maximal amplitude become positive on Ti and Au. The frequency shift is always higher on Ti, in contrast to the maximal amplitude, which is larger on Au. In summary, desorption occurs on both surfaces with a decrease of the adlayer thickness and/or a decrease of the viscosity-elasticity ratio.

3.2.3 Adsorbed Fibronectin as a function of concentration

The adsorption of fibronectin after rinsing has been determined for different concentrations of fibronectin in solutions, as shown in figure 10. No clear correlation can be established between the Fibronectin concentration and the measured frequency shifts, because local maxima are present on Au and Ti at different concentrations. We repeated each experiment at least twice and always measured similar values. On Ti the frequency shifts in-
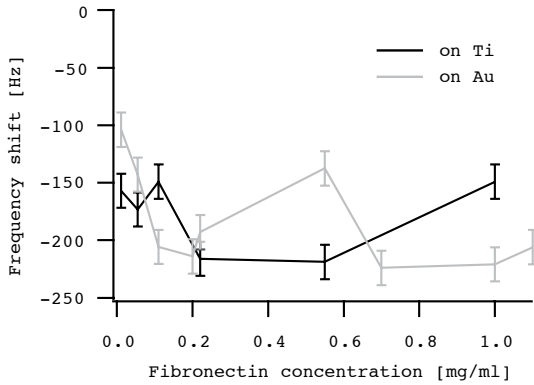
Figure 10: Frequency shift of adsorbed Fibronectin on Au and Ti surfaces vs protein concentration.

crease with increasing concentration and decrease thereafter at larger concentrations. On Au Δf increases with increasing concentrations but local minimum in the adsorption is present at $0.5 mg/ml$. Even if no difference in A_0 are observed between all concentrations, differences in viscoelastic properties of the adlayer can explain such phenomena.

4   DISCUSSION

It has been shown that the adsorption affinity of protein A is higher on Au surfaces because larger frequency shifts are measured on Au and less energy is dissipated. Furthermore, the adsorbed proteins are more squeezed and form stiff adlayers, dissipating less energy than for
those on Ti. Nevertheless, the biological activity of adsorbed protein A is smaller on Au. Therefore, the spatial arrangement of adsorbed proteins can be closely related to their biological activity. Small changes of protein conformation due to adsorption can be sufficient to destroy their biological activity. Adsorbed proteins,
which keep their native conformation have therefore rather small adsorption affinities. In turn, protein desorption occurs easily when rinsing

the surface. For biosensor applications, this leads to the difficulty of finding the correct balance between the attachment of proteins on the surface and their biofunctionality in order to perform reproducible medical diagnostics.

The measurement of energy losses allows us to compare the mechanical properties of the adsorbed protein layers on different surfaces. The maximal oscillation amplitude A_0 shows larger shifts for proteins having low adsorption affinity. Nevertheless, it remains difficult at the moment to quantify the contribution of the different phenomena, which lead to energy dissipation. An increase in adlayer thickness is the first parameter, as this can increase the energy losses due to an increase of mass-dissipating energy. Nevertheless, it has been shown that a dramatic decrease of maximal amplitude occurs in the second phase of protein   A   adsorption, where the adsorption rate is low, so that the thickness cannot be the only important parameter. An increase of the adlayer viscosity-elasticity ratio also increases the motional resistance of the QCM [33] and therefore decreases the maximal amplitude. Water molecules, which are trapped between the adsorbed proteins, vibrate with the adlayer and bring an added measured mass [39]. Depending on the arrangement of the adsorbed proteins, the presence of these entrapped water molecules can also influence the viscosity and elasticity of the total adlayer. Furthermore, trapped water dissipates energy also due to the generation of non-laminar motion of the liquid [40]. The measured frequency is also influenced by the mechanical properties of the liquid and of the adlayer. It is therefore essential to measure the energy losses in order to detect and evaluate possible artefacts in the frequency. Nevertheless, systematic studies will be required in order to separate the different sources of energy losses that contribute to the QCM signals. One example is the Fibronectin adsorption, which shows local maxima in the total frequency shift as a

function of protein concentration. The stock solution was in a buffer, but we diluted it in nanodeionized water in order to get the different concentrations. Therefore, ionic strength differences are present between the different concentrations, which can lead to different Fibronectin conformations in solution [29], and/or influence the interactions with the surface and modify the amount of entrapped water molecules, and/or the mechanical behavior as well as the height of the adsorbed layer. Under low salt conditions Fibronectin forms clusters, in contrast to high salt concentrations, where each molecule adsorbs independently [41]. No significant differences of maximal amplitude are present for Fibronectin adsorbed on Au and Ti at the different concentrations. Further microscopy studies will have to be performed in order to determine the thickness and the topography of the adlayer. The ionic strength of the different buffers induces conformation changes of the Fibronectin, so that the thickness and the mechanical properties of the adlayer are modified. After immersion in Hepes solution larger energy losses are present for adsorbed Fibronectin on Au. The total frequency shift is zero on Au and Ti, which does not necessarily imply that no desorption occurs, because viscoelastic properties of the adlayer can influence the frequency. In Citrate-Phosphate solution small desorption is observed for Fibronectin adsorbed on Ti. Similar behavior have been observed for other proteins [42] because phosphate is known to stabilize the native structure, so that desorption can occur. The explanation is always the same: ions from the buffer change the screening of the different amino acids of the proteins, so that the interactions are modified inside the proteins, between proteins, and between proteins and the surface.

5 CONCLUSION

In summary, we have shown that the higher adsorption affinity of proteins on Au surfaces in comparison to Ti diminishes the biological activity of the irreversible adsorbed protein A. This phenomenon is especially valid at high protein concentrations. Furthermore, the protein A adlayers dissipate less energy on Au. The estimation of the changes of the adlayer properties was improved with the measurement of the maximal amplitude. It allowed us to determine that immersion of a fibronectin adlayer in citrate-phosphate buffer induces desorption when adsorbed on Au and on Ti, and this effect is larger on Ti. In Hepes buffer, desorption occurs with stiffening of the adlayer or no desorption arises with an increase of the thickness or viscosity- elasticity ratio of the adlayer. Further studies are required to separate the different contributions of liquid and adlayer properties.

BIBLIOGRAPHY

[1] C. A. Haynes, W. Norde, Globular proteins at solid/liquid interfaces, Colloids Surfaces B: Biointerfaces 2 (1994) 517–566.

[2] S. Ravichandran, J. Talbot, Mobility of adsorbed proteins: a brownian dynamics study, Biophysical journal 78 (2000) 110–120.

[3] C. Galli, M. Collaud Coen, R. Hauert, V. L. Katanaev, M. P. Wymann, P. Gröning, L. Schlapbach, Protein adsorption on topographically nanostructured titanium, Surf. Sci. 474 (2001) L180–L184.

[4] C. Galli, M. Collaud Coen, R. Hauert, V. L. Katanaev, P. Gröning, L. Schlapbach, Creation of nanostructures to study the topographical dependency of protein adsorption, Colloids and Surfaces B: Biointerfaces 26 (2002) 255–267.

[5] Y. F. Dufrêne, T. G. Marchal, P. G. Rouxhet, Influence of substratum surface properties on the organization of adsorbed collagen films: in situ characterization by atomic force microscopy, Langmuir 15 (1999) 2871–2878.

[6] H. Fitzpatrick, P. F. Luckham, S. Eriksen, K. J. Hammond, Use of x-ray phtoelectron spectroscopy to study protein adsorption to mica surfaces, J. Colloid Interface Sci. 149 (1992) 1–9.

[7] E. Blomberg, P. M. Claesson, J. C. Froberg, Surfaces coated with protein layers: a surface force and ESCA study, Biomaterials 19 (1998) 371–386.

[8] M. Collaud Coen, R. Lehmann, P. Gröning, M. Bielmann, C. Galli, L. Schlapbach, Adsorption and bioactivity of protein A on silicon surfaces studied by AFM and XPS, J. Colloid Interface Sci. 233 (2001) 180–189.

[9] F. Caruso, D. N. Furlong, P. Kingshott, Characterization of ferritin adsorption onto gold, J. Colloid Interface Sci. 186 (1997) 129–140.

[10] B. Liedberg, B. Ivarsson, P. O. Hegg, I. Lundström, On the adsorption of β-lactoglobulin on hydrophilic gold surfaces: studies by reflection-absorption spectroscopy and ellipsometry, J. Colloid Interface Sci. 114 (1986) 386–396.

[11] T. Arnebrant, T. Nylander, Sequential and competitive adsorption of β-lactoglobulin and κ-casein on metal surfaces., J. Colloid Interface Sci. 111 (1986) 529–533.

[12] T. Nylander, N. M. Wahlgren, Competitive and sequential adsorption of beta-casein and beta-lactoglobulin on hydrophobic surfaces and the interfacial structure of beta-casein, J. Colloid Interface Sci. 162 (1994) 151–162.

[13] P. Tengvall, I. Lundstrom, B. Liedberg, Protein adsorption studies on model organic surfaces: an ellipsometric and infrared spectroscopic approach, Biomaterials 19 (1998) 407–422.

[14] M. Robers, I. J. Rensink, C. E. Hack, L. A. Aarden, C. P. Reutelingsperger, J. F. Glatz, W. T. Hermens, A new principle for rapid immonoassay of protein based on in situ precipitate-enhanced ellipsometry, Biophys. J. 76 (1999) 2769–2776.

[15] R. J. Green, J. Davies, M. C. Davies, C. J. Roberts, S. J. B. Tendler, Surface plasmon resonance for real time in situ analysis of protein adsorption to polymer surfaces, Biomaterials 18 (1997) 405–413.

[16] G. B. Sigal, C. Bamdad, A. Barberis, J. Strominger, G. M. Whitesides, A self-assembled monolayer for the binding and study of histidine-tagged proteins by surface plasmon resonance, Anal. Chem. 68 (1996) 490–497.

[17] E. E. M. G. Loomans, T. A. M. Beumer, K. C. S. Damen, M. A. Bakker, W. J. G. Schielen, Real-time monitoring of peptide-surface and peptide-antibody interaction by means of reflectometry and surface plasmon resonance, J. Colloid Interface Sci. 192 (1997) 238–249.

[18] Z. Xu, R. E. Marchant, Adsorption of plasma proteins on polyethylene oxide-modified lipid bilayers studied by total internal reflection fluorescence, Biomaterials 21 (2000) 1075–1083.

[19] C. Calonder, P. R. Van Tassel, Kinetic regimes of protein adsorption, Langmuir 17 (2001) 4392–4395.

[20] R. Kurrat, M. Textor, J. J. Ramsden, P. Böni, N. D. spencer, Instrumental improvements in optical waveguide light mode spectroscopy for the study of biomolecule adsorption, Rev. Sci. Instrum. 68 (5) (1997) 2172–2176.

[21] B. S. Murray, C. Deshaires, Monitoring protein fouling of metal surfaces via a quartz crystal microbalance, J. Colloid Interface Sci. 227 (2000) 32–41.

[22] J. Rickert, A. Brecht, W. Göpel, Quartz crystal microbalance for quantitative biosensing and characterizing protein multilayers, Biosensors and Bioelectronics 12 (7) (1997) 567–575.

[23] F. Höök, M. Rodahl, P. Brzezinski, B. Kasemo, Energy dissipation kinetics for protein and antibody-antigen adsorption under shear oscillation on a quartz crystal microbalance, Langmuir 14 (1998) 729–734.

[24] C. Galli Marxer, M. Collaud Coen, H. Bissig, U. F. Greber, L. Schlapbach, Interpretation of quartz crystal microbalance measurements improved using the maximal oscillation amplitude and the transient decay time constant, submitted to Analytical and Bioanalytical Journal .

[25] Brookhaven Database of Proteins .

[26] J. J. Langone, Protein A of staphylococcus aureus and related immunoglobulin receptors produced by streptococci and pneumonococci, Adv. Immunology 32 (1982) 157–252.

[27] A. Müller, E. Diemann, A. banding, M. Richter, J. Frey, W. Engelhardt, Comment on the imaging of immunoglobulin G by scanning tunneling microscopy, J. Vac. Sci. Technol.B 11 (2) (1993) 337–338.

[28] J. Engel, E. Odermatt, A. Engel, J. Madri, H. Furth-mayr, H. Rohde, R. Timpl, Shapes, domain organizations and flexibility of laminin and fibronectin, two multifunctional proteins of the extracellular matrix, J. Mol. Biol 150 (1981) 97–120.

[29] S. Alexander, G. Colonna, H. Edelhoch, The structure and stability of human plasma cold-insoluble globulin, J. Biol. Chem 254 (5) (1979) 1501–1505.

[30] M. Rodahl, F. Höök, B. Kasemo, QCM operation in liquids: an explanation of measured variations in frequency and Q factor with liquid conductivity, Anal. Chem. 68 (1996) 2219–2227.

[31] K. K. Kanazawa, J. G. Gordon, Frequency of a quartz microbalance in contact with liquid, Anal. Chem. 57 (1985) 1770–1771.

[32] M. V. Voinova, M. Rodahl, M. Jonson, B. Kasemo, Viscoelastic acoustic response of layered polymer films at fluid-solid interfaces: continuum mechanics approach, Physica Scripta 59 (1999) 391–396.

[33] M. A. M. Noël, P. A. Topart, High-frequency impedance analysis of quartz crystal microbalances. 1. General considerations, Anal. Chem. 66 (1994) 484–491.

[34] K. K. Kanazawa, QCM physical theory extended to include liquid immersion, Electrochemical society proceedings 23 (1999) 306–313.

[35] C. Zhang, G. Feng, Contributions of amplitude measurement in QCM sensors, IEEE Trans. Ultrason., Ferroelect. Freq. Control 43 (5) (1996) 942–947.

[36] H. L. Bandey, S. J. Martin, R. W. Cernosek, Modeling the responses of thickness-shear mode resonators under various loading conditions, Anal. Chem. 71 (1999) 2205–2214.

[37] M. Yang, M. Thompson, Multiple chemical information from the thickness shear mode acoustic wave sensor in the liquid phase, Anal. Chem. 65 (1993) 1158–1168.

[38] K. K. Kanazawa, Mechanical behaviour of films on the quartz microbalance, Faraday Discuss 107 (1997) 77–90.

[39] W. Saenger, In Annual review of biophysics and biophysical chemistry, annual reviews Palo Alto, CA Edition, Engelman DM Cantor RC Pollard TD, 1987.

[40] L. Daikhin, M. Urhakh, Effect of surface film structure on the quartz crystal microbalance response in liquids, Langmuir 12 (1996) 6354–6360.

[41] L. Guemouri, J. Ogier, Z. Zekhnini, J. J. Ramsden, The architecture of fibronectin at surfaces, J. Chem. Phys. 113 (18) (2000) 8183–8186.

[42] R. Kurrat, J. E. Prenosil, J. J. Ramsden, Kinetics of human and bovine serum albumin adsorption at silica-titania surfaces, J. of Colloid and interface science 185 (1997) 1–8.

Paper V

Cell viscosity increase during spreading induces positive frequency shifts in Quartz Crystal Microbalance measurements

C. Galli Marxer[a,1], M. Collaud Coen[a], T. Greber[b], U.F. Greber[c], and
L. Schlapbach[a,d]

[a] *Solid State Physics Research Group, University of Fribourg, Pérolles, CH-1700 Fribourg (Switzerland)*
[b] *Institute of Physics, University of Zürich, Winterthurerstrasse 190, CH-8057 Zürich (Switzerland)*
[c] *Institute of Zoology, University of Zürich, Winterthurerstrasse 190, CH-8057 Zürich (Switzerland)*
[d] *Swiss federal laboratories for materials testing and research, Ueberlandstr. 129, CH-8600 Dübendorf (Switzerland)*

Abstract

Cell attachment and spreading was investigated with a home-made Quartz Crystal Microbalance (QCM), which measures the frequency, the maximal oscillation amplitude and the transient decay time constant. In a first phase the mass adsorption induces mainly a decrease of the frequency. After about $80 min$ the frequency begins to increase continuously and after several hours passes the initial frequency of neat quartz measured before the cell adsorption. Nevertheless, phase contrast and fluorescence microscopy measurements demonstrate that at this moment the cells are still attached to the quartz surface, so that cell desorption cannot explain this phenomenon. The measurements of the maximal oscillation amplitude and the transient decay time constant, however, reveal changes in the viscoelastic properties of the spreaded cells. Such changes can be reproduced when the attached cells are treated with agents (Jasplakinolide, Cytochalasin D, Latrunculin B, Taxol and Nocodazole) affecting the actin and microtubule filaments. Our results indicate that viscosity variations of cell affect the frequency in the absence of cell desorption. The analysis of QCM experiments performed with cells therefore requires the measurement of the maximal oscillation amplitude and the transient decay time constant in addition to the frequency shift in order to detect variations in mechanical properties of the spreading cells.

Keywords: cell, drug, adsorption, QCM, amplitude, decay time constant, frequency

1 INTRODUCTION

Many functions of the cells are directly related to the control of their shape, such as cell growth, motility, apoptosis and differentiation [1–7], which are mainly governed by the cytoskeleton. It has been shown that structural and mechanical alterations of the cytoskeleton are important for controlling the cell deformability [8, 9]. Different methods have been used to determine the mechanical properties of the cytoskeleton after treatment with different agents. Light microscopy provides images of the dynamic shape of living cells, the structure and organization of the cytoskeleton over time [10]. Magnetic twisting cytometry [11–15] measures the rotation of magnetic particles in contact with the cell membrane in order to determine the cytoplasmic viscosity and consistency. Magnetic bead microrheometry gives similar information by measuring the position of the particles [16–18]. Nevertheless, invasive methods were necessary to measure contractile forces generated in the cytoplasm or exerted by the cytoplasm on the

[1]Corresp. author: Carine.Galli@unifr.ch, Tel: ++41 26 300 90 76, Fax:++41 26 300 97 47

cell surface by pulling adsorbed cells with a needle [19], by micropipette aspiration of cells [20–23] or with the cell poker [24, 25].

In contrast, the Quartz Crystal Microbalance (QCM) allows non-invasive measurements [26]. The frequency of an oscillating quartz is measured, which is linearly proportional to the adsorbed mass according to the Sauerbrey equation [27]. The QCM has been first developed to measure molecule adsorption under vacuum [28, 29]; nevertheless, this method can also be applied under liquid environment [30], where additional physical properties have to be considered, such as the liquid density and viscosity [31]. When the quartz is vibrating at its resonance frequency and is immersed in a fluid, an exponentially damped wave is coupled into the liquid to a penetration depth δ. Under water loading at 37^oC, our QCM is only sensitive to $\delta = 146.5nm$ above the electrode surface. It is therefore possible to follow in time phenomena occurring near the electrode surface during cell spreading, such as cell attachment and modification of the mechanical properties of adsorbing cells. Experiments have been performed with different cell types by measuring the frequency and the resistance using a steady state technique [32–35], or the dissipation factor D [36–38] using a transient technique. Unfortunately since D contains the frequency, it is impossible to distinguish the contribution of an adsorbed mass to that of a viscoelastic modification of spreaded cells, since both influence the measured frequency.

Our Quartz Crystal Microbalance corresponds to a transient technique, where the quartz excitation is stopped each $300ms$ and the oscillation amplitude decay is measured. This allows us to differentiate between the contribution of viscosity to mass changes by measuring the frequency f, the maximal oscillation amplitude A_0 and the transient decay time constant τ [39]. The characterization of predominant phenomena arising during cell attachment and spreading, such as rigidification of attached cells inducing positive frequency shifts, is therefore possible. Using different drugs, which disturb the polymerization state of some cytoskeleton proteins (actin and microtubules) and therefore modify the mechanical properties of spreaded cells, we could observe variations of the measured parameters.

2 MATERIALS AND METHODS

2.1 Cells

TC7 african green monkey kidney epithelial cells and HeLa cells (American Type Culture Collection) were grown on plastic dishes in a humidified $5\%CO_2$ air atmosphere at 37^oC in Dubelcco's Modified Eagle's Medium (DMEM) (Gibco) containing 10% Fetal Calf Serum (FCS) (Hyclone) and $2mM$ L-glutamine as described earlier [40].

A549 (lung carcinoma) cells were grown in similar conditions in DMEM (Gibco) containing 7% Clone III (Hyclone) and $2mM$ glutamine.

Near confluency cells were detached from the substrate by short trypsinisation ($0.5mg/ml$) at 37^oC and immediately resuspended in RPMI medium (Gibco) supplemented with $20mM$ Hepes and 10% FBS (TC7 and HeLa) or 7% Clone III (A549), $2mM$ Glutamine, 1% nonessential amino acids, $100U/ml$ penicillin and $0.1mg/ml$ streptomycin. Cells were immediately transferred to the QCM.

2.2 Drugs

Different drugs were used in order to disturb the polymerization state of actin filaments and microtubules of spreaded cells on the quartz crystal. The drugs have been conserved in DMSO and were diluted in the media lacking cell.

Jasplakinolide (jas)(a gift from Phil Crews, Santa Cruz, Calif.) induces actin polymerization by stimulating actin filament nu-

cleation and competes with phalloidin for actin binding [41–43]. It was used at a concentration of $500nM$.

Latrunculin B (LatB)(Calbiochem, Juro Supply), which was used at a concentration of $1\mu M$, forms $1:1$ complexes with actin monomers and inhibits therefore actin polymerization [44, 45]. Cytochalasin D (CD)(Calbiochem, Juro Supply) has a similar effect as LatB, it binds to the faster-growing end of actin [46] and disrupts the filaments [47]. The concentration was $2\mu M$.

In order to induce microtubules polymerization Taxol (Sigma) [48] was used at a concentration of $2\mu M$.

In contrast, Nocodazole (Noc)(Sigma) depolymerises the microtubules [49] and increases the time that microtubules spend in pause [50, 51]. The concentration was $20\mu m$.

2.3 The Quartz Crystal Microbalance (QCM)

The sensor of the QCM consists of a thin quartz plate with 2 Au-evaporated electrodes on each side. The application of an alternative voltage with a frequency near the quartz resonance frequency will induce the oscillation of the quartz at its resonance frequency. Under vacuum a change of resonance frequency Δf is proportional to the amount of adsorbed mass Δm according to the Sauerbrey relation [27]

$$\Delta m = -C \cdot \Delta f$$

where C represents the quartz sensitivity, which is $4.5ng/Hzcm^2$ for our $10MHz$ AT-cut Au crystals (Internal Crystal Manufacturing Co,Inc, OK, USA). Under liquid loading an additional frequency shift arises, which is proportional to the liquid density ρ_l and viscosity η_l [31]:

$$\Delta f = -f_0^{3/2}\sqrt{\frac{\rho_l \eta_l}{\pi \mu_q \rho_q}}$$

where f_0 is the unloaded resonance frequency, μ_q the shear modulus and ρ_q the density of the quartz crystal. Nevertheless, artefacts due to viscoelasticity of the adsorbed mass can occur, what concerns especially spreaded cells.

It is therefore essential to measure additional parameters. With our home-made QCM we are able to measure not only the frequency f, but also the maximal oscillation amplitude A_0 and the transient decay time constant τ. The maximal amplitude characterizes energy losses occurring in the system. It decreases with an increase of the viscosity-elasticity ratio of the adsorbed mass. The decay time constant τ, which corresponds to the ratio of mass over the energy losses, decreases with a more viscous adlayer. Finally a frequency decrease corresponds either to an increase of adsorbed mass in the case of a thin and rigid adlayer, and/or to a softening of the adlayer since it has been shown that the resolution in frequency increases for more viscous adlayers [52]. The setup has been completely described elsewhere as well as the correspondence between the measured parameters, the physical properties and the equivalent circuit model [39].

Experiments were performed at constant a temperature of $37 \pm 0.1^o C$. Each solution was tempered before introduced in the liquid cell in order to avoid changes in liquid density and viscosity. Moreover the surface with spreaded cells was rinsed with a mixture of $RPMI+x\%DMSO$, where x represents the drug dilution before injection. Therefore, no changes of the measured parameters can be attributed to viscosity modification of the new solution.

The quartz has smooth electrodes; the smaller one has a diameter of $5mm$ and the other, which is in contact with liquid, covers completeley the quartz in order to prevent any influence of the conductivity and dielectric constant of the liquid [53]. The quartz is entrapped between two plexiglas pieces sealed with VITON O-rings, where solution exchange are possible with a tubing system where no evaporation occurs. $80\mu l$ of liquid are directly in contact with the quartz electrode over an area having a diameter of $8mm$. Nevertheless, if

we consider that the sensitive area corresponds to the smaller electrode, the sensitive area becomes $19.6mm^2$ large and $3.12\% \cdot cell\ concentration$ of cells reach this region.

3   RESULTS AND DISCUSSION

3.1   Cell attachment and spreading

Different cell types have spread at different concentrations on the Au electrode of the QCM. Before the introduction of cell solution, the QCM was preequilibrated with media lacking cell, inducing protein adsorption. Figure 1 represents the frequency shift measured during cell attachment and spreading of different cell types. It can be seen that the TC7, HeLa and A549 cells induce similar behaviors of Δf. During the first $40sec$ after the
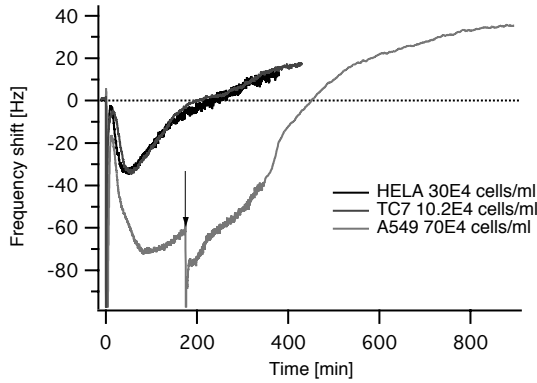
Figure 1: Adsorption of different cells at different concentrations. A decrease of frequency corresponds to a mass adsorption in accordance to the Sauerbrey's relation. After 180min the surface with spreaded A549 is rinsed (arrow). Nevertheless, the frequency continues to increase.

introduction of cell solution, the frequency decreases dramatically and reaches Δf ranged between $-190Hz$ and $-370Hz$ for the different cell types. Then f increases during $16min$ and frequency shifts of $\Delta f \approx -5Hz$ are measured before the subsequent frequency decrease. Similar frequency shifts are measured for HeLa and TC7 cells, although cell concentrations are different $(30\cdot$

$10^4cells/ml$ and $10.2 \cdot 10^4cells/ml$, respectively). A549 induce larger frequency shift for a larger cell concentration of $70 \cdot 10^4cells/ml$. The maximal frequency shift is reached after $80min$ for A549 and $50min$ for the HeLa and TC7 cells and are $\Delta f = -64Hz$ and $\Delta f = -33Hz$, respectively. Surprisingly, the frequency begins to increase continuously thereafter, and passes the initial frequency measured with no cells present at the surface of the quartz. After $6h15min$ the frequency shift $\Delta f = +13Hz$ is even positive for HeLa and TC7 cells. Rinsing of the surface with RPMI (arrow in figure 1) does not disturb this behavior and after $14h50min$ the frequency shift reaches $\Delta f = +43Hz$ for A549. Stopping the quartz excitation during several hours induces no change in the frequency behavior since the frequency shift continues to increase (data not shown). Therefore quartz oscillation does not perturb the cell spreading. Optical measurements performed directly on the QCM cell show a 80% full electrode coverage of living cells, as it can be seen in figure 2A. Staining of the spreaded HeLa and TC7 cells on quartz electrode shows the actin filaments (figure 2B, C), which are well developed. Therefore the increase of frequency does not correspond to a mass desorption, as the Sauerbrey equation would suggest, because living spreaded cells are present at the surface of the electrode when positive frequency shifts are measured. Kanazawa's equation demonstrates that without any mass adsorption, frequency shifts can occur by modifying the liquid properties, such as liquid viscosity and density [31]. In our case liquid properties remain constant during and after the introduction of the cell solution and we consider that they are not significantly affected due to biochemical reactions of the living cells. Therefore variations of the measured frequency are mainly due to spreading cells.

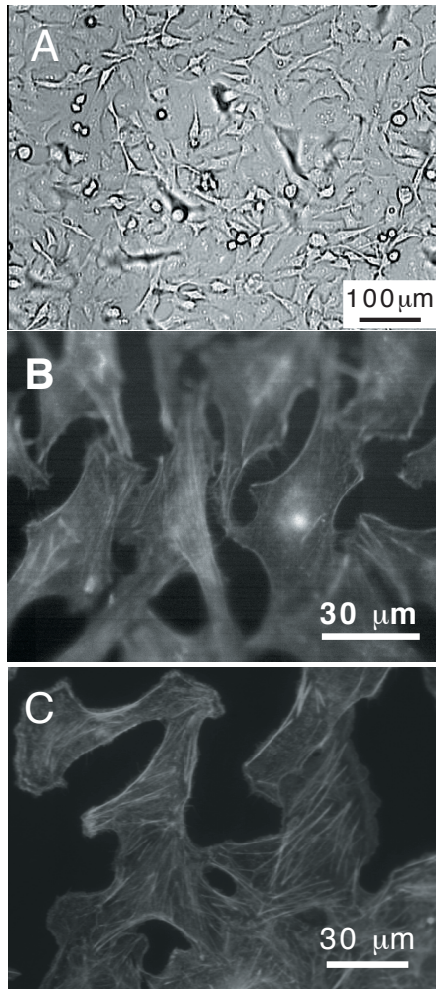A similar behavior was observed with neu-

Figure 2: Microscopy measurements of the quartz surface after cell spreading when the frequency shift is positive. For each cell type the surface is covered with living cells. Frequency increase does therefore not correspond to cell desorption. A: phase contrast measurement directly above the QCM liquid cell, where the surface is full of spreaded A549. B: actin staining of spreaded HeLa. C: actin staining of spreaded TC7.

trophils deposited on HSA-coated linebreak polystyrene [37]. The authors tentatively attributed the increase in frequency to protein detachment. Nevertheless, it is not shown how the frequency would continue to increase, and which positive value it would reach. In other studies [32, 54] it is also shown that a fre-

quency increase can appear, nevertheless positive frequency shifts were never reached and no explanation were given. But concerning our experiments, the increase in frequency cannot be only attributed to protein detachment, and an other explanation has to be found.
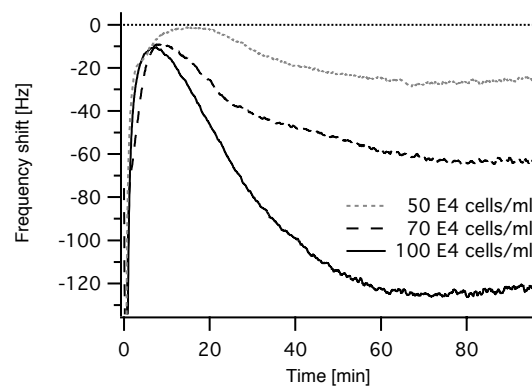
Figure 3: Adsorption of A549 cells at different concentrations. Larger frequency shifts are measured at larger solution concentrations.

During cell attachment and spreading focal points are developed, where actin is mostly present [55]. Actin filaments and microtubules represent two of the main proteins, which participate in the building of the cytoskeleton and determine cell shape and mechanical properties. The attachment and spreading of cells occurs in successive phases, where the first attachment of the cell to the solid surface is followed by the extension of lamellae with development of the focal points [56]. Adsorption of A549 from solutions with different concentrations shows different negative frequency shifts during the first $80min$, as it can be seen in figure 3. The first frequency decrease, which occurs during $40sec$ after the introduction of the cell solution, corresponds to an increase of the surface pressure due to cells entering in contact with the electrode during the solution exchange (see explanation of fig.4, [39]). Thereafter equilibrium in the solution arises and cells leave the electrode sur-

face, inducing an increase of the frequency, which reaches about the initial value. After $10 - 16min$ the frequency decreases due to the spreading of the attached cells and attachment of new cells. This phase will be defined as the "first adsorption phase". With higher cell concentration larger frequency shifts are measured (figure 3). Therefore during the first adsorption phase, Δf is proportional to the amount of adsorbed mass as soon as confluency is not reached, what was also measured with different cell lines [32, 54]

During the "second adsorption phase" the frequency begins to increase and Δf remains higher for smaller cell concentrations. In order to determine what phenomena becomes predominant during this second phase, other measured parameters have to be considered, such as maximal amplitude ΔA_0 and decay time constant τ, which concern energy losses and stiffness of the adsorbed mass [39], respectively. Since the sensitive thickness of our QCM is $146.5nm$ above the electrode surface under water loading at 37^oC, only changes appearing at the cell surface above the electrode can be detected. Moreover, the ventral part of the cell does not entirely enter in contact with the surface. When fibroblasts grow on a culture dish, most of their cell surface is separated from the substratum by a distance of more than $50nm$ [55]. At focal contacts this gap is reduced to about $10nm$. Therefore, only a small part of the adsorbed cells can be detected. Moreover, the cell density approaches the water density, what can explain the small frequency shifts measured during the first adsorption phase. In this study the liquid interlayer present under the cell will not be distinguished from the cell. We are aware that such a simplification does not correspond to the reality. Nevertheless it allows us to describe quite well modifications arising in the cell under agent treatments.

Figure 4 shows the maximal amplitude versus the decay time constant for the different cell adsorptions shown in figure 1. The water-
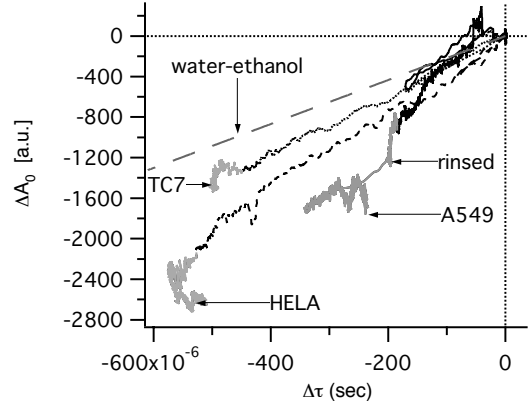

Figure 4: Maximal amplitude versus decay time constant during cell attachment and spreading of TC7, HeLa and A549 cells and solution exchange of water with ethanol. The water-ethanol curve corresponds to A_0 and τ changes as a result of only modifications of the liquid viscosity and sensity, without any mass adsorption. The second adsorption phase (Δf increases) of each cell adsorption is represented with a brighter colour.

ethanol line represents changes in ΔA_0 and τ only due to solution change with no mass adsorption. Both parameters are inversely proportional to the product of the liquid viscosity and density [39]. Since all different curves lie under the water-ethanol line, mass adsorbs on the electrode surface with dissipation of energy. Energy losses arise firstly due to the slip of cells over the surface since the formation of the focal contacts may not be instantaneous; secondly cell cytoplasm does not act as a standard solution in contact with the electrode surface because it is confined inside the cell membrane. With the introduction of the cell solution as well as during the first adsorption phase, A_0 is a linear function of τ and all slopes follow nearly the water-ethanol one. Moreover, the slope remains constant for a given cell type at different cell concentrations (data not shown). ΔA_0 decreases during the first $40sec$ and increases thereafter during about $16min$ with $\Delta\tau$. Therefore inverse phenom-

ena of adsorption and desorption have to occur. After this, ΔA_0 and $\Delta \tau$ decrease linearly for all cell types with the same slope as during the first $40sec$. Nevertheless, slopes are different for each cell type, the largest is found for A549 and the smallest for TC7. Since A_0 decreases with an increase of energy losses, and τ decreases with a decrease of the ratio of adsorbed mass over energy losses, A549 dissipate less energy per adsorbed mass than HeLa, which dissipate less energy than TC7. Differences in stiffness of spreaded cells can therefore be determined for different cell types.

In figure 1 it has been shown that frequency kinetics are similar for HeLa and TC7 cells in the first and second adsorption phase, but that the concentration of TC7 is smaller and, in accordance to what has been shown in figure 3, the frequency shift should be smaller with less cells. TC7 are softer because ΔA_0 versus $\Delta \tau$ slope is smaller than that of HeLa. Moreover, it has been shown that the quartz sensitivity in frequency decreases for stiffer adsorbed mass [52]. Therefore, since HeLa are stiffer than TC7 cells, the amount of spreaded HeLa is greater than that of TC7 for a given Δf. Then, similar frequency shifts are measured for both cell types because of different cell concentrations.

During the second adsorption phase (brighter color in figure 4) the behavior of the ΔA_0 versus $\Delta \tau$ curves is no more linear. When the surface is not rinsed τ reaches a minimal value and increases thereafter at a constant maximal amplitude, as it is shown for the experiment with HeLa and TC7 cells. This phenomenon is particularly visible when the surface covered with spreaded cells is rinsed. In the case of A549 cells, the rinsing of the surface provokes in a first time jumps of $\Delta \tau = -120 \cdot 10^{-6} sec$ and $\Delta A = -500 a.u.$, which correspond to the washing of some cells. Then ΔA_0 remains constant and τ increases, characterizing a stiffening of the spreaded cells. Therefore, an increase of the cell stiffness seems to become predominant during the second ad-

sorption phase, what induces a decrease of the quartz sensitivity in frequency and therefore, the measurement of a frequency increase.

In summary the attachment and spreading of cells influence mostly the decrease of frequency in the first adsorption phase, where the amplitude decreases linearly as a function of the decay time constant. During the second adsorption phase the frequency increases mainly due to stiffening of spreaded cells.

3.2 Cell cytoskeleton disturbed with drugs

In order to confirm our hypothesis, in which stiffening of spreaded cells influence mostly the frequency increase during the second adsorption phase, the cytoskeleton of spreaded A549 cells was disturbed with different drugs, and induced changes of f, A_0 and τ were stored.

The cytoskeleton is principally composed of actin filaments, microtubules and intermediate filaments. Depending on the polymerization state of each protein, cells will present different mechanical properties. Specific drugs have been chosen to disturb actin or microtubules and the effects were observed during the following $30min$.

Figure 5 presents the different steps of a complete experiment performed with drugs. After adsorption of A549 cells and during the frequency increase linked to the second adsorption phase, the surface is rinsed with the media lacking cell, which contained a similar concentration of DMSO as the future drug solution. The frequency decreases due to modification of the solution density and viscosity. Thereafter the drug solution is introduced and subsequent shifts in f, A_0 or τ are only induced by modification of the cell state since drug solution presents similar properties to the previous one. The next figures only present drug effect on the measured parameters and the reference time corresponds to the introduction of the drug solution. Parallel experiments were per-
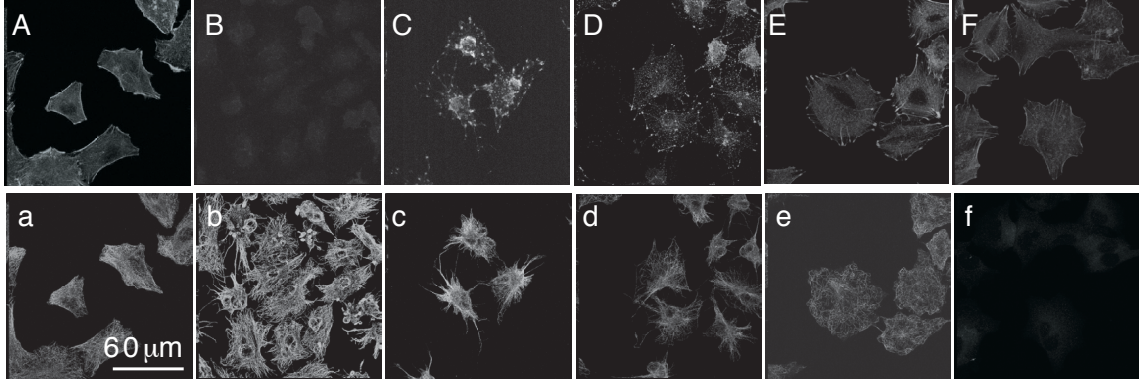
Figure 6: Confocal images of actin (top) and microtubules (bottom) staining of adsorbed cells on coverslips. The cytoskeleton of A549 cells (A and a) has been disturbed with jas (B and b), CD (C and c), LatB (D and d), Taxol (E and e) and Noc (F and f). The scale in a is the same for all images.
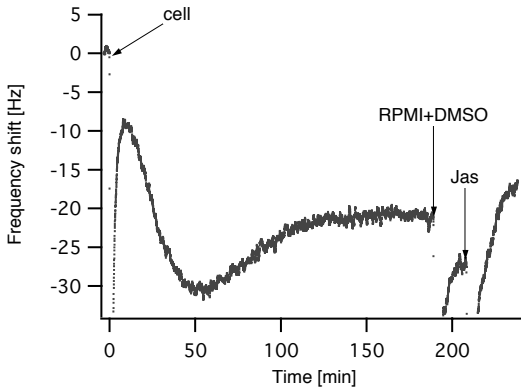

Figure 5: The cytoskeleton of adsorbed A549 cells is disturbed by jas. The surface was first rinsed with RPMI+DMSO, which has a similar viscosity than the drug solution.

formed on coverslips in order to visualize the effect of different drugs on actin and microtubules of A549 spreaded cells (figure 6A,a). As expected the cytoskeleton proteins are modified under drug treatment (figure 6B-F, b-f).

Jas increase actin polymerization by stimulating actin filament nucleation. In figure 6B actin filaments are not visible because jas binding with actin prevents the staining, which would require phalloidin binding to actin at the same place. Jas induces a rapid increase

of the frequency shift, as it can be seen in figure 7 inset. After only $25min$ the positive frequency shift reaches $+9Hz$, what represents a high value in comparison to the larger frequency shift ($\Delta f = -32Hz$) obtained at the end of the first adsorption phase (figure 5). Parallel experiments performed on coverslips show that no cells desorb after jas treatment (figure 6B,b), so that the frequency increase cannot be attributed to cell desorption, similarly to the second phase of cell adsorption. The maximal amplitude versus the decay time constant curve follows very well the water-ethanol one, and this behavior is generalized with each drug modifying the actin filaments (see figures 7, 8). Therefore, changes of the total measured cell mass and/or cell viscosity occur under jas, CD or LatB treatments. A decrease of τ corresponds to an increase of mass density and/or viscosity and a decrease of amplitude is induced by an increase of the viscosity-elasticity ratio of the adlayer [39]. We consider that cell density remains constant under any drug treatment, but cell adsorption/desorption can occur, as well as modification of cell viscosity. During the first $40sec$ after each drug introduction the maximal amplitude A_0 and the decay time constant τ decrease and in-
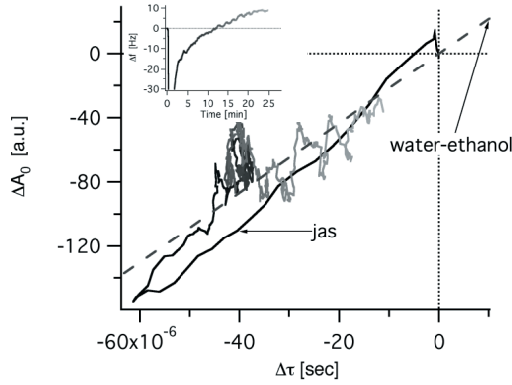
Figure 7: polymerization of actin filaments with jas drug. Inset: frequency versus time under jas treatment.

crease thereafter, similarly to what is measured after the introduction of the cell solution. Cells are therefore slightly disturbed by each solution exchange. During the next $15min$ the maximal amplitude and the decay time constant remain constant under jas treatment, $\Delta A_0 = -70a.u.$ and $\Delta \tau = -40 \cdot 10^{-6} sec$. The cell
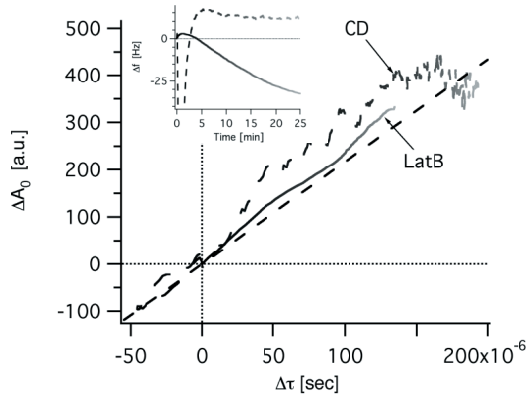

Figure 8: Depolymerization of actin filaments with CD and LatB drugs. Inset: frequency versus time under CD and LatB treatment.

viscosity has therefore increased, inducing a positive
frequency shift $\Delta f = +4Hz$. After this, frequency continues to increase simultaneously with τ ($\Delta \tau = 30 \cdot 10^{-6} sec$) and the max-

imal amplitude shows a small increase following the water-ethanol line. This second phase characterizes a stiffening of cell. Therefore, cell viscosity increase under jas treatment decreases the quartz sensitivity in frequency, which induces frequency increase.

In order to produce a reverse effect on the polymerization state of actin filaments, we also treated spreaded cells with CD (figure 6C,c) and LatB (figure 6D,d). In this case the larger frequency shifts at the end of the first adsorption   phase reached $\Delta f = -20Hz$ and $\Delta f = -23Hz$, respectively. Figure 8 shows that the behavior of ΔA_0 and $\Delta \tau$ for both drugs is in opposition to that observed for jas. The decay time constant and the maximal amplitude increase of about $\Delta \tau \approx +150 \cdot 10^{-6} sec$ and $\Delta A_0 \approx +400a.u.$ in $25min$, so that the total cell density and/or viscosity decreases. A similar result has been measured with a steady state technique [34] with MDCK-II cells. They observed a decrease of resistance and inductance, which corresponds to a decrease of energy losses and mass desorption, respectively. In figures 6C and c it can be seen that under CD treatment the projection of the cell area on the solid surface diminishes and that some cells desorb. Moreover it has been shown that no change of cell viscosity occurs with CD [57–59]. Therefore, the frequency increase of $\Delta f = +11Hz$ (inset fig. 8) under CD treatment is principally due to the decrease of the measured cell mass in contact with the electrode surface. In contrast the frequency decreases continuously under LatB treatment, reaching $-32Hz$ after $25min$ (inset figure 8), and parallel experiments (figure 6D,d) show that no significant cell desorption occurs. Therefore, the cell viscosity decreases under LatB treatment, increasing the quartz sensitivity in frequency,
which induces a frequency decrease for a constant amount of spreaded cells.

We were also interested in measuring possible changes of adsorbing cells, whose mi-

crotubule polymerization state is modified by Taxol and Noc. ΔA_0 versus $\Delta \tau$ curves in fig-
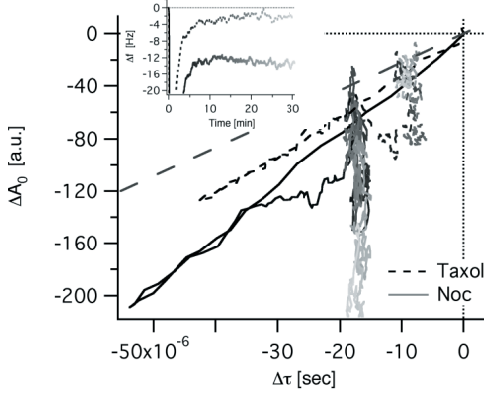

Figure 9: polymerization of microtubules with Taxol and depolymerization with Noc. Inset: frequency versus time under Taxol and Noc treatment.

ure 9 do not follow the water-ethanol line but lie under it, corresponding to cell spreading with modification of the viscoelastic properties of attached cells. This effect is especially important for cells under Noc treatment.

Taxol facilitates microtubule polymerization, what induces no significant change in frequency ($\Delta f = -2Hz$) in comparison to the maximal frequency shift $\Delta f = -30Hz$ reached at the end of the first adsorption phase. The small $\Delta A = -40a.u.$ and $\Delta \tau = -8 \cdot 10^{-6} sec$ decreases correspond to an insignificant increase of the cell viscosity, which is in accordance to measurements performed by N.Wang [57]. Parallel experiments show no significant changes of the actin state, but a large microtubules polymerization and an increase of the cell area projection (figure 6E,e). Therefore the very small decrease of frequency is induced by the small cell spreading.

Microtubules depolymerization was achieved under Noc treatment, which decreases the cell viscosity [57]. The larger frequency shift reached at the end of the first adsorption phase was $\Delta f = -20Hz$. After the succes-

sive decrease and increase of the maximal amplitude and of the decay time constant during the first $6min$ (see figure 9), τ remains constant at $\Delta \tau = -18 \cdot 10^{-6} sec$ and the maximal amplitude decreases from $-80a.u.$ to $-210a.u.$ in $30min$. During this time the frequency remains constant at $\Delta f = -14Hz$ and the parallel measurements show that similarly to Taxol, cell spreading arises under Noc treatment (figure 6F,f). Therefore the cell spreading participates in the frequency decrease, as well as the viscosity decrease of the spreaded cells, which increases the measurement sensibility in frequency. Marx et al. also treated spreaded cells with Noc, but with smaller concentrations ($0.33 - 15\mu M$) [32]. The endothelial cells also induce a decrease of frequency, which then increases during attachment and spreading. Under Noc treatment a frequency decrease was also measured, as well as a drop in resistance, which decreases then very slowly. It was interpreted as restoration of rounded cell shape, which is in contradiction to our results. It may be due to the different cell line and the different cell confluency.

Modifications of actin and microtubule polymerization state induce different changes in spreaded cells, which can be detected with the QCM and can be well explained by measuring the maximal amplitude, the decay time constant and the frequency. An increase in cell stiffness can effectively induce a frequency increase and therefore explain that positive frequency shifts can be measured during the second adsorption phase of spreading cells.

In reality contacts between quartz electrode and the ventral side of the cells are not continuous but separated by gaps filled with solution. At the present time the quartz responsivity of such systems is unknown and at our knowledge no theoretical models have been developped to treat such cases. Nevertheless, it is obvious that any modification of the liquid present between the cell and the solid sur-

face will contribute to the quartz responsivity, due to a different penetration depth of the damped wave coupled to the quartz.

4 CONCLUSION

The QCM is a very promising technique to study kinetics of spreading cells as well as their viscoelastic properties at the only condition that complementary parameters to f are measured, such as the maximal oscillation amplitude of the quartz and the decay time constant. The different phenomena analysis is therefore possible since the Sauerbrey relation is no longer valid with spreaded cells.

In this paper we showed that the frequency measured during the cell attachment and spreading is composed of two main adsorption phases. In the first one the frequency decreases during almost $80 min$ and is mainly due to cell attachment and spreading. During the second one the frequency increases and even passes the initial value and positive frequency shifts are measured after several hours. Nevertheless, optical measurements have shown that the surface of the quartz crystal is covered with living cells. Therefore no cell desorption occurs during this phase. In fact the frequency increase is mainly due to an increase of the cell stiffness, which modifies the measure sensibility in frequency.

In order to confirm this hypothesis, we treated spreaded cells with different agents, which affect the polymerization state of actin and microtubule filaments. Positive frequency shifts are measured when viscosity of the spreaded cells increases and/or when cell desorption occur, and negative frequency shifts arise when cells become softer and/or the projection area of spreaded cells increases.

Since many factors can influence the quartz responsivity, further experiments on systems with phase transitions have to be performed in order to better characterize the different parameters. In this view we are currently trying to built a QCM under an optical microscope.

BIBLIOGRAPHY

[1] R. Singhvi, A. Kumar, G. P. Lopez, G. N. Stephanopoulos, D. I. C. Wang, G. M. Whitesides, D. E. Ingber, Engineering cell shape and function, Science 264 (1994) 696–698.

[2] J. T. Emerman, D. R. Pitelka, Maintenance and induction of morphological differentiation in dissociated mammary epithelium on floating collagen membranes, In Vitro 13 (1977) 316–322.

[3] D. E. Ingber, J. Folkman, Mechanochemical switching between growth and differentiation during fibroblast growth factor-stimulated angiogenesis in vitro: role of extracellular matrix, J. Cell Biol. 109 (1989) 317–330.

[4] J. Folkman, A. Moscona, Role of cell shape in growth control, Nature 273 (1978) 345–349.

[5] D. E. Ingber, Fibronectin controls capillary endothelial cell growth by modulating cell shape, Proc. Natl. Acad. Sci. USA 87 (1990) 3579–3583.

[6] M. J. Bissel, H. G. Hall, G. Parry, How does extracellular matrix direct gene expression?, J. Theor. Biol. 99 (1982) 31–68.

[7] C. S. Chen, M. Mrksich, S. Huang, G. M. Whitesides, D. E. Ingber, Goemetric control of cell life and death, Science 276 (1997) 1425–1428.

[8] K. A. Barbee, P. F. Davies, L. Ratneshwar, Shear stress-induced reorganisation of the surface topography of living endothelial cells imaged by atomic force microscopy, Circ. Res. 74 (1994) 163–171.

[9] J. Pourati, A. Maniotis, D. Spiegel, J. L. Schaffer, J. P. Butler, J. Fredberg, D. Ingber, D. Stamenovic, N. Wang, Is cytoskeletal tension a major determinant of cell deformability in adherent endothelial cells?, Am J Physiol. 274 (1998) C1283–C1289.

[10] R. D. Allen, New observations on cell architecture and dynamics by video-enhanced contrast optical microscopy, Ann. Rev. Biophys. Biophys. Chem. 14 (1985) 265.

[11] N. Wang, I. M. Tolic-Norrelykke, J. Chen, S. M. Mijailovich, J. P. Butler, J. J. Fredberg, D. Stamenovic, Cell prestress.I. Stiffness and prestress are closely associated in adherent contractile cells, Am. J. Physiol. Cell Physiol. 282 (3) (2002) C606–C616.

[12] M. Puig-De-Morales, M. Grabulosa, J. Alcaraz, J. Mullol, G. N. Maksym, J. J. Fredberg, D. Navajas, Measurement of cell microrheology by magnetic twisting cytometry with frequency domain demodulation, J. Appl. Physiol. 91 (3) (2001) 1152–1159.

[13] J. C. Berrios, M. A. Schroeder, R. D. Hubmayr, Mechanical properties of alveolar epithelial cells in culture, J. Appl. Physiol. 91 (1) (2001) 65–73.

[14] Q. Wang, E. T. Chiang, M. Lim, J. Lai, R. Rogers, P. A. Janmey, D. Shwpro, C. M. Doerschuk, Changes in the biomechanical properties of neutrophils and endothelial cells during adhesion, Blood 97 (3) (2001) 660–668.

[15] N. Wang, D. Stamenovic, Contribution of intermediate filaments to cell stiffness, stiffening, and growth, Am. J. Physiol. Cell Physiol. 279 (1) (2000) C188–C194.

[16] A. R. Bausch, U. Hellerer, M. Essler, M. Aepfelbacher, E. Sackmann, Rapid stiffening of integrin receptor-actin linkages in endothelial cells stimulated with thrombin: a magnetic bead microrheology study, Biophys. J. 80 (6) (2001) 2649–2657.

[17] A. R. Bausch, F. Ziemann, A. A. Boulbitch, K. Jacobson, E. Sackmann, Local measurements of viscoelastic parameters of adherent cell surfaces by magnetic bead microrheometry, Biophysical Journal 75 (1998) 2038–2049.

[18] F. Ziemann, J. Rädler, E. Sackmann, Local measurements of viscoelastic moduli of entangled actin networks using an oscillating magnetic bead microrheometer, Biophysical Journal 66 (1994) 2210–2216.

[19] J. Kolega, Effects of mechanical tension on protrusive activity and microfilament and intermediate filament organization in an epidermal epithelium moving in culture, J. Cell Biol. 102 (1986) 1400–1411.

[20] R. M. Hochmuth, R. E. Waugh, Erythrocyte membrane elasticity and viscosity, Annu. Rev. Physiol. 49 (1987) 209–219.

[21] E. Evans, A. Yeung, Apparent viscosity and cortical tension of blood granulocytes determined by micropipet aspiration, Biophys. J. 56 (1989) 151–160.

[22] E. Evans, D. Berk, A. Leung, Detachment of agglutinin-bonded red blood cells, Biophysical Journal 59 (1991) 838–848.

[23] K. L. P. Sung, M. K. Kwan, F. Maldonado, W. H. Akeson, Adhesion strength of human ligament fibroblasts, J Biomech Eng 116 (1994) 237–242.

[24] N. O. Petermon, W. B. McConnaughey, E. L. Elson, Dependence of locally mesured cellular deformability on position on the cell, temperature and cytochalasin b, Proc. Natl. Acad. Sci. USA 79 (1982) 5327–5331.

[25] C. Pastermank, S. Wong, E. L. Elson, Mechanical function of dystrophin in muscle cells, C. Cell Biol. 128 (1995) 355–361.

[26] A. Janshoff, H.-J. Galla, C. Steinem, Piezoelectric mass-sensing devices as biosensors - An alternative to optical biosensors?, Angew. Chem. Int. Ed. 39 (2000) 4004–4032.

[27] G. Sauerbrey, Verwendung von Schwingquartzen zur Wägung dünner Schichten und zur Mikrowägung, Z. Phys. 155 (1959) 206–222.

[28] J. L. Jones, J. P. Meiure, A piezoelectric transducer for determination of metals at the micromolar level, Anal. Chem. 41 (1969) 484.

[29] J. P. Meiure, J. L. Jones, Electrogravimetric trace analysis on a piezoelectric detector, Talanta 16 (1969) 149–150.

[30] T. Nomura, M. Iijima, Electrolytic determination of nanomolar concentrations of silver in solution with a piezoelectric quartz crystal, Anal. Chim. Acta 131 (1981) 97–102.

[31] K. K. Kanazawa, J. G. Gordon, Frequency of a quartz microbalance in contact with liquid, Anal. Chem. 57 (1985) 1770–1771.

[32] K. A. Marx, T. Zhou, A. Montrone, H. Schulze, S. J. Braunhut, A quartz crystal microbalance cell biosensor: detection of microtubule alterations in living cells at nM nocodazole concentrations, Biosensors and Bioelectronics 16 (2001) 773–782.

[33] T. Zhou, K. A. Marx, M. Warren, H. Schulze, S. J. Braunhut, The quartz crystal microbalance as a continuous monitoring tool for the study of endothelial cell surface attachment and growth, Biotechnol. Prog. 16 (2000) 268–277.

[34] J. Wegener, J. Seebach, A. Janshoff, H.-J. Galla, Analysis of the composite response of shear wave resonators to the attachment of mammalian cells, Biophys. J. 78 (2000) 2821–2833.

[35] A. Janshoff, J. Wegener, M. Sieber, H.-J. Galla, Double-mode impedance analysis of epithelial cell monolayers cultured on shear wave resonators, Eur. Biophys. J. 25 (1996) 93–103.

[36] K. Otto, H. Elwing, M. Hermansson, Effect of ionic strength on initial interactions of escherichia coli with surfaces, studied on-line by a novel quartz crystal microbalance technique, Journal of Bacteriology 181 (17) (1999) 5210–5218.

[37] G. Nimeri, C. Fredriksson, H. Elwing, L. Liu, M. Rodahl, B. Kasemo, Neutrophil interaction with protein-coated surface studied by an extended quartz crystal microbalance technique, Colloids and surfaces B: Biointerfaces 11 (1998) 255–264.

[38] C. Fredriksson, S. Khilman, B. Kasemo, In vitro real-time characterization of cell attachment and spreading, J. Mater. Sci. Mater. Med. 9 (1998) 785–788.

[39] C. Galli Marxer, M. Collaud Coen, H. Bissig, U. F. Greber, L. Schlapbach, Interpretation of quartz crystal microbalance measurements improved using the maximal oscillation amplitude and the transient decay time constant, submitted to Analytical and Bioanalytical Journal .

[40] M. Suomalainen, M. Y. Nakano, S. Keller, K. Boucke, R. P. Stidwill, U. F. Greber, Microtubule-dependent plus- and minus end-directed motilities are competing processes for nuclear targeting of adenovirus, J. Cell Biol. 144 (1999) 657–672.

[41] A. Holzinger, Jasplakinolide. an actin-specific reagent that promotes actin polymerization, Methods Mol Biol 161 (2001) 109–120.

[42] M. R. Bubb, I. Spector, B. B. Beyer, K. M. Fosen, Effects of jasplakinolide on the kinetics of actin polymerization. An explanation for certain in vivo observations, J Biol Chem 275 (2000) 5163–5170.

[43] M. R. Bubb, A. M. Senderwicz, E. A. Sausville, K. L. Duncan, E. D. Korn, Jasplakinolide, a cytotoxic natural product, induces actin polymerization and competitively inhibits the binding of phalloidin to F-actin, J Biol Chem 269 (1994) 14869–14871.

[44] M. Coue, S. L. Brenner, I. Spector, E. D. Korn, Inhibition of actin polymerization by latrunculin A, FEBS Lett 213 (1987) 316–318.

[45] I. Spector, N. R. Shochet, D. Blasberger, Y. Kashman, Latrunculins-novel marine macrolides that disrupt microfilament organization and affect cell growth: I. Comparison with cytochalasin D, Cell Motil. Cytoskel. 13 (1989) 127–144.

[46] E. Urbanik, B. R. Ware, Actin filament capping and cleaving activity of cytochalasins B, D, E, and H, Arch Biochem Biophys 269 (1989) 181–187.

[47] J. A. Cooper, Effects of cytochalasin and phalloidin on actin, J. Cell Biol. 105 (1987) 1473–1478.

[48] P. B. Schiff, J. Fant, S. B. Horwitz, Promotion of microtubule assembly in vitro by taxol, Nature 277 (1979) 665–667.

[49] J. Hoebeke, G. Van Nijen, M. DeBrabender, Interaction of nocodazole (R17934) a new antitumoral drug, whith rat brain tubulin, Biochem. Biophys. Res. Commun. 69 (1976) 319–324.

[50] L. Wilson, R. J. Toso, M. A. Jordan, Vinblastine, nocodazole, and colchicine suppress the dynamic instability of microtubules: implications for the mechanism of antimitotic action, Cell. Pharmacol. (Suppl.) I (1993) S35–S40.

[51] L. Wilson, M. A. Jordan, Pharmacological probes of microtubule function, Wiley-Liss, 1994.

[52] K. K. Kanazawa, Mechanical behaviour of films on the quartz microbalance, Faraday Discuss 107 (1997) 77–90.

[53] M. Rodahl, F. Höök, B. Kasemo, QCM operation in liquids: an explanation of measured variations in frequency and Q factor with liquid conductivity, Anal. Chem. 68 (1996) 2219–2227.

[54] J. Wegener, A. Janshoff, H.-J. Galla, Cell adhesion monitoring using a quartz crystal microbalance: comparative analysis of different mammalian cell lines, Eur. Biophys. J. 28 (1998) 26–37.

[55] K. Burridge, K. Fath, T. Kelly, G. Nuckolls, C. Turner, Focal adhesions: transmembrane junctions between the extracellular matrix and the cytoskeleton, Annu. Rev. Cell. Biol. 4 (1988) 487–525.

[56] J. Bereiter-Hahn, M. Luck, T. Miebach, H. K. Stelzer, M. Voth, Spreading of trypsinized cells: cytoskeletal dynamics and energy requirements, J. Cell Sci. 96 (1) (1990) 171–188.

[57] N. Wang, Mechanical interactions among cytoskeletal filaments, Hypertension 32 (1998) 162–165.

[58] O. Thoumine, O. Cardoso, J.-J. Meister, Changes in the mechanical properties of fibroblasts during spreading: a micromanipulation study, Eur Biophys J 28 (1999) 222–234.

[59] T. Wakatsuki, B. Schwab, N. C. Thompson, E. L. Elson, Effects of cytochalasin D and latrunculin B on mechanical properties of cells, J. Cell Science 114 (5) (2001) 1025–1036.

Conclusion and outlook

The thesis work presents two different studies. In the first one the fundamental question addressed was to know, whether proteins can "sense" the topography, similarly to what had been shown for cells. It required to find a method, which allowed us to modify the topography at the nanometer scale without any change of the surface chemistry. Moreover it was necessary to visualize the nanostructured surface before and after protein adsorption. The AFM is the only technique, which allows us to modify the surface at a nanometric scale and to measure in situ adsorbed biological molecules such as proteins, which are insulators. Nanostructured surfaces by LAO have been characterized by XPS, demonstrating that LAO treatment effectively induces no change of the surface chemistry. Therefore ideal systems can be created by LAO to study the only influence of the topography on protein adsorption. Globular protein A shows no adsorption difference between parallel $1nm$ high nanostructures and neat Si. The bounded IgG also shows no preferential adsorption on or outer the nanostructures covered with protein A. In contrast, preferential adsorption of filamentous F-actin has been measured on $1nm$ high created lines on Si, and the density of adsorbed protein on neat Si is higher than on nanostructures. Ti nanostructures of different heights have been created. The F-actin adsorption is the greatest on $1 - 2nm$ high lines with a preferential orientation along them. In contrast the adsorption density is low on $4nm$ high nanostructures, and no defined orientation is noted. On neat Ti adsorbed F-actin shows a smaller density than on the $1 - 2nm$ high nanostructures. Therefore proteins are able to react to modifications of the topography at the nanometer scale, what has to be taken into account in the design of new biomaterials.

In order to approach in vivo conditions, further studies have to be performed under aqueous conditions and with the presence of protein mixtures. Moreover the next experimental step consists on the adsorption of cells on the proteins oriented by such nanostructured surface. In this view new methods would be required, because the work area of most actual commercial AFM is restricted to $10^4 \mu m^2$ and the method is too slow to create nanostructures over larger areas. The lithography technique will be perhaps the solution to produce nanostructures at large scale, because its resolution is becoming improved and its work area is in the cm^2 range. Nevertheless further developments are required before the lithography reaches the LAO resolution.

The second part of this work was concentrated on the development of the QCM technique, and especially on the improvement of the interpretation of QCM data. At the moment the QCM is the only method, which allows us to follow the adsorption kinetics and to get simultaneously viscoelastic information of the adlayer. Nevertheless the interpretation of measurements performed with commercial QCM is still difficult, because modifications of liquid and mass properties can not be separated from the variation of adsorbed mass. We have demonstrated that the introduction of the maximal oscillation amplitude and the decay time constant improves the determination of the phenomena arising at the quartz surface. Con-

tribution of adsorbed mass can effectively be distinguished from the one of modification of viscosity or density of the liquid or of the mass. Using the protein A-BSA-IgG system, the biological activity of adsorbed protein A has been investigated on Au and on Ti. At concentration of $160\mu M$ no difference is noted, but divergences have been measured at higher concentrations. More proteins always adsorb on Au surfaces and the adlayers dissipate less energy than on Ti. However the biological activity is better on Ti. Further experiments with other protein systems are required in order to determine if the biological activity can be directly related to the viscoelastic properties of the protein layer. The effect of buffer properties on adsorbed fibronectin has also been investigated. Immersion in Citrate-Phosphate buffer induces only delamination of the adlayer. In contrast the mechanical properties of the fibronectin are modified in Hepes solution.

The QCM open new applications in cell biology and biotechnologies, because the interactions occurring between a surface and a cell can be directly investigated. We have demonstrated that different phenomena influence the frequency, the amplitude and the decay time constant during cell adsorption. During the first $80min$ the frequency decreases due to an increase of adsorbed cells. Thereafter the frequency begins to increase, what would correspond to mass desorption. Nevertheless living cells are still present at the surface. We demonstrate that the development of the cytoskeleton induces stiffening of the cell and increases the total cell viscosity. This phenomenon influences the QCM sensitivity in frequency, although no modification of the amount of adsorbed cells occurs. The cytoskeleton state has also been modified with drugs, which increase or decrease the polymerisation state of actin and microtubules. It allowed us to reproduce rapid increasing and decreasing of frequency in less than $30min$ due to fast changes of the cell viscosity and cell adsorption.

The understanding of complex systems such as cells requires nevertheless the combination of different technique. We tried to combine a QCM with a fluorescence microscopy. The quartz electrode has to be modified in order to avoid fluorescence bleaching on Au. Moreover it is essential to work with oil objectives, which have very short working distances. The building of the whole setup is therefore complicated in order to fulfill all requirements, such as temperature stabilization and exchange of fluid. To date no reproducible measurements could be performed during several hours. Nevertheless this process is the only one, which would allows us to correlate the number of developed focal points with the measured frequency, amplitude and decay time constant. Moreover this method combination would allow us to track modification of cell properties during for example virus infection. In order to quantify the variation of the frequency, the amplitude and the decay time constant during viscoelastic modifications of adlayer, colloidal systems can be very interesting. They are firstly much less complex than living cells and secondly they allow us to study phase transitions. Our first tests are very promising.

Thank you!

Curriculum Vitae

Name	Galli Marxer
First name	Carine
Date and place of birth	22 April 1974, Fribourg (CH)
Nationality	Swiss (Valcolla/TI)
Marial status	married
Languages	French, German, Swiss German, English, French Sign Language
Home address	Untereyfeldweg 25, 3063 Ittigen
Email address	carine@carinegalli.ch

Education

since 2002	Post-doc in the Solid State Physics Research Group, University of Fribourg, Switzerland
1998-2002	PhD thesis in the Solid State Physics Research Group, University of Fribourg, Switzerland, Supervisor: Prof. L. Schlapbach
1996-1998	DMG (Diplôme de maître de Gymnase) to teach physics and mathematics in high schools
1993-1998	Undergraduate degree in Physics, University of Fribourg, Switzerland
1995-1996	Studies of Physics one year at the Physics Institute, University of Bayreuth, Germany
1989-1993	Maturity diploma Type C, Collège Ste-Croix, Fribourg, Switzerland
1980-1989	Obligatory school, Fribourg, Switzerland

Additional training

1998	Cours postgrade en biomatériaux (postgrade course on biomaterials) EPFL, Lausanne, Switzerland
1998	Short course on microsystem technology, NanoTech98, Montreux, Switzerland
1999	NeutronenPraktikum (neutron course), Forschungszentrum Jülich, Germany
2000	Protein Folding, Enrico Fermi Summer School, Varenna, Italy
2000	Einführung in die Telekommunikation (Introduction in telecommunications), Course for computer scientists, University of Fribourg, Switzerland
2001	Introduction to Object Oriented Programming using C++ and Java, Cours du 3ème Cycle de Physique, EPFL, Lausanne, Switzerland

Publications

1. **Adsorption and bioactivity of protein A on silicon surfaces studied by AFM and XPS**
   M. Collaud Coen, R. Lehmann, P. Gröning, M. Bielmann, Carine Galli and L. Schlapbach,
   J. Colloid and Interf. Sci., 233 (2001) 180-189

2. **Protein adsorption on topographically nanostructured titanium**
   Carine Galli, M. Collaud Coen, R. Hauert, V.L. Katanaev, M.P. Wymann, P. Gröning and L. Schlapbach, Surface Science 474, L180-L184 (2001)

3. **Protein and cell adsorption kinetics**
   Carine Galli, M. Collaud Coen, Urs Greber, Thomas Greber and Louis Schlapbach, European Cells and Materials, Vol.2, Suppl. 1 (2001) 33

4. **Dynamic measurements of bound water in proteins and protein-resistant polymers: a combined OWLS and QCM-D study**
   J. Vörös, S.M. DePaul, I. Reviakine, C.Galli, M. Collaud Coen, M. Textor and N.D. Spencer, European Cells and Materials Vol. 2, Suppl.1 (2001) 49

5. **Creation of nanostructures to study the topographical dependency of protein adsorption**
   Carine Galli, M. Collaud Coen, R. Hauert, V.L. Katanaev, P. Gröning and L. Schlapbach, Colloids and Surfaces B: Biointerfaces, 26 (2002) 255-267

6. **Interpretation of Quartz Crystal Microbalance measurements improved using the maximal oscillation amplitude and the transient decay time constant**
   C. Galli Marxer, M. Collaud Coen, H. Bissig, U.F. Greber and L. Schlapbach, submitted to Analytical and Bioanalytical Journal

7. **Study of adsorption and viscoelastic properties of proteins with a Quartz Crystal Microbalance by measuring the oscillation amplitude**
   C. Galli Marxer, M. Collaud Coen and L. Schlapbach, J. Colloid Interface Sci., accepted 2002

8. **Cell viscosity increase during spreading induces positive frequency shifts in Quartz Crystal Microbalance measurements**
   C. Galli Marxer, M. Collaud Coen, T. Greber, U.F. Greber and L. Schlapbach, submitted to Analytical and Bioanalytical Journal